UNIVERSITY OF TRENTO - Italy
Department of Civil, Environmental and Mechanical Engineering

Doctoral School in Civil, Environmental and Mechanical Engineering
XXIX cycle 2014/2017

Doctoral Thesis - July 2018

Narges Ataollahi

Anion Exchange Membranes (AEMs), based on Polyamine Obtained by Modifying Polyketone, for Electrochemical Applications

Supervisors

Prof. Rosa Di Maggio, University of Trento, Italy
Prof. Paolo Scardi, University of Trento, Italy

In memory of my father

To my mother
with love and unending appreciation

ACKNOWLEDGEMENTS

I would like to acknowledge all the people who have made crucial contributions to this work. I would like to express my gratitude to my supervisor Prof. Rosa Di Maggio for her continuous support, endless inspiration, and immense knowledge. I also thank my co-supervisor Prof. Paolo Scardi, for his helpful advice and support throughout my PhD research studies. Special thanks go to Prof. Vito Di Noto too, whose great knowledge and guidance benefited me enormously. I am also very grateful to Prof. Gianni Cavinato, Prof. Sandra Dirè, and Prof. Claudio Della Volpe for their valuable advice and contributions. Sincere thanks go to Dr. Keti Vezzù, Dr. Wilma Vaona, Dr. Elisa Cappelletto, Dr. Mirco D'Incau, and Dr. Emanuela Callone for their kind help. I would like to thank my family, to whom I owe a great deal, especially my mother: she has been a constant source of support and encouragement. I am also grateful to the friends I made in Trento, and particularly Angela, Rocco, Roberto, Vincenzo and Camilo, who were all part of my second family in Italy, and fond memories will always remain.

ABSTRACT

Polymeric anion exchange materials can be key components for forming membranes for use in several electrochemical applications. Polyketones seem particularly promising as materials for making anion exchange membranes (AEMs), not only because the starting monomers, carbon monoxide and ethylene, are relatively inexpensive (pointing to the feasibility of producing polyketone at a more competitive cost than other membranes), but also because the presence of 1,4-dicarbonyl units along the backbone is an important chemical feature for the purposes of chemically modifying these polymers. It allows for post-manufacturing functionalization through the so-called Paal-Knorr reaction, which introduces N-substituted pyrrole units along the polymer backbone. An anion exchange membrane (AEM) was made with a modified polyketone using a solvent casting method, followed by iodomethylation and ion exchange with KOH (PK-PDAPm). Every step in the synthetic process was confirmed by Fourier Transform InfraRed spectroscopy (FTIR). Nuclear Magnetic Resonance (NMR) spectroscopy was also used to characterize the structure of the modified polyketone in detail. The results obtained revealed the formation of a pyrrole ring along the polyketone backbone. Polyamines modified in this way are amenable to structural rearrangements to form N-substituted pyrrole crosslinked with dihydropyridine units. Scanning electron microscopy, differential scanning calorimetry, and X-ray diffraction techniques were also used to study the morphological, thermal, and structural characteristics of the modified polyketone, as well as the membranes derived therefrom. Thermogravimetric analyses demonstrated the thermal stability of the material up to 200ºC, with no significant mass loss or degradation. The conductivity of the AEM was studied at temperatures up to 120ºC, and the highest value of $9x10^{-4}$ $S.cm^{-1}$ was reached at 120ºC for the ionic conductivity of the membrane in iodide form, with values of the same order of magnitude (10^{-4} $S.cm^{-1}$) for the membrane in OH form.

Polyamine $(PA\text{-}SiNH_2)_m$, membranes containing silica formed by sol-gel reactions of 3-aminopropyltriethoxysilane (APTES) in hydrolytic conditions were prepared by solution casting, followed by methylation and an ion exchange process, in an effort to improve the properties of the AEM. FTIR and NMR were used to investigate the chemical

features of the silica and its interaction with the polyamine polymer. The influence of amino-functionalized silica (Si-NH_2) on the properties of the membrane obtained was investigated. The results demonstrated: a significant improvement in thermal stability up to 300°C, and an increase in water uptake and ion exchange capacity by comparison with the AEM (PK-PDAPm) containing no silica. The maximum conductivity obtained for (PA-SiNH_2)m-I and (PA-SiNH_2)m-OH was 2.4×10^{-4} S cm^{-1} at 130°C, and 4.8×10^{-4} S cm^{-1} at 120°C.

These details may serve as an initial guide to the use of the above-described AEM in electrochemical applications.

PUBLICATIONS

The following publications were produced as a result of the work conducted by the author during her years of doctoral studies.

Journal publications

- **N. Ataollahi**, K. Vezzù, G. Nawn, G. Pace, G. Cavinato, F. Girardi, P. Scardi, V. Di Noto, R. Di Maggio. 2017, A polyketone-based anion exchange membrane for electrochemical applications: synthesis and characterization. *Electrochimica Acta*, (226)148-157.

- **N. Ataollahi**, F. Girardi, E. Cappelletto, K. Vezzù, V. Di Noto, P. Scardi, E. Callone, R. Di Maggio. 2017, Chemical modification and structural rearrangements of polyketone-based polymer membrane. *Journal of Applied Polymer Science*, DOI: 10.1002/APP.45485

- **N. Ataollahi,** E. Cappelletto, K. Vezzù, V. Di Noto, G. Cavinato, E. Callone, S. Dirè, P. Scardi, R. Di Maggio. 2018, Properties of anion exchange membrane based on polyamine: effect of functionalized silica particles prepared by sol-gel method. *Journal* of *Solid State Ionic*, (322) 85-92.

- **N. Ataollahi,** V. Di Noto, C. Della Volpe, P. Scardi, R. Di Maggio. 2018, Conductivity measurements on anion exchange membrane based on polyamine by EMS. In *progress*.

Other topics

- C. S. Wong, K. H. Badri, **N. Ataollahi,** K. P. Law, M. S. Su'ait, N. I. Hassan. 2014, Synthesis of new bio-based solid polymer electrolyte polyurethane-$LiClO_4$ via prepolymerization method: Effect of NCO/OH ratio on their chemical, thermal properties and ionic conductivity. *International Journal of Chemical, Molecular, Nuclear, Materials and Metallurgical Engineering*, (8) 1168-1175.

- L. Tian Khoon, **N. Ataollahi,** N. H. Hassan, A. Ahmad. 2016, Studies of porous solid polymeric electrolytes based on poly (vinylidene fluoride) and poly (methyl methacrylate) grafted natural rubber for applications in electrochemical devices. *Journal of Solid State Electrochemistry*, (20) 203-213.

- F. Girardi, L. Bergamonti, C. Isca, G. Predieri, C. Graiff, P.P. Lottici, E. Cappelletto, **N. Ataollahi**, R. Di Maggio. 2017, Chemical-physical

characterization of ancient paper with functionalized polyamidoamines (PAAs). *Cellulose*, (24) 1057-1068.

- C. Malerba, E. Cappelletto, **N. Ataollahi,** R. Ciancio, R. Edla, R. Di Maggio, P. Scardi. Control of composition and grain growth in Cu_2ZnSnS_4 thin films from nanoparticle inks. Submitted to the *Journal of Thin Solid Films* (April 2018).

Conference proceedings

- **N. Ataollahi**, E. Cappelletto, C. Malerba, R. Di Maggio, P. Scardi. Effect of annealing cycles on the properties of CZTS layers for thin film solar cells. 21st International Conference on Solid State Ionics, 18-23 June 2017, Padova, Italy. Oral presentation.

- **N. Ataollahi**, K. Vezzù, V. Di Noto, P. Scardi, E. Callone, S. Dire, R. Di Maggio. Properties of anion exchange membrane based on polyamine: effect of functionalized silica particles prepared by sol-gel method. 21st International Conference on Solid State Ionics, 18-23 June 2017, Padova, Italy. Oral presentation.

Contents

List of Figures

List of Tables

Foreword

A high hydroxide conductivity and excellent stability of anion exchange membranes (AEMs) are essential in electrochemical applications. Ion-exchange membranes are used in a wide range of industrial applications involving separation processes [1,2], and ion-selective transport in many electrochemical processes and solid-state devices. The most famous membrane separation systems rely on electrodialysis, electrolysis, diffusion dialysis, pervaporation, and reverse osmosis, which operate on the basis of a concentration, potential, or pressure gradient serving as a driving force. There are also electrochemical devices that use ion exchange membranes in the alternative energy field, including fuel cells, batteries and sensors [3-7].

Numerous works in the literature describe the development of different AEMs, but the resulting membranes usually suffer from poor stability under humidified conditions after incorporating anionic sites by chloromethylation and quarternization. Degradation causes the loss of anionic exchange groups, a drop in ionic conductivity, and an increase in production costs. In order to be able to use membranes on a large and commercially-viable scale, inexpensive and non-toxic starting materials need to be used in simple reactions. With the collaboration of Prof. Vito Di Noto, who has conducted an abundance of remarkable scientific research in the field of electrolytes for energy conversion and storage devices, we used polyketone (PK) as the host polymer for three main reasons: 1) ease of modification; 2) high thermal and mechanical stability; and 3) low cost of the starting materials. This thesis aims to give an account of the use of polyamine (PA) obtained from modified aliphatic polyketone in this setting. PA emerges as a suitable candidate AEM for electrochemical applications. Modified silica was also incorporated in the PA to obtain a membrane with improved thermal stability and electrochemical properties.

Outline of the thesis

This thesis illustrates the main outcomes of the research conducted by the author during her PhD activities. It is divided into three main topics, for a total of three chapters, as briefly outlined below.

Chapter 1 provides a detailed introduction to the main electrochemical applications of membranes, and discusses fuel cells, types of membranes, and ionic mechanisms.

Chapter 2 describes the synthesis of an anion exchange membrane (AEM) based on modified polyketone. Particular attention is paid to the pathway reactions, proposed on the strength of the ^{1}H NMR, UV-Vis, and FTIR results. The membranes obtained are characterized in terms of their thermal properties, conductivity, water uptake, and ion exchange capacity. Scanning electron microscopy, and X-ray diffraction techniques were used to study the morphological, and structural characteristics of the modified polyketone, as well as the corresponding membrane. The main results were reported in two publications titled: 'A polyketone-based anion exchange membrane for electrochemical applications: synthesis and characterization'. [8] and 'Chemical modification and structural rearrangements of polyketone-based polymer membrane'. [9].

Chapter 3 deals with the surface modification of silica using 3-aminopropyltriethoxysilane (APTES), followed by the preparation of AEMs with the addition of this modified silica. The influence of the amino-functionalized silica (Si-NH_2) on the properties of the membranes obtained was investigated, and many details of their characterization are provided. The main results were reported in the publication titled: 'Properties of anion exchange membrane based on polyamine: effect of functionalized silica particles prepared by sol-gel method'. [10].

This thesis ends with a summary of the main conclusions and future prospects.

Chapter 1

1. Introduction

1.1 An overview on alternative energy sources

Traditional fossil energy sources, such as fossil fuel, natural gas, coal and oil, are ultimately limited, and the widening gap between increasing demand and decreasing supply will overlap at some point in the future. With an expanding world population, a globalized economy, and advances in civilization, the global demand for energy is growing at an alarming rate, prompting various efforts around the world to explore alternative energy sources. More efficient and cleaner alternative energy sources are strongly preferable due to a heightened awareness of the need to safeguard the environment. Electrochemical power generation is one such alternative energy option that is attracting considerable interest due to its sustainability and environmental friendliness [11]. Fuel cells (FC) are one of the principal systems for converting chemical energy into electrical energy. The chemical processes occur at the electrodes and the flows of electronic and ionic species are separated by an electrolyte. FC derive their power from the fuel supplied, which can be replenished almost instantaneously when exhausted. The FC is therefore an excellent energy system that can be refilled and ready to go without any prolonged downtime [11-13].

1.2 Ion exchange membranes

A membrane is a selective barrier that separates and/or unites two adjacent phases, and enables or promotes the exchange of matter, between them [14]. It is known as an ion

exchange membrane when the barrier carries charged groups. Ion exchange membranes can be divided into three categories:

1) cation exchange membranes;
2) anion exchange membranes; and
3) amphoteric ion exchange membranes.

Cation exchange membranes contain negatively-charged groups, such as $-SO_3^-$, -COO, $-PO_3^{2-}$, $-PO_3H^-$, and $C_6H_4O^-$, fixed to the membrane's backbone, which enable the transfer of cations, but not of anions. Conversely, anion exchange membranes (AEMs) contain positively-charged groups, such as $-NH_3^+$, $-NRH_2^+$, $-NR_2H^+$, $-NR_3^+$, $-PR_3^+$, and $-PR_2^+$, attached to the membrane backbone, and allow for the passage of anions, but retain cations. The matrix of cation and anion exchangers are shown in Figure 1.1. Amphoteric ion exchange membranes consist of two polymer layers carrying both negatively and positively charged groups that randomly distributed within the polymer matrix of the membrane [3,14,15].

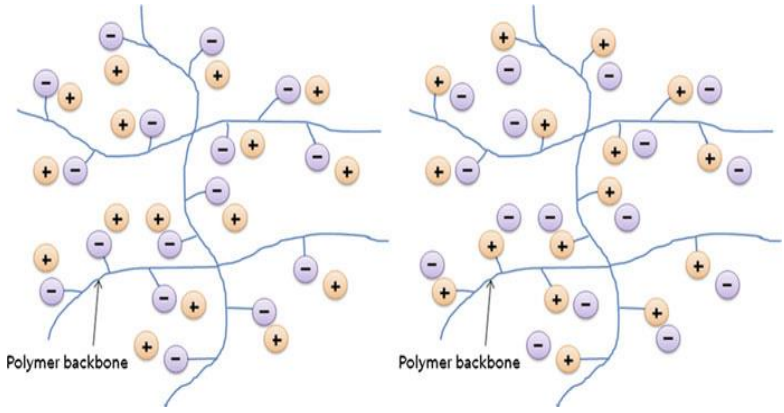

Figure 1.1: Schematic of the chemical structure of a cation exchanger (left), and an anion exchanger (right) [3]

Ion exchange membranes can also be classified according to their structure and preparation procedure as:

1) heterogeneous membranes, in which the charged groups are physically mixed with the membrane matrix;
2) homogeneous membranes, in which the charged groups are chemically bonded to the matrix.

An example of a heterogeneous membrane is poly(ethylene oxide) (PEO) with oxyethylene chains, discovered by Fenton et al. [16], and Armand et al. [17]. Complexes of PEO with a salt combine the mechanical properties of the polymer with the electrochemical properties of the salt, resulting in a good ionic conductivity ($1x\ 10^{-3}\ S{\cdot}cm^{-1}$). With increasing salt concentrations, PEO tends to crystallize, however, and this leads to a decrease in the membrane's ionic conductivity [18]. Poly(benzimidazole) (PBI) doped with KOH has been used in alkaline FCs for its high thermal and chemical stability, even though this polymer is not water-soluble [19-21]. Ionic conductivities between $5x10^{-5}$ $S{\cdot}cm^{-1}$ and $1x10^{-1}$ $S{\cdot}cm^{-1}$ were obtained for PBI with KOH at a concentration of 6 M at 70-90ºC [21].

Homogeneous membranes exhibit good electrochemical properties, but their mechanical strength is limited, whereas heterogeneous membranes have a good mechanical strength and a comparatively poor electrochemical performance [3-5,22].

Homogeneous ion exchange membranes can be prepared by:

1) polymerizing or polycondensing monomers, which usually contain a specific functional group capable of forming anionic or cationic exchange groups. AEMs based on the copolymerization of vinyl pyridines and divinyl benzene are best known in the literature for their applications in electrodialysis or desalination [23]. Sata and coworkers [24] developed poly(vinyl pyridinium) membranes, but these membranes are unsuitable for use in alkaline fuel cells (AFCs) because of the instability of pyridinium in alkaline conditions [25];

2) adding anionic or cationic moieties to a preformed solid film. Fluorinated films like poly (fluorinated ethylene propylene) (FEP) [26,27],

poly(tetrafluoroethylene-fluoroethylenepropylene) (PTFE-FEP) [28], and poly(ethylene-co-tetrafluoro ethylene) (ETFE) [29] have been used as AEMs. The reported method for synthesizing ETFE involves irradiating the film with an electron beam, then immersing it in vinyl benzyl chloride solution. The resulting grafted poly(vinyl benzyl chloride) copolymer film is soaked in trimethylamine solution to obtain quaternary ammonium groups. The last step consists of an alkaline exchange process obtained by dipping the membrane into KOH solution [30]. The same method has been used to obtain AEMs from FEP and PTFE-FEP;

3) adding anionic or cationic moieties to a polymer, then dissolving the polymer and casting it into a film [30,31]. Chitosan-based membranes have been used as novel polyelectrolytes in AFCs. These membranes contain the quaternary ammonium groups attached to the chitosan matrix, and exhibit a conductivity that comes close to 10^{-2} $S \cdot cm^{-1}$[32].

Heterogeneous ion exchange membranes can be made by incorporating powdered ion exchange resin in sheets of rubber, poly vinyl chloride (PVC), acrylonitrile copolymers, or some other matrix, and processing the resulting material by means of extrusion or molding [33].

The materials for ion exchange membrane can be further divided into three broad classes:

1) high-molecular-weight membranes based on polymers containing ionic moieties;
2) inorganic membranes; and
3) hybrid membranes composed of organic/inorganic materials [3,34].

The chemical and thermal stability of the membrane depends largely on the nature of the functional group capable of transporting the hydroxyl anions, and partly also on the nature of the backbone. AEM degradation is due to hydroxide ions being excellent nucleophiles, and attacking the bound cationic groups to create a neutral polymer. Examples of functional groups in the '-onium' class of AEMs are shown in Figure 1.2. Among these

different groups, the quaternary ammonium groups are chemically and thermally more stable than the quaternary phosphonium or tertiary sulfonium groups [35,36]. The stability of the backbone is just as important as the stability of the ion exchange sites because the membrane's mechanical properties, and conductivity in particular, can be reduced if it is damaged [37].

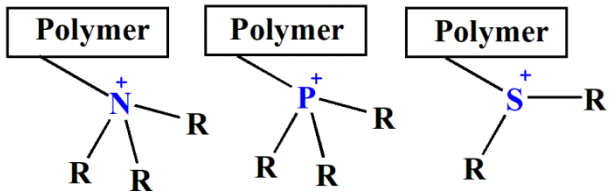

Figure 1.2: "-onium" class AEMs: (from left to right) ammonium, phosphonium and sulfonium

1.3 Fuel cells

Fuel cells are galvanic cells in which the free energy of a chemical reaction is converted directly into electrical energy, promising a highly-efficient power generation with a low environmental impact [12]. The basic physical structure of a FC consists of an electrolyte layer in contact with an anode and a cathode on either side, as first demonstrated by Sir William Grove in 1839. Their first major application came when the NASA used hydrogen-powered FCs to produce electricity and water for the Gemini space missions [38]. FC technology has evolved since then, but the fundamental components in a modern FC remain the same [11-13].

In a typical FC, fuel is fed continuously to the anode (negative electrode) and an oxidant (often oxygen from air) is fed continuously to the cathode (positive electrode). The electrochemical reactions taking place at the electrodes produce an ionic current through the electrolyte, while driving a complementary electric current that performs work on the load [12]. Batteries and FCs are similar in nature: in both devices, the chemical

processes occur at the electrodes, and the flows of electronic and ionic species are separated by an electrolyte. Batteries are energy storage devices, however, in which all the available energy is stored inside the battery itself (or the reductant at least). Batteries will stop generating electrical energy when the chemical reactants have been consumed (i.e., discharged). FCs, on the other hand, are energy conversion devices to which fuel and oxidant are supplied continuously, so they continue to generate power as long as there is a supply of fuel [11,12].

FCs are used in a variety of products, ranging from the very small FCs in portable devices such as mobile phones and laptops, through mobile applications like cars, delivery vehicles, buses, ships and space craft, to heat and power generators in stationary applications in the domestic and industrial sector [11-13,38,39]. They are classified by choice of electrolyte and type of fuel, which determine the electrode reactions and the type of ions that convey the current across the electrolyte. The general categories are: solid oxide fuel cells (SOFCs) [39]; molten carbonate fuel cells (MCFCs) [39]; alkaline fuel cells (AFCs) [39]; phosphoric acid fuel cells (PAFCs) [39]; and proton exchange membrane fuel cells (PEMFCs) [39].

SOFCs work at temperatures around 600-1000^{o}C, high enough to enhance the oxygen reduction kinetics, and this leads to a reduction in the loads of precious catalysts required. It has a solid oxide or ceramic material as the electrolyte for conducting negative oxygen ions from the cathode to the anode to form oxygen gas and generate electrons for the external circuit. SOFCs are among the most efficient FCs, thanks to their high operating temperature, but this high operating temperature also demands longer start-up times [12,13,38,39].

MCFCs are highly efficient too, again because of their high operating temperature. They use a molten lithium or potassium carbonate salt suspended in a porous ceramic matrix as the electrolyte. They were developed for industrial and military applications. The major disadvantage of the MCFC technology concerns the durability of

the electrolyte as the high temperatures involved accelerate its breakdown and corrosion, reducing the FC's life [12,13,38,39].

PAFCs work with liquid phosphoric acid as the electrolyte. The operating temperature is in the range of 150-200^{o}C. The water expelled can be converted into steam for building and water heating purposes (in combined heat and power applications), raising these FCs' energy efficiency by up to 80%. One of the drawbacks of PAFCs, however, lies in the use of an acidic electrolyte, which promotes the corrosion or oxidation of its components. PAFCs are also expensive due to the use of platinum catalysts [12,13,38,39].

PEMFCs work at low temperatures, between 60^{o}C and 120^{o}C, and use a polymeric proton exchange membrane as an electrolyte, platinum as the catalyst, and hydrogen as fuel. They are generally used in transportation systems and portable devices [12,13,38-41].

1.4 Alkaline fuel cells

The initial development of AFCs dates back to 1960, when they were used to provide electrical power on board the Apollo space vehicle. Since then, they have met with considerable success in space-related applications [41]. AFCs are the most efficient of all FC technologies. They use potassium hydroxide (KOH) solution as a liquid electrolyte. Unlike PEMFCs, AFCs convey hydroxide ions from cathode to anode. The oxygen reduction reaction is faster under alkaline conditions than in acidic conditions, and this enables the use of a broad choice of non-noble catalysts (e.g., Ni, metal oxides, spinels), as well as noble metals [42,43]. AFCs are consequently attractive from a cost perspective. On the other hand, carbon dioxide (CO_2) - present in both hydrogen and air - reacts with potassium hydroxide to form potassium carbonate, which precipitates on the electrodes, blocking the surface, and reducing the cells' efficiency. This makes it necessary to use very pure H_2 as fuel [44,45]. The leakage problem due to the use of a liquid electrolyte

also limits the development of AFCs. Alkaline anion exchange membrane fuel cells (AAEMFCs) were recently developed to tackle the problems with liquid electrolytes. AFCs and AAEMFCs have similar functions, the difference lying in that the solution of potassium hydroxide used as the electrolyte is replaced with a polymeric anion exchange membrane. The main types of FC and their characteristics are summarized in Figure 1.3.

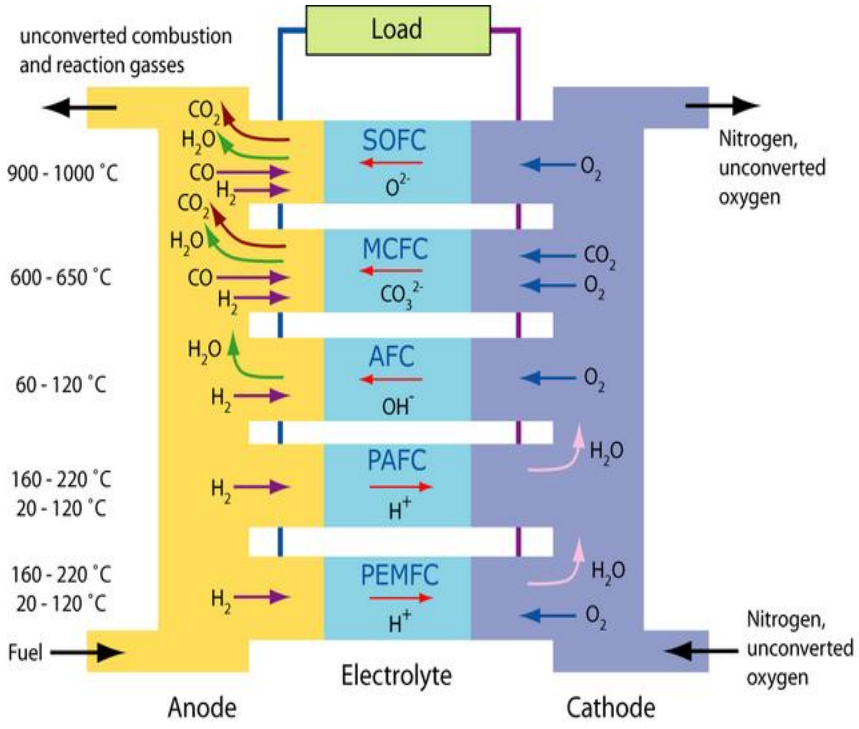

Figure 1.3: Main types of fuel cell and their characteristics

1.5 Filtration

AEMs have attracted a lot of attention for use in filtering applications because they are stable in water and impermeable to positive ions, and they can be tailored to make them selective for specific ions [46]. In filtering applications, AEMs act as barriers between two phases. The membranes filter on the basis of molecular (or particle) size, retaining constituents larger than their pores. Depending on the pore size of the membrane, the

filtering process may be classified as microfiltration, ultrafiltration, nanofiltration, or reverse osmosis [47-50].

1.6 Electrodialysis

Electrodialysis is a process that uses direct current electric power to move ions from one solution to another, giving rise to a concentration of ions in order to retrieve them later [51,52]. This technique is widely used in applications such as recovering acids or bases from industrial wastewater, concentrating or deionizing aqueous electrolyte solutions [53-55], desalinating saltwater to make it suitable for drinking, and purifying the resulting brine for us as salt [50]. Electrodialysis can also be used to separate acidic gases with the aid of a carrier [56,57].

1.7 Batteries

Vanadium redox flow batteries (VRFB) are a type of rechargeable flow battery that exploits vanadium ions in different oxidation states to store chemical potential energy and generate electricity [58]. AEMs can be used in such batteries to separate the cathode and anode solutions, preventing vanadium crossover, and a decline in capacity [59].

1.8 Hydroxide conduction mechanisms in anion exchange membranes

The initial idea of ionic conduction in a polymer electrolyte dates back to the 1970s, when long polyethylene oxide (PEO) chains were thought to wrap around cations. Ion hopping between vacant sites should result in ionic conduction. Although there is a similarity between the cation conduction mechanism and that of conventional solid-state ionic conductors, the findings reported by Berthier et al. (1983) [60] gave the impression that ion conduction in a PEO-based electrolyte was taking place in the amorphous phase. Although the actual mechanism of hydroxyl transport through an AEM is still being debates, more recent literature on proton exchange membranes (PEMs) has clarified the

mechanism behind hydroxyl formation. The transport in PEMs can be described on the grounds of two main mechanisms: proton hopping (or the Grotthuss mechanism), and diffusion (or the vehicle mechanism of water) [61-63].

In proton hopping, a proton (H^+) hops across the membrane, from one hydrolyzed ionic site to another, based on the mechanism proposed by Theodor von Grotthuss in 1804 [64]. The proton formed in the oxidation reaction of hydrogen gas at the anode adheres to water molecules and forms a short-lived hydronium ion. Then another proton from the same hydronium ion hops onto the neighboring water molecule. This mechanism prompts the formation of ionic clusters that swell in the presence of water. That is how the proton percolation mechanism can take effect [61, 64].

In the vehicle mechanism, the hydrated proton is transferred in the form of a hydrated ion by the carrier species spreading through the electrolyte. The protons thus attach themselves to a vehicle such as water and spread through the medium. The rate of this transport process depends on whether there are free volumes in the polymer chains, and also on the rate of diffusion of the vehicle [62-65].

Proton conductivity generally depends on environmental conditions, such as relative humidity, temperature and pressure. Anion conductivity depends on much the same parameters, so some researchers assume that proton and hydroxyl are both carried by similar mechanisms [66]. Hydroxide transport in AEMs is influenced by the Grotthuss (proton hopping) mechanism. Like protons, OH^- exhibits Grotthuss behavior in aqueous solutions, [67-69]. As a result of this mechanism, the excess negative charge for hydroxide is shuttled through a chain of water molecules by means of a series of O-H bond-breaking and bond-forming processes [69]. The vehicle mechanism is just as important as the Grotthuss mechanism in hydroxide ion transport. Surface diffusion is one of the mechanisms by which the hydroxide ion spreads, by hopping between strongly-interacting groups in the polymer chain [70]. Figure 1.4 shows a schematic representation of the Grotthuss and vehicle mechanisms in AEMs.

Convective transport results from a pressure gradient and/or from a species being carried by a net ionic concentration subject to an electrostatic potential gradient [71]. Hydroxyl anions hop over surface site on quaternary ammonium groups present on the membrane, and recognized as being of secondary importance. In this mechanism, the water in the system acts as a permanent dipole, interacting with the fixed charges of the membrane. This strong coordination of water molecules around the ammonium groups makes their interaction with ionic species less likely [71-73].

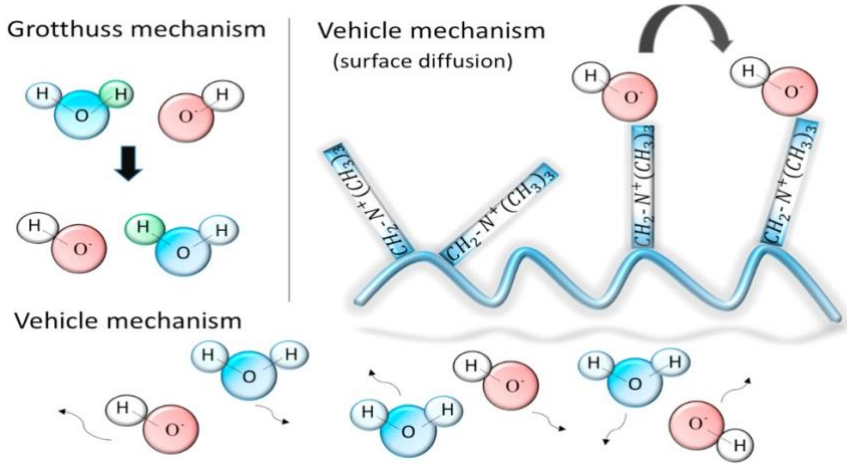

Figure 1.4: Schematic of hydroxide transport mechanisms in AEMs [70]

1.9 Polyketone (PK)

The first study on the copolymerization of ethylene with carbon monoxide was conducted in the 1940s. Dintses [74], and researchers at the Farbenfabriken Bayer [75] demonstrated that harsh conditions (200-250 MPa and 290-310°C) were needed for the free-radical copolymerization of ethylene and carbon monoxide. Following their research, studies were conducted on copolymerization under milder conditions (20 MPa and 200°C) [75-78]. A considerable effort focused on developing catalysts derived from Group VIII transition-metal complexes, and capable of producing linear, perfectly-alternating

copolymers [79,80]. Then Drent and co-workers at Shell went on to develop an alternating PK of carbon monoxide with olefins using a highly-efficient homogeneous palladium catalyst (Figure 1.5) [81].

Aliphatic PK copolymers are semicrystalline materials that crystallize in a planar zig-zag conformation with an orthorhombic unit cell. Two crystalline structures known as α and β have been identified. They have an identical backbone conformation, the only difference being in the chain packing mode: the carbonyl groups are closer together in the α form than in the β form [79,82-84]. PKs are insoluble in common organic solvents, and only dissolve in highly polar and acidic solvents, such as hexafluoroisopropanol and m-cresol. They have a high melting point (250-260^{o}C), which reflects the strong contribution of the polar group resulting from a great regularity in an arrangement of repeating units [85].

One of the most crucial points in the field of AEMs for large-scale production concerns the cost of the membrane, as well as its good thermal stability. The main interest in PKs thus relates to: (a) the cost of the starting materials; (b) their versatility, or modifiability; and (c) their excellent thermal and mechanical properties.

1.10 Polyketone preparation

Carbon monoxide and simple olefins are abundantly available and inexpensive. PK is a polar polymer that has a set of desirable properties, including excellent mechanical strength, and pressure and heat resistance [86], chemical resistance to acids, bases and solvents [87], amenability to chemical modification, great stiffness, impact strength, and stability against electrolytic corrosion [88]. PK synthesis procedures have been improving constantly in terms of selectivity, productivity, environmental impact, and economy [79,85]. The unique properties of PK make it a suitable candidate for use in a broad range of applications in engineering, barrier packaging, fibers, film coatings, adhesives and blends [83,89,90].

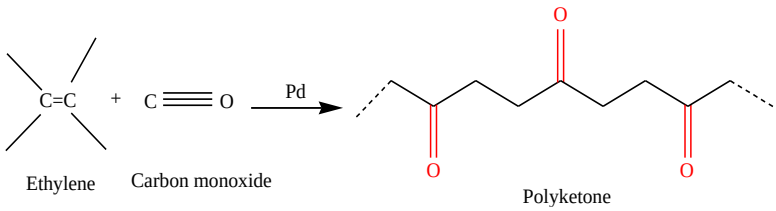

Figure 1.5: Polyketone formation by alternating CO/ethylene copolymerization.

1.11 Polyketone modification

Chemical modification is important in the preparation of functional polymers [91]. Polymer modifications have been used to combine different desirable properties in a new (modified) material [92-94], enhancing its thermal stability, stiffness, flexibility, compatibility, degradability, biological resistance, and/or impact resistance [94].

PKs have polar carbonyl groups as part of their backbone. Typical chemical reactions applied to single ketone molecules could provide a simple means for modifying PKs to extend the portfolio of new materials. Huge industrial and academic interest has led to the generation of a vast number of derivatives. To give an example, there have been reports of ketone groups being converted into: furans [95], pyrroles [96], thiophenes [95], oximes [97,98], cyanohydrins [95], acetals [99], hemiacetals [100], amines [101], α-hydroxy-phosphonic acids [102], methylenes [103], thiols [104] and amides [105], among others (Figure 1.6).

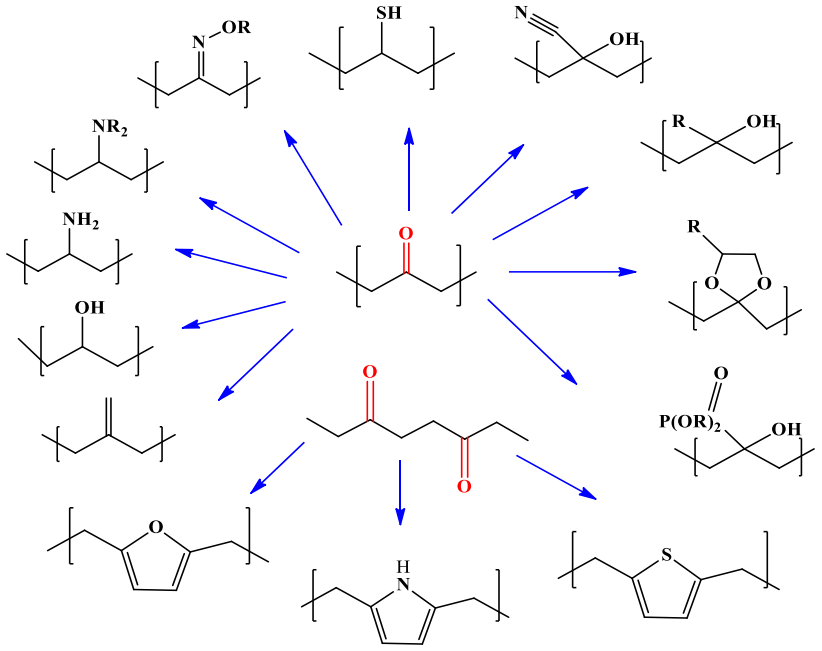

Figure 1.6: Some reported polyketone modifications [96]

The conversion of carbonyl to pyrrole groups (known as the Paal-Knorr reaction) seems to be one of the easiest modification reactions achievable in PKs [106-109]. The Paal-Knorr reaction has aroused a great deal of interest in the world of synthetic chemistry, for the preparation of pyrrole, pyrazoles, and their derivatives, as naturally-occurring organic compounds and intermediates for synthetic pharmaceuticals [109,110].

In a typical Paal-Knorr reaction, the 1,4-dicarbonyl moiety of the PKs reacts with a primary amine function, yielding a pyrrole unit as shown in Figure 1.7. This route consists of a two component/one-pot reaction in the absence of any catalyst or organic solvent, with water as the only by-product, and mild conditions throughout the process. It is a good example of a simple, low-cost, straightforward approach to the preparation of polymeric amines, that is easy to apply on an industrial scale [111-113].

With the conversion of PK into polyamines we have a dual functionality: the N-substituted 2,5-pyrrole-diyl group incorporated in the polymer backbone; and a substituent

with an amino functionality, which can be primary, secondary, or tertiary, and either aliphatic or aromatic [111-116].

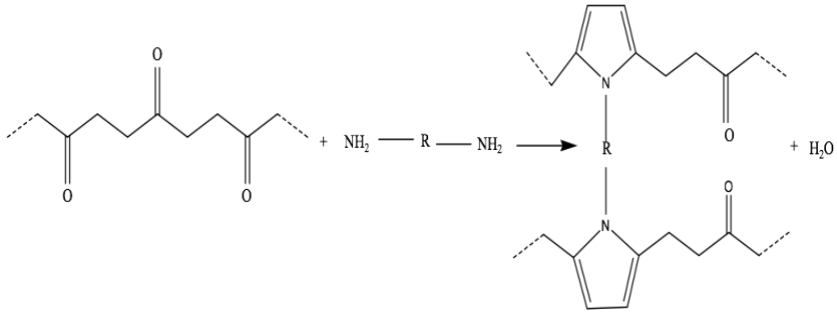

Figure 1.7: Paal-Knorr reaction of polyketone with primary amine

Chapter 2

A Polyketone-based Anion Exchange Membrane for Electrochemical Applications: Synthesis and Characterization

2.1 Introduction

Anion exchange membranes (AEMs) have promising features for the purpose of overcoming some of the problems associated with cation exchange membranes [36, 117-121], and they are already key components of various electrochemical devices. Among their potential applications, electrochemical energy conversion [122], storage systems [123], electrolyzers [124], and even electrodialysis for water desalination [125], are some of the most important and best known.

The selective transport by anionic charge carriers, lower crossover of cationic redox couples, and trouble-free reaction kinetics in AEM energy conversion processes stem mainly from the density and distribution of the positively-charged functional groups, associated with a macromolecular polymer backbone. There has consequently been a growing demand for the development of AEMs that are more selective, with a higher chemical stability and conductivity, and a great deal of work has been done in this area. Good mechanical properties, good dimensional stability, and a high hydroxide conductivity and stability are key properties for an AEM, but efforts to manufacture high-performance AEMs have shown that it is very difficult to maximize all of them at the same time.

The polymer electrolyte membrane is usually made of positively-charged groups fixed to the backbone of the polymer (typically a quaternary ammonium functional group), which enables the transfer of anions such as I^-, Cl^-, Br^- and OH^-. The challenge lies, however, in developing an AEM [126-130] that has not only excellent thermal and

mechanical properties, but also an OH^- ion conductivity comparable with that of H^+ in a proton exchange membrane (PEM). This means that the ion-conducting groups (which are usually quaternary ammonium groups) attached to the main chain of the polymer suffice to achieve a high hydroxide conductivity. Quaternary ammonium ion groups are less dissociated than sulfonic acid ion groups, and hydroxide ions have a lower diffusion coefficient, giving rise to a lower conductivity than that of PEMs. For AEMs to achieve results similar to those obtained with PEMs, a higher concentration of OH^- is required.

Various types of membrane have consequently been developed, using polymerization [131], chemical grafting [27], radiation-induced grafting, and copolymerization [132,133]. Another suitable way to obtain AEMs is by inducing chemical changes in a polymer [32]. The last of these solutions gives rise to a structure tailored so as to improve certain properties for a specific application. This has to be achieved without negatively affecting other characteristics of the pristine polymer. The main issue with this method is how to introduce the functional group, and chloromethyl methyl ether is often used in this approach [134].

The aim of the present study was to prepare a new polyamine-based AEM. Polyketone (PK) was obtained from the reaction of ethylene with carbon monoxide in the presence of a palladium catalyst [135]. This procedure was first described in 1941 [75], and PK production subsequently became popular in academic and industrial circles, partly thanks to the low cost and availability of ethylene and carbon monoxide [79,81]. The costs of polymerizing PK are much lower than for the quaternary ammonium-functionalized radiation-grafted poly(ethylene-co-tetrafluoro ethylene) (ETFE) [26]. The production of such membranes on a large scale is expensive and physically impracticable due to the use of electron beam technology for irradiation. On the other hand, this polar polymer has a set of desirable properties, including an excellent mechanical strength, pressure and heat resistance [86], chemical resistance to acids, bases and solvents [87], high stiffness and impact resistance, and stability against electrolytic corrosion [88]. Another reason why PK is so appealing is because its functional properties can be modulated by changing the carbonyls into a great variety of other functional groups [136-139]. In the present study,

the reaction of 1,4-dicarbonyl moieties of PK with primary amine led to the formation of N-substituted pyrrole units which is known as Paal-Knorr condensation. This occurred under mild reaction conditions, without using any solvents. Chemical modification is a simple way to create a new polymer with a stable pyrrole ring along the backbone, and a reactive pendant amino functional group [91,111,140], which allows for the introduction of quaternary ammonium cation groups with iodomethane, followed by OH^- ion exchange processes. The composition of the membrane and starting materials was characterized using elemental analysis. The chemical structure of the modified PK was studied using NMR, UV-Vis, and FTIR analyses. The thermal, structural, and morphological characteristics of the prepared membrane were assessed using thermogravimetric analysis, differential scanning calorimetry, X-ray diffraction, and scanning electron microscopy. The membrane's conductivity was measured after appropriate ion exchange treatments. This work serves as a proof of concept that amination of an inexpensive polymer, PK, gives rise to a new type of membrane family with an exceptional thermal and chemical stability, and potentially suitable for use in a variety of applications, such as electrodialysis for water desalination [125], alkaline water electrolysis [141], and vanadium redox flow batteries [142].

2.2 Experimental

2.2.1 Reagents

1,2-diaminopropane (99%), 1,1,1,3,3,3,-hexafluoroisopropanol (99%), 1,3-bis (diphenylphosphino) propane [dppp] (97%), diethyl ether (99.8%), methanol (99.8%), petroleum ether (95%), and trimethylamine (99%) were purchased from Sigma-Aldrich. Potassium hydroxide was obtained from VWR. p-toluene-sulfonic acid [p-TsOH] (99%) was purchased from ACROS. Ammonium hydroxide (28-30%) was obtained from JT Baker, and iodomethane (99%) was purchased from ABCR GmbH. Carbon monoxide (N37) (99.97%) and ethylene (N25) (99.5%) were supplied by Air Liquide. Bi-distilled water was used in all procedures. All reagents and solvents were used as received.

2.2.2 Polyketone synthesis

PK was synthesized at the Department of Chemical Sciences at the University of Padova, thanks to the cooperation of Prof. Gianni Cavinato. The reaction was conducted in a 250 mL Hastelloy C stainless steel autoclave equipped with a self-aspirating turbine using a 150 mL Pyrex glass beaker to avoid contamination from metallic species. The instrumental setup for PK synthesis is shown in Figure 2.1. The [Pd(p-TSO)(H_2O)(DPPP)] p-TSO catalyst was prepared as described in the literature [143,144]. Ten mg of catalyst [Pd(p-TSO)(H_2O)(DPPP)] p-TSO (0.011 mmol), 20 mg of p-TsOH (0.10 mmol), 0.3 mL of deionized water, and 80 mL of methanol were mixed in a 150 mL Pyrex glass beaker, then placed in the autoclave. The autoclave was sealed and the contents were degassed by flushing with a 1/1 mixture of CO/C_2H_4 at 0.5 MPa, followed by depressurizing to atmospheric pressure; this was done three times. The autoclave was then brought to 90°C before ethylene (pressurized to 2.25 MPa) was added, followed by carbon monoxide (2.25 MPa). The pressure in the reactor was maintained at 4.5 MPa throughout the reaction by supplementing the reactor from a CO/C_2H_4 reservoir. The reaction ran for 1 hour at a stirring rate of 700 rpm. After cooling to room temperature, a solid product was collected, filtered and washed three times with methanol and petroleum ether. The resulting white powder PK was dried in a vacuum for approximately 1 hour before it was placed in an oven at 70°C for 5 hours.

Figure 2.1: The instrumental setup for polyketone synthesis

2.2.3 Polyketone amination

In a 100 mL round-bottomed flask equipped with a reflux condenser (Figure 2.2), 1,2-diaminopropane (1.53 mL, 0.018 mol) and triethylamine (6.97 mL, 0.05 mol) were added to a suspension of 1.0 g of PK in 50 mL of methanol. The reaction mixture was brought to reflux and then left for 25 days at 100°C. The product was then filtered and washed with methanol and diethyl ether to remove the residual solvent and amine. Then it was dried in a vacuum for 5 hours at 10^{-2} mbar and ambient temperature. The final product (PK-PDAP) was a light brown powder. The polyamine thus prepared proved to be insoluble in water and common organic solvents, except for 1,1,1,3,3,3-hexafluoroisopropanol (HFIP).

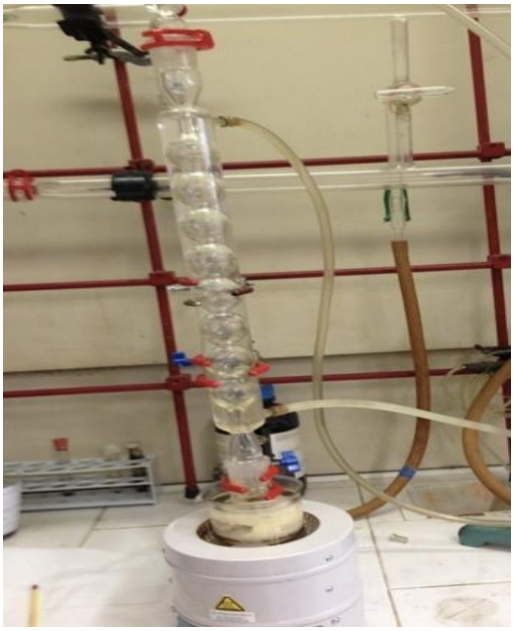

Figure 2.2: The instrumental setup for polyketone amination

2.2.4 Membrane casting

After adding 0.3 g of PK-PDAP to 7 mL of HFIP and stirring for 30 minutes at 40°C, 120 mL of ammonium hydroxide vapor was bubbled directly into the solution using a syringe. The solution was homogenized in an ultrasonic bath (TRANSSONIC 46O/H) for 45 minutes at 40°C, and stirred overnight at 40°C. The solution was then poured onto a Petri dish. A homogeneous membrane (PK- PDAPm) was obtained, as shown in Figure 2.3, which was dried in a vacuum at 40°C for 24 hours. The average thickness of the membrane was about 100 μm (thicker membranes can be prepared in the same way, simply by increasing the amount of polyamine).

Figure 2.3: Photo of the polyamine membrane

2.2.5 Methylation

The PK-PDAPm was immersed in an excess amount of iodomethane at room temperature for 24 hours under a fume hood. The methylated membrane was removed from the remaining iodomethane, then washed thoroughly with deionized water and dried at 40°C in a vacuum for 24 hours to obtain PK-PDAPm(I).

2.2.6 Anion exchange

Anion exchange was induced under a nitrogen atmosphere by soaking the methylated membrane (PK-PDAPm(I)) in a solution of 1 M KOH for 1 hour; this step was repeated three times, using a fresh KOH solution each time. The PK-PDAPm(OH) membrane was then washed with distilled water and stored under a nitrogen atmosphere. To assess its stability, the PK-PDAPm(OH) was immersed in a 2 M NaOH solution and kept at 80°C, taking samples of membrane after 24, 40 and 64 hours, and analyzing them using HR-TGA.

2.2.7 Water uptake

The water content of the PK-PDAPm(I) and PK-PDAPm(OH) membranes was ascertained by measuring the change in the weight of the membrane before and after its immersion in distilled water. The membrane samples were first washed with distilled water, then immersed in distilled water for 24 hours. They were then removed from the water and the humidified membranes were weighed immediately after blotting to remove free surface water. They were then dried at 40°C for 6 hours and weighed again. The water content was calculated based on the following formula:

$$WU = \left[\left(M_{wet} - M_{dry}\right)\right]/M_{dry}\ ]\ X\ 100\% \tag{2.1}$$

where M_{wet} is the mass of the wet membrane, and M_{dry} is the mass of the dry membrane. The water uptake was 34% for the PK- PDAPm(I), and 38% for the PK-PDAPm(OH).

2.2.8 Ion exchange capacity

The PK-PDAPm(OH) membrane was washed several times with distilled water to remove any traces of KOH solution, then immersed in 30 mL of 0.01 M HCl solution for 24 hours at room temperature. The solution was then titrated with 0.01 M NaOH solution, using phenolphthalein as an indicator. The ion exchange capacity (IEC) was 1.11 mmol/g based on the following equation:

$$IEC = \left[\left(V_{0,NaOH} - V_{NaOH}\right)C\right]/m_{dry} \tag{2.2}$$

where $V_{0,NaOH}$ and V_{NaOH} are the volumes of NaOH solution consumed for back titration without and with the membrane, respectively, C is the concentration of NaOH solution, and m_{dry} is the mass of the dry membrane.

2.2.9 Instrumental methods

The elemental analysis was done with a LECO-CHN628 instrument (Michigan, USA), which uses a combustion technique. The samples were ground and homogenized. About 0.1 g of sample material was accurately weighed, encapsulated, and placed in the instrument's furnace. The sample was burned in an excess of oxygen, and several traps collected the products of combustion (carbon dioxide, water, and nitric oxide). The masses of these products of combustion were used to calculate the composition of the sample. The iodine content of the PK-PDAPm(OH) was ascertained using inductively-coupled plasma atomic emission spectroscopy (ICP-OES), with an ICP SPECTRO Arcos and an EndOnPlasma torch. The analyses were run using the emission lines of 178.276 nm for λ(I).

Fourier transform infrared spectroscopy (FTIR) was conducted using a Nicolet FT-IR Nexus spectrometer, averaging 1000 scans with a resolution of 4 cm^{-1} in the wavenumber range between 400 and 4000 cm^{-1}.

NMR spectroscopy was done on a Bruker 400WB spectrometer (Billerica, Massachusetts, USA) at room temperature under the following conditions: ^{1}H NMR with a frequency of 400.13 MHz, a π/2 pulse of 10 μs, and a delay of 10 s, obtaining 128 scans using 1,1,1,3,3,3-hexafluoro-2-propanol-d2 as the solvent, and a BBO 5 mm liquid probe; Cross-Polarization - Magic Angle Spinning (CP/MAS) ^{13}C NMR with a frequency of 100.49 MHz, a π/2 pulse of 3.5 μs, a contact time of 2 ms, and a decoupling pulse of 6.2 μs, for 3000 scans. Samples were spun at 11 kHz in a 4 mm zirconia rotor, double-channel 4 mm CP/MAS probe. Adamantane was used as a secondary external standard for the chemical shift.

UV-Vis measurements were obtained using a Perkin Elmer spectrometer (Lambda 40). All absorption spectra were collected under identical conditions, i.e. scanning from 200 to 600 nm at a rate of 120 nm/min.

Differential scanning calorimetry (DSC) was done to obtain the thermal properties, with a DSC92 SETARAM (Caluire, France) equipped with a liquid N_2 cooling

system. The data were collected in the temperature range between -100ºC and 400ºC, with a heating rate of 10ºC min^{-1}. The measurements were obtained by loading a weighed amount of sample inside a closed aluminum pan. Further DSC analysis was done on membranes, in both the iodide and the hydroxide forms to get more detailed thermal properties within the working temperature. This analysis was done with a DSC 2920 Differential Scanning Calorimeter (TA Instruments) equipped with the LNCA low-temperature attachment operating under a helium flux of 30 cm^3/min. Data were collected in the temperature range from -150 ºC to 150ºC, at a heating rate of 3ºC/min. The measurements were obtained by loading 3 mg of membrane sample in a watertight aluminium pan.

High-resolution thermogravimetric analysis (HR-TGA) was conducted with a high-resolution modulated TGA 2950 (TA Instruments) thermobalance, and a working N_2 flux of 100 cm^3/min. Thermogravimetric measurements were collected from room temperature up to 850ºC, using open platinum pans. The heating rate was adjusted dynamically over the ramp, based on the derivative of the weight change, from 50 to 0.001ºC/min. Sensitivity was set for changes in weight from 0.1% to 2% per minute. The balance has a resolution of 1 mg.

X-ray diffraction (XRD) measurements were obtained with an X'TRA diffractometer (Thermo ARL, Ècublens, Switzerland), based on conventional powder geometry, and with a solid-state Si-Li detector using Cu Kα radiation. The data were collected at a diffraction angle 2θ ranging from 1º to 60º, and at a scanning rate of 0.0258 s^{-1}. For scanning electron microscopy (SEM), a Philips SEMTMP (Eindhoven, Netherlands) XL30 was used, with magnifications of 2000x and 5000x, and the microanalysis was conducted with a Falcon-EDAX, with a carbon-uranium detector connected to the microscope. The membranes were quenched in liquid nitrogen and manually fractured immediately after removal from the quenching liquid. The fractured surface was coated with gold, and the fractured surfaces and cross-sections of the membrane were analyzed. The samples were prepared by putting a fine powder of PK and PK-PDAP on the smooth surface of the sample holder and coating it with gold.

Conductivity was measured using broadband electrical spectroscopy (BES) in the range of frequencies from 30 mHz to 10 MHz using a Novocontrol Alpha-A Analyzer, over a range of temperatures from -100 to 120°C. The temperature was controlled using a home-made cryostat operating with a N_2 gas jet heating and cooling system. The membranes were sandwiched between two circular platinum electrodes inside a sealed cylindrical cell, which was placed inside a glovebox filled with nitrogen.

2.2.10 Quantum mechanical calculations

The geometries and infrared spectra of the models for PK and PK-PDAP were ascertained using the methods of density functional theory (DFT), based on an all-electron code, using the double numerical plus polarization basis set and gradient-correlated (GCA) BLYP functions of the DMol3 program (San Diego, California, USA) [145]. The internal modes were identified by animating the atomic motion of each mode calculated, with the aid of the features available in the Materials Studio package (San Diego, California, USA).

2.3 Results and discussion

2.3.1 Elemental analyses

Table 2.1 shows the chemical composition of all the samples, as emerged from elemental analysis (CHNS) and ICP-OES (iodine). The composition of the PK synthesized in the present study is consistent with the theoretically expected stoichiometry. The negligible differences in the amounts of C, H and O are due to the presence of traces of water. PK amination at 374 K and 1 Pa was obtained under different reaction times, after 10 (PK-PDAP-10), 15 (PKPDAP-15), and 25 days (PK-PDAP-25). The results indicate that the amination increased with longer reaction times, meaning that the reaction time is an essential factor influencing the amount of conversion. The amination process was expected to take place as a result of two adjacent carbonyl groups of the polymeric chain

reacting with amine to form a pyrrole ring. The reaction mechanism of 1,4-dicarbonyl with 1,2-diaminopropane is shown in Figure 2.4.

In the absence of any catalyst, this type of (Paal-Knorr) reaction can occur to a small extent with much longer reaction times, producing some pyrrole units. PK amination gave rise to a product (PK-PDAP) with about 5.3 wt% of nitrogen. This N content is quite low, and suggests that a fraction of the ketone groups remained unreacted in the functionalized PK (PK-PDAP). Judging from the elemental analysis, the structure of the PK-PDAP could be as hypothesized in Figure 2.5, with x/y about 5. In the light of the experimental results (discussed in the next section), and the theoretical chemical formula derived from the elemental analysis, there is also a six-atom ring. This type of N ring can form as a result of the mechanism shown in Figure 2.6. The experimental evidence discussed below also suggests that amination is hindered by some degree of crosslinking. The six-atom ring can account for crosslinking being favored by long reaction times and high temperatures, and possibly following the mechanism shown in Figure 2.6. Of course, the occurrence of crosslinking gives rise to a stiffer structure. The percentage of nitrogen remained more or less the same in the polyamine membranes (PK-PDAPm), suggesting that the preparation conditions prevented any decomposition or loss of amine groups. The low N content would also account for the low degree of PK-PDAPm(I) and PK-PDAPm(OH) methylation. In fact, only 10% of the N contained in the material was functionalized as quaternary groups (see Table 2.1). These anionic membranes consequently have a low concentration of mobile anion, even though the experimental IEC of PK-PDAPm(OH), as measured by back titration, was 1.11 mmol/g, and therefore comparable with that of commercially-available AEMs (Neosepta AMX; ASTOM Corp., Tokyo, Japan) [146,147].

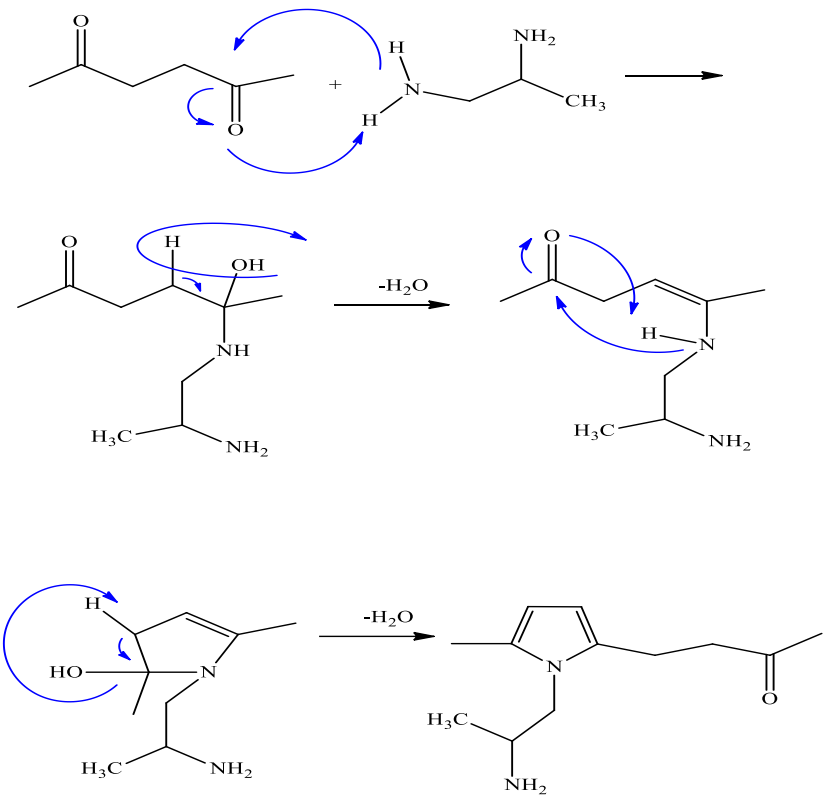

Figure 2.4: Reaction mechanism of 1,4-dicarbonyl with 1,2-diaminopropane (Paal-Knorr reaction)

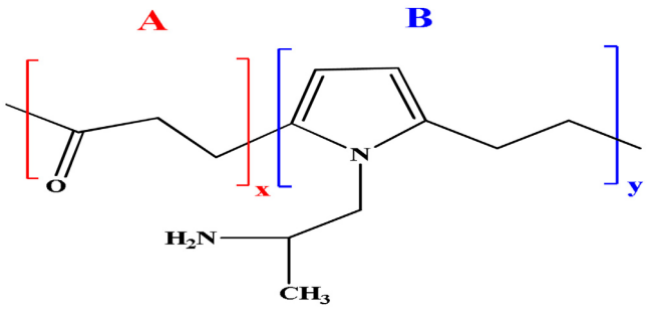

Figure 2.5: Chemical structure of polyketone (A), and product of the reaction of PK with 1,2-diaminopropane (B)

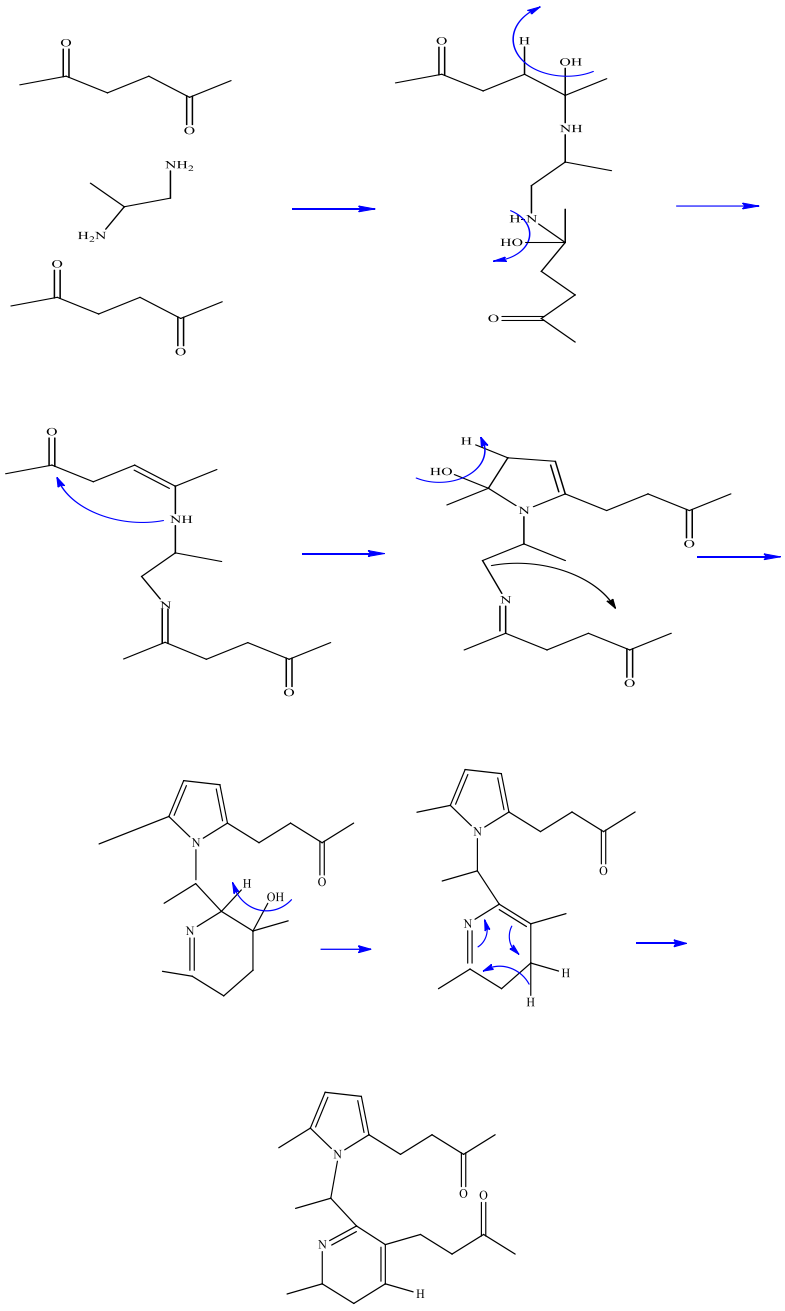

Figure 2.6: Reaction mechanism for the 1,4-dicarbonyl group with 1,2-diaminopropane and the formation of dihydropyridine.

Table 2.1: Composition of the samples.

Sample	**%C***	**%H***	**%O#**	**%N***	**%I**	**nC**	**nH**	**nO**	**nN**	**nI**	**nH/nC**	**nO/nC**	**nI/nN**
Theoretical PK	64.27	7.19	28.54	/	/	3.00	4.00	1.00	/	/	1.333	0.333	/
PK	61.83	7.17	31.00	/	/	5.15	7.11	1.94	/	/	1.382	0.376	/
PK-PDAP-10	64.85	7.62	24.01	3.49		5.40	7.55	1.50	/	/	1.398	0.277	/
PK-PDAP-15	63.58	7.22	25.21	3.99		5.30	7.21	1.57	/	/	1.360	0.296	/
PK-PDAP-25	62.00	7.34	25.32	5.34	/	5.16	7.28	1.58	0.381	/	1.411	0.307	/
PK-PDAPm	60.57	8.07	25.55	5.81	/	5.04	8.01	1.60	0.415	/	1.588	0.317	/
PK-PDAPm(I)	62.01	7.54	19.41	5.96	5.08	5.16	7.48	1.21	0.426	0.04	1.449	0.235	0.094
PK-PDAPm(OH)	60.73	7.92	25.63	5.72	/	5.06	7.86	1.60	0.408		1.554	0.0317	/

*ascertained from elemental analyses and § ICP measurements: # %O is obtained as the difference with respect to 100. PK-PDAP-10, -15, and -25 refer to different reaction times, i.e. 10, 15, and 25 days, respectively. PK-PDAPm is the membrane obtained from PK-PDAP-25.

2.3.2 FTIR studies

FTIR spectra were obtained for PK, PK-PDAP, PK-PDAPm, PK- PDAPm(I) and PK-PDAPm(OH), as shown in Figure 2.7 (a and b). Peaks were assigned using the correlative method, and are shown in Table 2.2. The vibration spectra of PK gave rise to a strong peak, observed at 1688 cm^{-1}, corresponding to the stretching vibration frequency of the carbonyl (C=O) group [144,148,149]. The various modes (stretching, bending, wagging, and rocking) attributed to CH_2 are apparent at 1405, 1331, 1258,1055, 831, 810 and 666 cm^{-1} [144,148-152]. Bands at 591, 543 and 466 cm^{-1} correspond to the vibration of (CC=O) along the PK chain and the (CCC) polymer chain [144,150-152]. The bending vibration of CH_3, due to the PK terminal group, is detectable at 1351 and 1427 cm^{-1} [150,153]. The peaks at 2911 and 2947 cm^{-1} in Figure 2.7(a) correspond respectively to the symmetrical and asymmetrical vibration of CH_2 [144,148-150,152,153]. The peak at 3390 cm^{-1} relates to the stretching of OH as a result of keto-enol tautomerism [114,143,150,152]. This is consistent with the presence of the shoulder at 1662 cm^{-1}, attributable to the stretching vibration of C=C. The modification of PK by amine leads to a lower intensity of the carbonyl (C=O) group at 1689 cm^{-1}, while new peaks occur: (a) a broad band at 754 cm^{-1}, corresponding to the out-of-plane vibration of C-C in the pyrrole ring; (b) a broad peak at 1567 cm^{-1}, which corresponds to the C=C stretching vibration [154] and is attributable to the presence of pyrrole; (c) a peak at 919 cm^{-1}, due to the out-of-plane bending vibration (=C-H) in the ring [137,148,149,151]; and (d) two shoulders at 1296 and 1076 cm^{-1}, attributed to the C-N stretching vibration of the rings [153]. This analysis led us to conclude that the reaction of 1,2-diaminopropane with PK leads to the formation of an N-substituted pyrrole ring along a chain containing carbonyl groups.

In PK-PDAPm, the main PK-PDAP peaks remain unchanged, but new features emerge as an effect of the molecular rearrangement and crosslinking occurring during the membrane's preparation as shown in Figure 2.8. These novel features include: (a) a new peak at 726 $cm^{-1,}$ due to CH_2 bending of the long-chain band [153]; (b) new peaks at 1173 and 1217 $cm^{-1,}$ corresponding to the C-N stretching vibration mode [152,153]; and (c) a

shift in the (=C-H) out-of-plane bending vibration from 919 cm^{-1} to a higher wavenumber (954 cm^{-1}). The formation of a six-atom ring (Figure 2.8) can account for the NMR results, as discussed in the next section, in accordance with the proposed mechanism, shown in Figure 2.6. A small amount of six-atom ring may be formed during the long reaction time at high temperatures, promoting not only crosslinking between two PK chains, but also other rearrangements, even in the absence of a catalyst.

In the PK-PDAPm(I) spectra, where a new carbon-amine bond has formed as a result of the amine attacking the electrophilic carbon of CH_3I due to the methylation reaction, the C-N stretching vibration gives rise to a new peak at 684 cm^{-1}, and to two weak shoulders at 1095 and 1291 cm^{-1} [152,153]. Some other new peaks are apparent in the PK-PDAPm(I) spectra, including: (a) peaks at 890 and 970 cm^{-1}, due to the (=C-H) out-of-plane bending vibration in the ring; and (b) a (C=C) shift of the aromatic ring (1567 cm^{-1}) to a higher wavenumber (1590 cm^{-1}). The IR spectra of PK-PDAPm(OH) show that the peaks due to the C-N stretching vibration at 890 and 1095 cm^{-1} in the PK-PDAPm(I) spectra shift to 917 and 1089 cm^{-1}, and this accounts for the anion exchange processes. Details of the assignment of the spectra for the materials proposed here are summarized in Table 2.2.

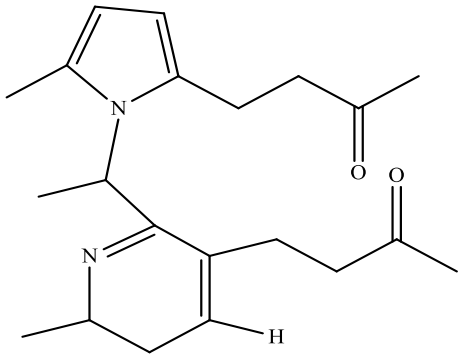

Figure 2.8: Rearrangement of the 1,4-dicarbonyl group with 1,2-diaminopropane.

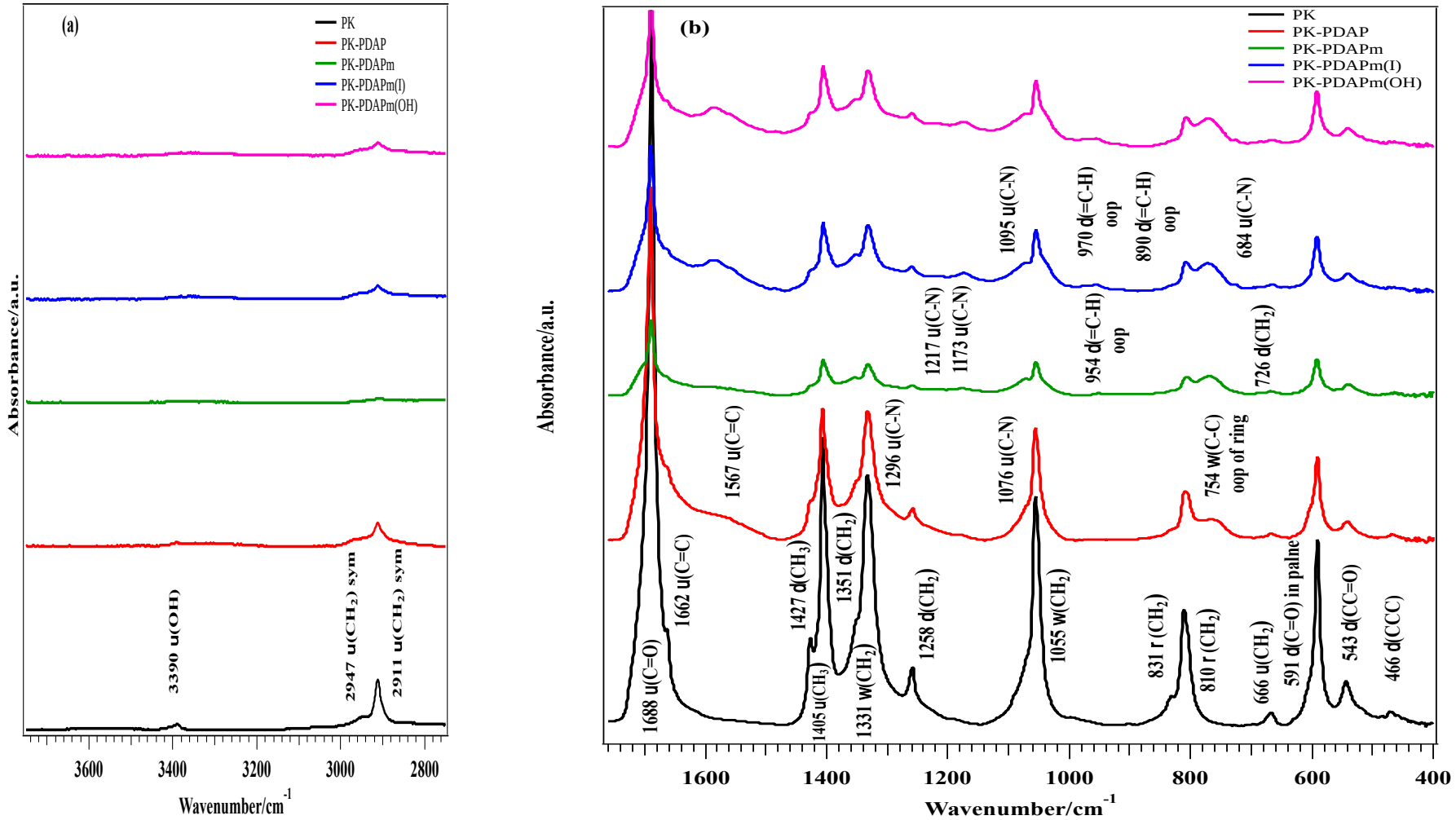

Figure 2.7: IR spectra of pristine PK, PK-PDAP, PK-PDAPm, PK-PDAPm(I) and PKPDAPm(OH): (a) in the range of 3700-2750 cm^{-1}; and (b) in the range of 1750-400 cm^{-1} (υ: stretching; δ: bending; *w*: wagging; *p*: rocking; *b*: broad; *oop*: out-of- plane; *asym*: asymmetric mode; *sym*: symmetric mode).

Table 2.2: FTIR peaks for pristine PK, PK-PDAP, PK-PDAPm, PK-PDAPm(I), and PKPDAPm(OH). Assignments were made correlatively.

Wavenumber (cm^{-1}) & intensity					**Band assignments**	**References**
PK	**PK-PDAP**	**PK-PDAPm**	**PK-PDAPm(I)**	**PK-PDAPm(OH)**		
466 (*vw*)	466 (*vw*)	462 (*vw*)	463 (*vw*)	462 (*vw*)	δ(CCC)	[144,152]
543 (*vw*)	541(*vw*)	539 (*vw*)	539 (*vw*)	538 (*vw*)	δ (CC=O)	[144,150,152]
591 (*w*)	590 (*w*)	592 (*vw*)	592 (*vw*)	592 (*vw*)	δ(C=O) in-plane	[144,150,152]
666 (*vw*)	665 (*vw*)	663 (*vw*)	665 (*vw*)	668 (*vw*)	*v* (CH_2)	[150]
			684 (*vw*)	684 (*vw*)	*v* (C-N)	[153]
		726 (*vw*)	726 (*vw*)	725 (*vw*)	δ (CH_2) long-chain band	[153]
	754 (*vw*)	770 (*vw*)	774 (*vw*)	768 (*vw*)	(C-C) oop of ring	[140,152,154]
810 (*vw*)	808 (*vw*)	808 (*vw*)	807 (*vw*)	807 (*vw*)	} *p* (CH_2)	[144,150,151]
831 (*sh,vw*)	831(*sh,vw*)	833 (*sh,vw*)	836 (*sh,vw*)	830 (*sh,vw*)		
	919 (*vw*)		890 (*vw*)	917 (*vw*)	} δ (=C-H) oop	[153]
		954 (*vw*)	954 (*vw*)	952 (*vw*)		
			970 (*vw*)	970 (*vw*)		
1055 (*w*)	1056 (*w*)	1054 (*vw*)	1054 (*vw*)	1054 (*vw*)	w (CH_2)	[144]
	1076 (*sh,vw*)	1072 (*sh,vw*)	1072 (*sh,vw*)	1070 (*sh,vw*)	*v* (C-N)	[152,153]
			1095 (*sh,vw*)	1089(*vw*)	*v* (C-N)	[152,153]

Wavenumber (cm^{-1}) & intensity					Band assignments	References
PK	**PK-PDAP**	**PK-PDAPm**	**PK-PDAPm(I)**	**PK-PDAPm(OH)**		
		1173 (*vw*)	1174 (*vw*)	1175 (*vw*)	*v* (C-N)	[152,153]
		1217(*vw*)	1213 (*vw*)	1216 (*vw*)	*v* (C-N)	[152,153]
1258 (*vw*)	1259 (*vw*)	1258 (*vw*)	1258 (*vw*)	1258 (*vw*)	δ (CH_2)	[144,148,149,151]
	1296 (*sh,vw*)		1282 (*sh,vw*)	1291 (*sh,vw*)	*v* (C-N)	[152,153]
1331 (*w*)	1330 (*w*)	1330 (*v*)	1331(*vw*)	1331(*vw*)	*w* (CH_2)	[148-150]
1351 (*sh,vw*)	1353 (*sh,vw*)	1351(*sh,vw*)	1352(*sh,vw*)	1351(*sh,vw*)	δ(CH_3) *sym*	[153]
1405 (*w*)	1405 (*w*)	1405 (*vw*)	1405 (*vw*)	1405 (*vw*)	*v* (CH_2)	[148-150]
1427 (*sh,vw*)	1427(*sh,vw*)	1426 (*sh,vw*)	1426 (*sh,vw*)	1424 (*sh,vw*)	δ(CH_3)	[150]
	1567 (*b,vw*)	1557 (*vw*)	1558 (*vw*)	1559 (*vw*)	} *v* (C=C) of ring	[154]
			1590 (*vw*)	1590 (*vw*)		
1662 (*sh,vw*)	1662 (*sh,vw*)	1663 (*sh,vw*)	1662 (*sh,vw*)	1662 (*sh,vw*)	*v* (C=C)	[144,152]
1688 (*vs*)	1689 (*m*)	1689 (*vw*)	1689 (*w*)	1689 (*vw*)	*v* (C=O)	[144-149]
2911(*vw*)	2912 (*vw*)	2910 (*vw*)	2910 (*vw*)	2908 (*vw*)	*v* (CH_2) *sym*	[144,150,152]
2947 (*sh,vw*)	2966 (*sh,vw*)	2951 (*sh,vw*)	2951 (*sh,vw*)	2946 (*sh,vw*)	*v* (CH_2) *asym*	[144,152,153]
3390 (*vw*)	3386 (*vw*)	3360 (*vw*)	3387 (*vw*)	3381(*vw*)	*v*(OH)	[114,144,150,152]

Relative intensities are shown in brackets: *vs*: very strong; *s*: strong; *m*: moderate; *w*: weak; *vw*: very weak; *sh*: shoulder. *v*: stretching; δ: bending; *w*: wagging; *p*: rocking; b: broad; oop: out-of-plane; *asym:* asymmetric mode*; sym:* symmetric mode.

2.3.3. NMR

An NMR investigation helped to shed light on some of the features of the chemical structures of all the products, and particularly of the membrane, which underwent more changes than PK and PK-PDAP during its preparation, as discussed earlier. The chemical shift assignments for the CP/MAS ^{13}C NMR [Figure 2.9(a)] and ^{1}H NMR spectra [Figure 2.9(b)] recorded for PK-PDAP are listed in Tables 2.3 and 2.4.

The chemical shifts assigned in the CP/MAS ^{13}C NMR spectrum of the membrane show two main signals attributable to the PK backbone, together with lesser, broad peaks in the aromatic and heteroaromatic region that would support a partial amination with the formation of the structure in Figure 2.8. In more detail, the ^{13}C resonances are grouped into three sets of signals: carbonyl carbons resonating at a low field (around 209 and 202 ppm), unsaturated carbons (of pyrrole or pyridine) in the range from 108 to 133 ppm, and aliphatic carbons from 18 to 35 ppm. The splitting of the two main resonances, at 210 and 35 ppm, points to the existence of heterogeneous chain packing.

Table 2.3: ^{13}C NMR chemical shift assignments.

δ (ppm)	**Assignment**	**Description**
209.9	>C=O	Sharp
201.6	>C=O	Broad
132.7	C-N (in pyrrole)	Broad
107.6	HC (in pyrrole)	Broad
46.2	HN-CH_2-	Broad
35.1	-CH_2-	Sharp
30.2	-CH_2-	Broad
17.9	-CH_3-	Broad

The ^{1}H NMR spectrum in solution [Figure 2.9(b)] shows different signals in the absorption region of the groups of aliphatic protons, CH_3 and CH_2 (from 3.2 to 0.5 ppm). The narrow peak around 2.7 ppm is due to the hexafluoro-2-isopropanol used as a solvent. In the downfield region, between 6 and 8.5 ppm, several signals can be assigned to the presence of rings of pyrrole (6.5 and 7 ppm) and 1,4-dihydropyridine. In particular, the resonance structures of the dihydropyridine enable us to account for the presence of a chemical shift at around 8.4 ppm [155,156]. The ^{1}H NMR spectrum of the membrane shows no specific changes vis-à-vis the PK-PDAP spectrum.

Table 2.4: ^{1}H NMR chemical shift assignments.

δ (ppm)	**Assignment**
7.9-8.4	N=CH=
6.5-7.3	CH pyrrole
4.7	Pyrrole-CH-CH_3 pyridine
1.2-3.9	Aliphatic protons

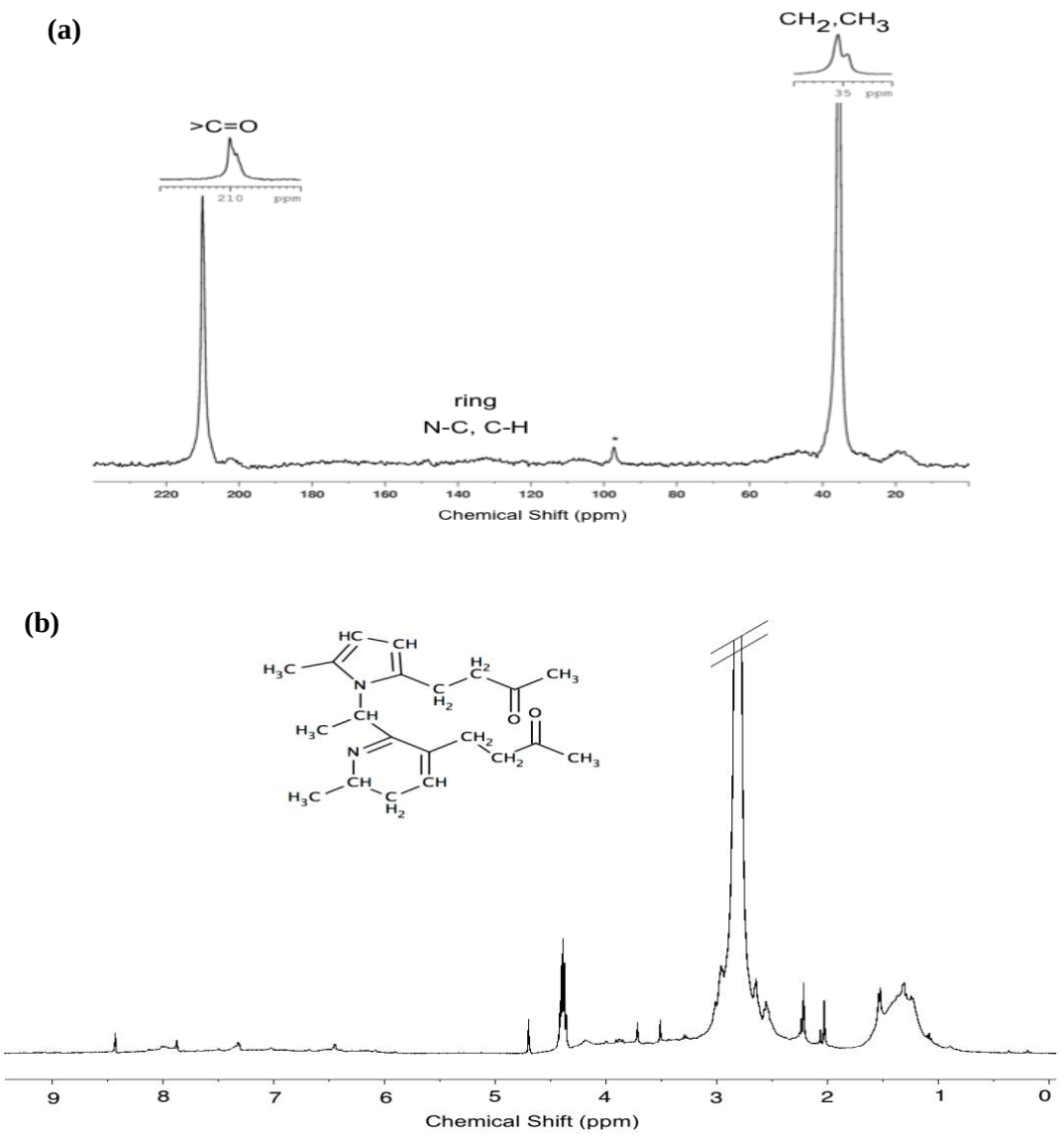

Figure 2.9: (a) CP/MAS ^{13}C NMR spectrum of PK-PDAP; (b) ^{1}H NMR spectrum of PK-PDAP (// indicates the solvent peak).

2.3.4. UV-Vis spectroscopy

UV-Vis spectroscopy was used to study structural and electronic changes. The absorption spectrum was recorded between 300 and 600 nm from PK-PDAP in HFIP solvent. The DFT calculation was used to ascertain the low-lying excited states of PK-PDAP, and the results were compared with the experimentally measured wavelength, as shown in Tables 2.5, 2.6 and 2.7. This electronic absorption corresponds to the transition from the ground to the first excited state, and is mainly described by one electron excitation from the highest occupied molecular orbital (HOMO) to the lowest unoccupied molecular orbital (LUMO). Figure 2.10(a) shows that UV-Vis absorption of the HFIP solvent occurs mainly at 230 and 276 nm, and no absorption is apparent beyond 300 nm. The transition from HOMO to LUMO can be seen from the UV-Vis spectrum for PK-PDAP, and the calculations predicted five electronic transitions at 305, 338, 354, 457, and 515 nm. This is consistent with the experimental measurements, as shown in Figure 2.10(b). Close examination of the absorptions indicates that the peaks observed correspond to the transition of both the N-substituted pyrrole [157,158] and the dihydropyridine structures, as shown in Figure 2.8.

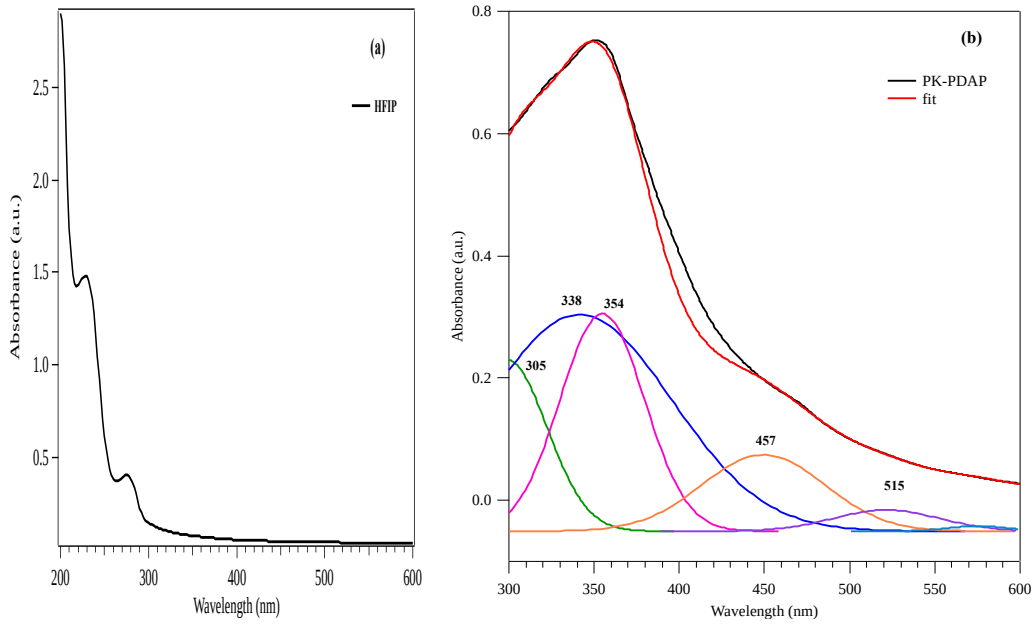

Figure 2.10: UV-Vis spectra of: (a) HFIP at 200-600 nm; and (b) PK-PDAP at 300-600 nm.

Table 2.5: Energy difference for some electronic transitions and the associated wavelength for the simulated A5 and A5+A6

A5		A5+A6	
# orbital	**E /eV**	**# orbital**	**E /eV**
86	-5.347	153	-5.277
87	-5.243	154	-5.156
88 HOMO	-4.432	155 HOMO	-4.342
89 LUMO	-1.44	156 LUMO	-1.650
90	-1.359	157	-1.498
91	0.141	158	-1.387
92	/	159	-1.370
		160	-0.777
		161	-320
		162	0.236

A5 refers to the pyrrole (Figure 2.5b), and A5+A6 refers to the pyrrole + dihydropyridine structure (Figure 2.8)

Table 2.6: Energy difference for some electronic transitions and the associated wavelength for the simulated A5

	A5	
Transition	**ΔE / eV**	**λ /nm**
E88 --> 89	2.992	414
E88 --> 90	3.073	403
E88 --> 91	4.573	271
E88 --> 92		
E87 --> 89	3.803	326
E87 --> 90	3.884	319
E87 --> 91	5.488	226
E87 --> 92		
E86 --> 89	3.907	317
E86 --> 90	3.988	311
E86 --> 91	5.488	226
E86 --> 92		

Table 2.7: Energy difference for some electronic transitions and the associated wavelength for the simulated A5+A6

	A5+A6	
Transition	**ΔE / eV**	**λ /nm**
E155 --> 156	2.692	461
E155 --> 157	2.844	436
E155 --> 158	2.955	420
E155 --> 159	2.972	417
E155 --> 160	3.565	348
E155 --> 161	4.022	308
E155 --> 162	4.578	271
E154 --> 156	3.506	354
E154 --> 157	3.658	339
E154 --> 158	3.769	329
E154 --> 159	3.786	327
E154 --> 160	4.379	283
E154 --> 161	4.836	256
E154 --> 162	5.392	230
E153 --> 156	3.627	342
E153 --> 157	3.779	328
E153 --> 158	3.890	319
E153 --> 159	3.907	317
E153 --> 160	4.500	276
E153 --> 161	4.957	250
E153 --> 162	5.513	225
E152 --> 156	3.679	337
E152 --> 157	3.831	324
E152 --> 158	3.942	315
E152 --> 159	3.959	313
E152 --> 160	4.552	272

2.3.5. Thermogravimetric analysis

Figure 2.11 (a and b) shows the thermal behavior of PK, PK-PDAP, PK-PDAPm, PK-PDAPm(I) and PK-PDAPm(OH), as measured by TGA in an inert atmosphere. The thermograms of all the samples show a small weight loss (1-2%) below 200ºC, due to moisture evaporation. PK remains stable up to 340ºC, when a first major weight loss of 14% occurs due to intra- and inter-molecular reactions accompanied by crosslinking and the formation of heterocyclic compounds [150]. A second major weight loss of 50% occurs at 377ºC, and is associated with fragmentation of the molecular backbone and the formation of alcohols, as already seen in ethylene-CO copolymers [150]. The thermal degradation of PK-PDAP occurs at lower temperatures than in PK, and in three distinct regions: (I) one at 215ºC, attributed to the loss of amine groups; (II) the next at 300ºC, tentatively attributed to decomposition of the aminated nitrogen heterocycle; and (III) the third, and most severe, at temperatures beyond 450ºC, due to degradation of the polymeric backbone. The thermal behavior of PK-PDAPm differed slightly from that of PK-PDAP because the decomposition events at higher temperatures (T > 300ºC) were negligible. Here again, decomposition occurred in three steps with: (I) a first 9% weight loss at 215ºC, due to the loss of the amine group; (II) a second 8% weight loss at 314ºC; and (III) a third 35% weight loss at 377ºC. In addition to the loss of the amine group (I), and the polymer backbone degradation (II), at low (200ºC) and high (445ºC) temperatures, respectively, the thermogravimetric profiles for PK-PDAPm(I) also reveal cleavage of the methylated group (III) at 300ºC with a 21% weight loss. The profiles for PK-PDAPm(OH) show three decomposition stages: (I) one at 212ºC with a 9% weight loss; (II) a second at 280ºC with a 16% weight loss; and (III) a third at 434ºC with a further 14% weight loss.

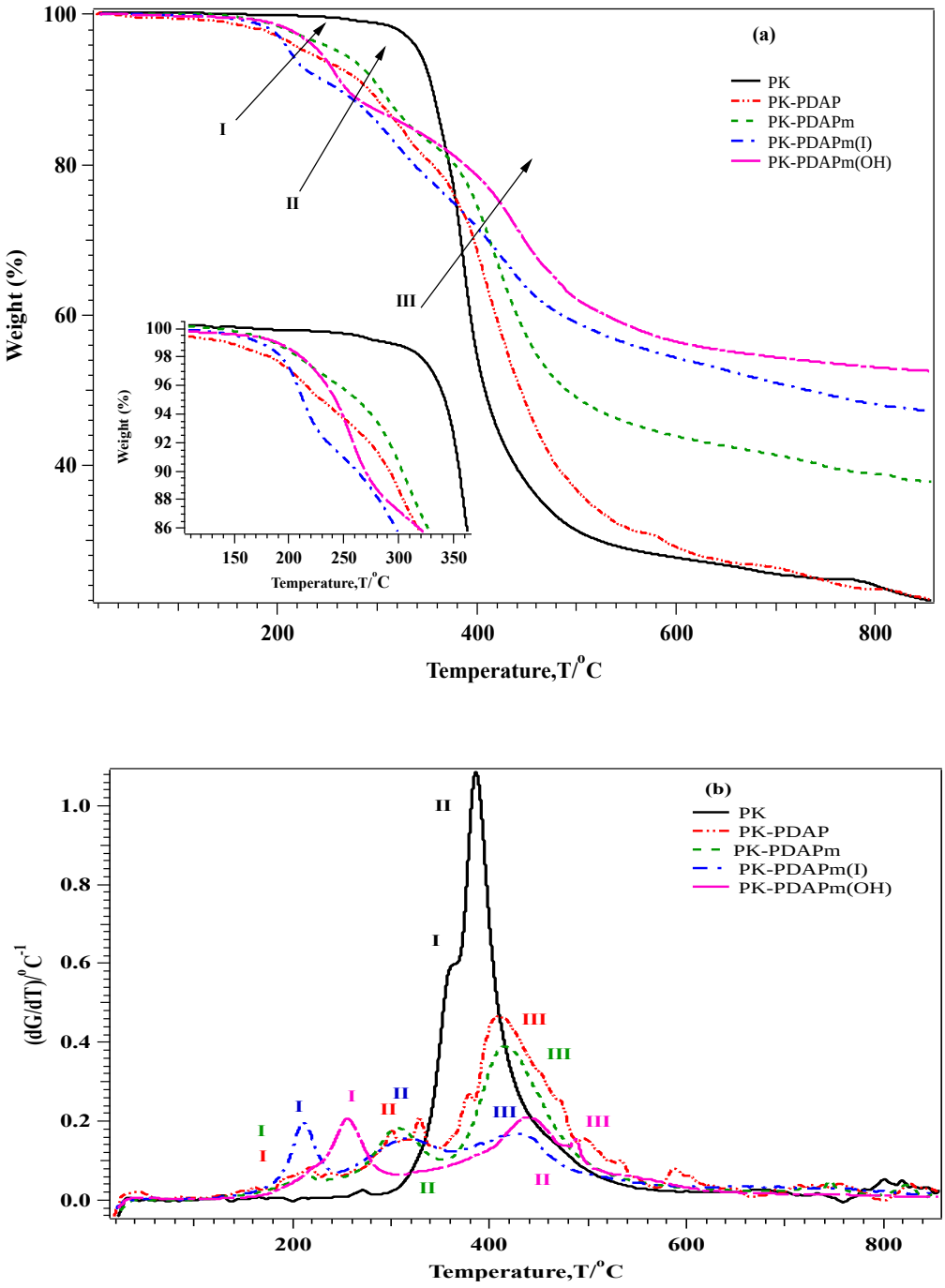

Figure 2.11: a) Thermographic profiles; and b) Dependence of the derivative of the profile on temperature for PK, PK-PDAP, PK-PDAPm, PK-PDAPm(I), and PK-PDAPm(OH)

2.3.6. Differential scanning calorimetry

The DSC thermograms of all the samples showed multiple exothermic events at temperatures in the range from -80 to 50ºC, that correspond to the order-disorder molecular rearrangement and melting of nanometric domains [8].

In the DSC curve for PK (Figure 2.12), the endothermic peak at 102ºC is identified as the α to β phase transition [79] typical of this material. These two crystalline phases correspond to two domains characterized by a different packing of the polymer domains. The chain is reorganized as a result of dipole interactions between neighboring carbonyl groups, which are closer in the α phase than in the β phase [82]. Two glass-transition temperatures (T_g) were also seen for the PK sample. The first T_g value obtained for the pristine PK was around 117ºC, and the corresponding step is broad and steep (indicating that most of the amorphous polymer is not very homogeneously arranged) by comparison with that of the second T_g, at about 163ºC. The sharp endothermic peak at 274ºC (enthalpy: -1000 kJ g^{-1}) represents the melting point of the β crystalline PK [159].

On the PK-PDAP curve, the endothermic peak at 98ºC relates to crosslinking and condensation phenomena, as depicted in Figure 2.8. This confirms what was said previously regarding the FTIR results: PK-PDAP is less well crosslinked than the membrane, and the thermal process involved in membrane formation promotes crosslinking without affecting the whole N content. The endothermic peak corresponding to the PK-PDAP melting point of appears at 224ºC (enthalpy: -71 kJ g^{-1}). This peak seemed broad, and not as sharp as expected for a melting phenomenon, because rearrangement in the PK-PDAP left a smaller amount of crystalline phase than in the pristine PK. All the samples were submitted to a second run (details not reported here), which indicated that the previously-described features became less evident, whatever the composition and nature of the samples. A thermosetting behavior was observed for all the samples, confirming that the reactions occurring in the first run were condensations and crosslinks.

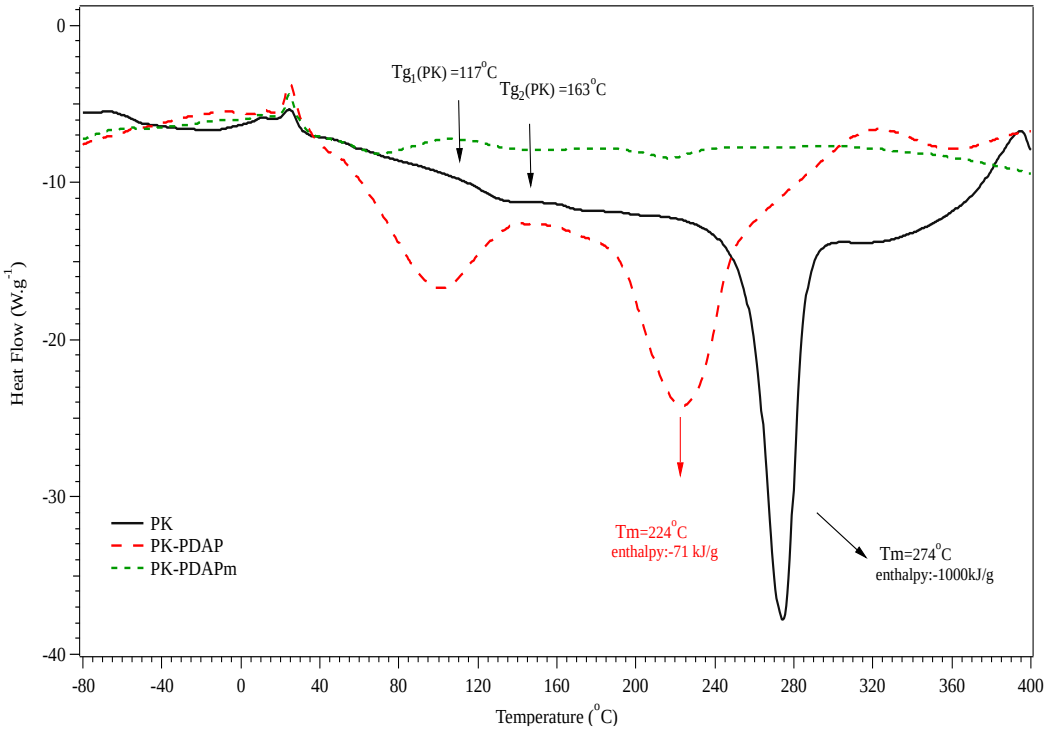

Figure 2.12: DSC thermographs of PK, PK-PDAP, and PK-PDAPm.

The DSC profiles of the dry and wet membranes, in both the iodide and the hydroxide forms, revealed four transitions (I, II, III & IV), as shown in Figure 2.13. Dry PK-PDAPm(I) undergoes one main endothermic transition at about 120°C, while the wet membrane reveals an overlapping endothermic event peaking in the temperature range of 80-120°C. This phenomenon is associated with the order-disorder transition attributed to the presence of cross-linking and inter-chain interactions. The transitions occurring at -75, -10 and 71°C (I, II, III), and at -78, -20 and 34°C (I, II, III), in dry and wet PK-PDAPm(I), respectively, correspond to order-disorder molecular rearrangements and melting of the nanometric domains. The DSC profiles for PK-PDAPm(OH) likewise indicate some order-disorder molecular rearrangements in both conditions, as well as melting of the nano domains below 60°C, followed by an endothermic peak at temperatures above 100°C. This

last event is more evident in the wet membrane, with a broad endothermic peak at 128ºC, probably due to water being removed as a result of the rearrangement of the hydroxide anions.

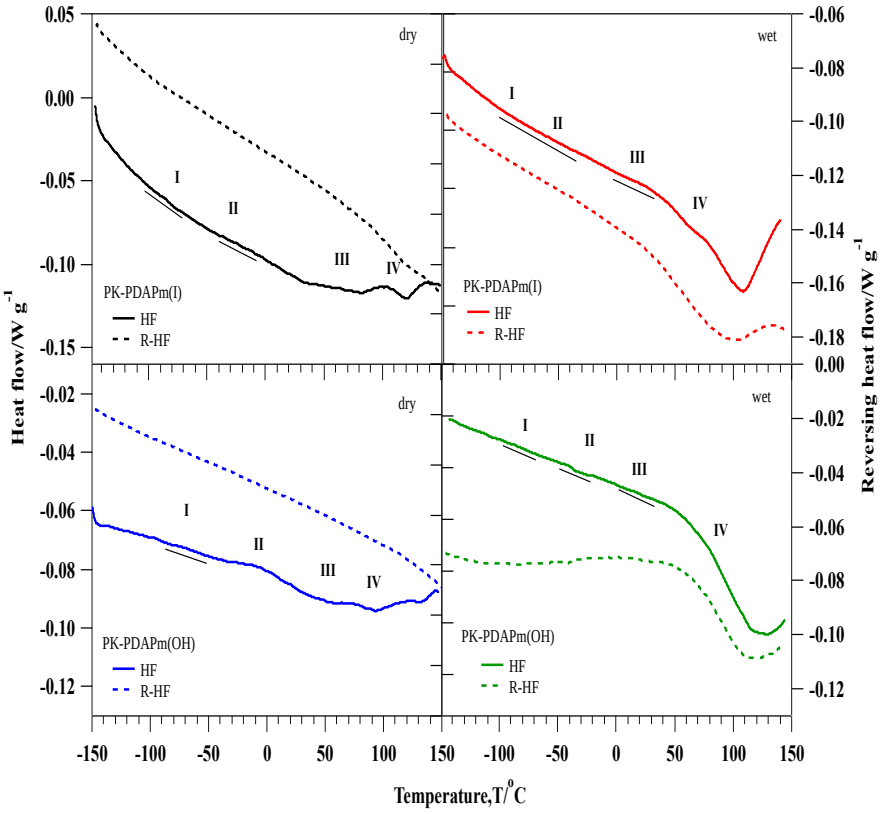

Figure 2.13: DSC profile of PK-PDAPm(I) and PK-PDAPm(OH) in dry and wet conditions.

2.3.7 Conductivity measurements

The conductivity of the iodide (PK-PDAPm(I)) and OH (PK- PDAPm(OH)) membranes was tested in dry and wet conditions using broadband electrical spectroscopy (BES) in the temperature range from -100 to 120ºC, and at frequencies ranging from 0.03 to 10^7 Hz. The 2D spectra of the real component of conductivity (σ') as a function of frequency and

temperature are shown in Figure 2.14: (a) the σ' of the dry and wet iodine membrane was higher than that of the hydroxyl membrane; and (b), as expected, the σ' values for the wet membranes were higher than those of the ionomer in dry conditions. The imaginary and real parts of the permittivity are shown in Figures 2.15 and 2.16 for the dry and wet membranes, respectively. As the temperature increased in the wet membranes, the 2D spectra of σ' reveal: (a) a shift in the dielectric relaxations at higher frequencies; (b) the appearance of electrode polarization (σ_{EP}) due to the charge accumulating between the sample and the electrode; (c) an enhanced conductivity for T > 0 due to water melting and giving rise to an increase in charge mobility; (d) inter-domain polarizations (σ_{IP}) [158] due to the charge accumulating at interfaces between the domains with a different permittivity in the bulk membranes. These results are consistent with the domains detected in the light of the previously-discussed DSC measurements. In the dry PK-PDAPm (I), the 2D spectra of σ' show a dielectric relaxation at low temperatures (T<0°C), and electrode polarization at higher temperatures (T>0°C) [150], while no such electrode polarization is visible in the dry PK-PDAPm(OH). The highest conductivity of the proposed materials was measured at 120°C and, for the wet PK-PDAPm(I) and PK-PDAPm(OH), it was 9×10^{-4} S cm^{-1} and 1×10^{-4} S cm^{-1}, respectively. These values are comparable with those of other anionic membranes [126,128,160-162].

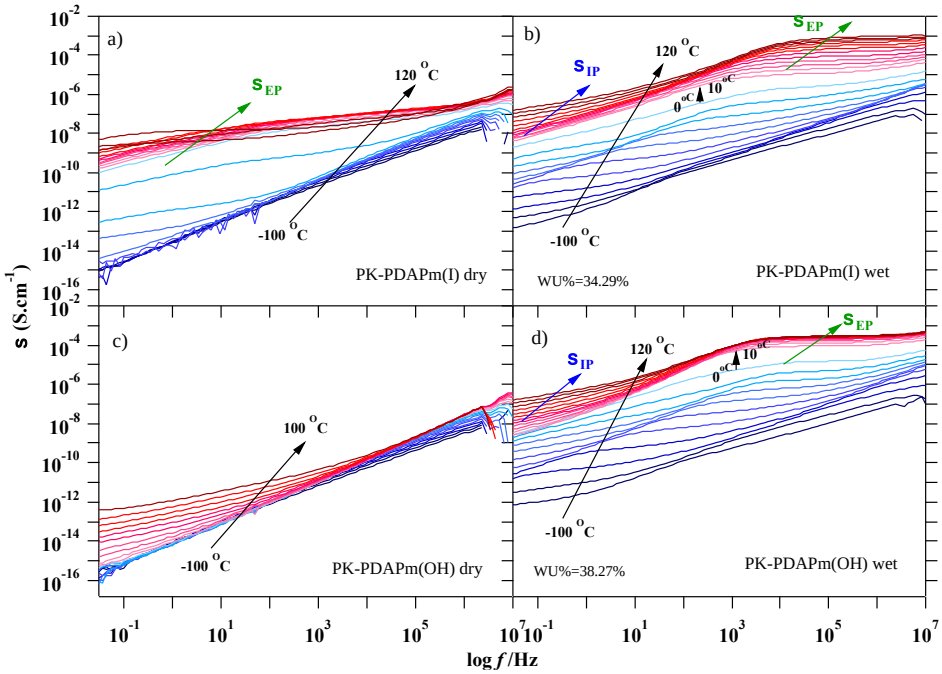

Figure 2.14: Real conductivity as a function of frequency and temperature for dry (a,c) and wet (b,d) iodide (a,b) and OH (c,d) conducting membranes. Black lines refer to temperature changes from -100 to 120°C, blue lines to the σ_{IP}, and green lines to the σ_{EP}.

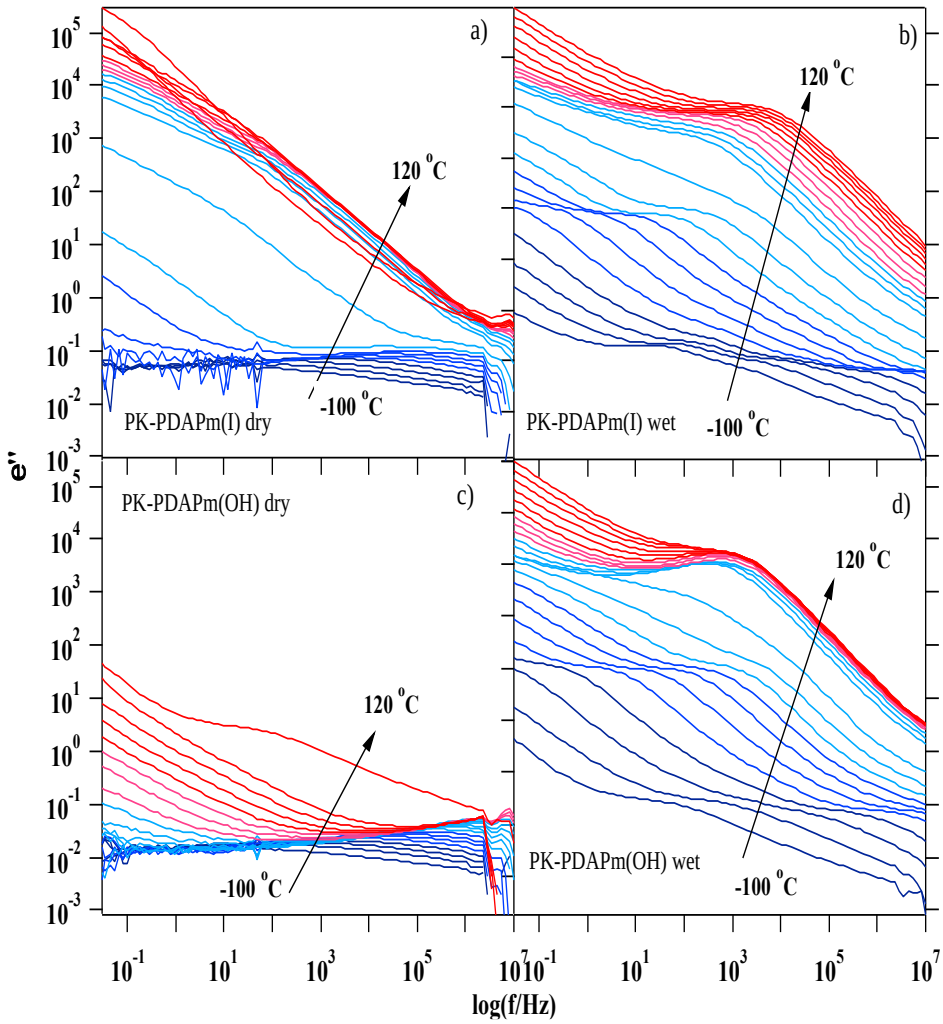

Figure 2.15: Imaginary part of permittivity for dry (a,c) and wet (b,d) iodide (a,b) and OH (c,d) conducting membranes. Black lines refer to temperature changes from -100 to 120°C.

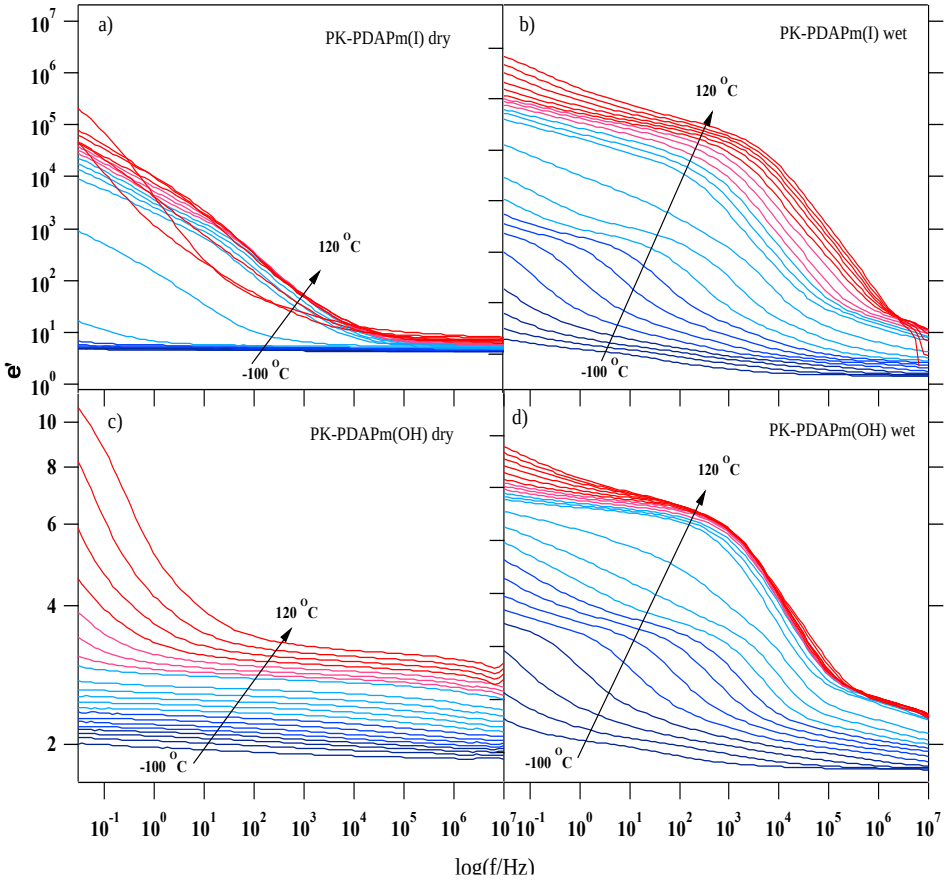

Figure 2.16: Real part of permittivity for dry (a,c) and wet (b,d) iodide (a,b) and OH (c,d) conducting membranes. Black lines refer to temperature changes from -100 to 120°C.

Figure 2.17 compares the real conductivity, by frequency and temperature, of PK-PDAPm(OH) and AMVOH membranes. Selemion AMV, a commercial reference AEM obtained from the Asahi Glass Company, is a functionalized polystyrene-based copolymer containing quaternary ammonium groups. It was studied in hydroxide anion form (AMVOH) by Giffin et al [163]. The AMVOH membrane exhibited a conductivity of 7 mS cm^{-1} at 25°C.

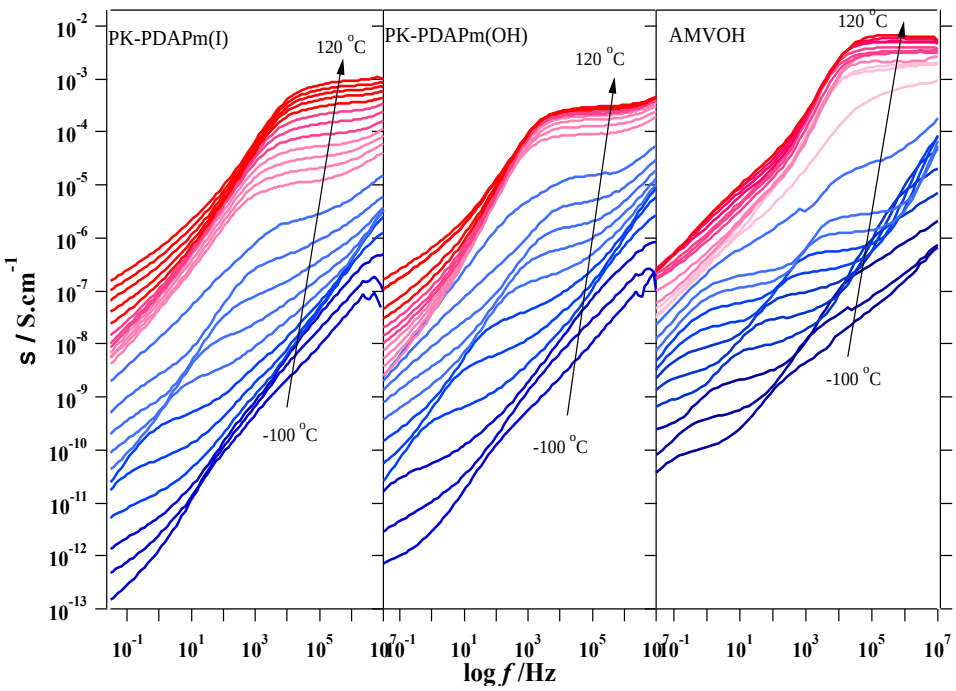

Figure 2.17: Real conductivity, by frequency and temperature, of PK-PDAPm(I), PK-PDAPm(OH), and AMVOH. Black lines refer to temperature changes from -100 to 120ºC.

The conductivity of the new membranes discussed in the present work could also be improved by raising the amine content of the modified polymer. These membranes are promising because of their thermal stability, as gauged by measuring the mass loss that occurred during their thermal decomposition (shown in Figure 2.18a). T_1 is the thermal event occurring at approximately 260ºC, associated with the loss of MeOH. After 60 hours under alkaline conditions, the mass loss becomes constant (approx. 6 wt%, as shown in Figure 2.18b), indicating that the membrane is stable under these conditions.

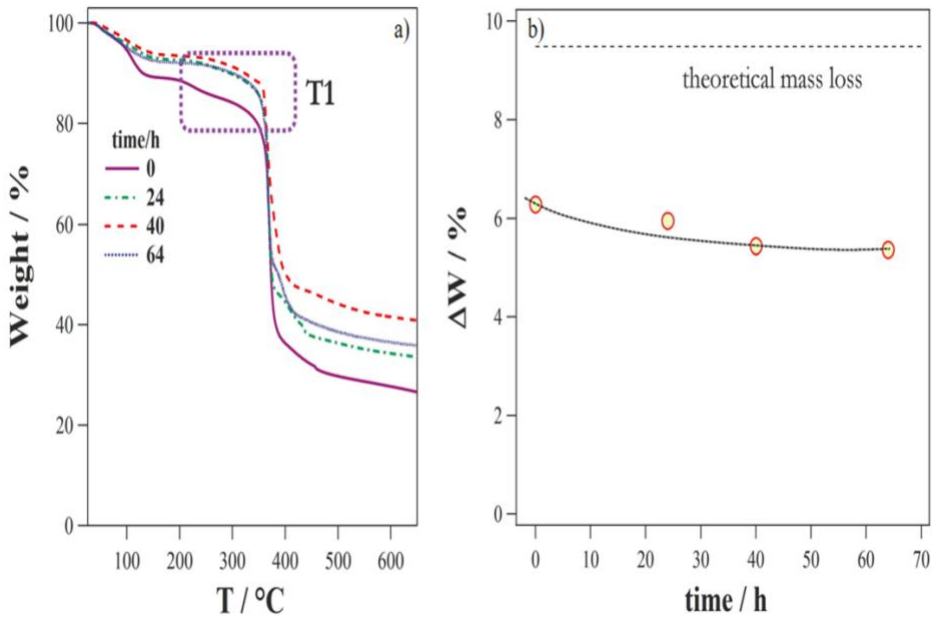

Figure 2.18: (a) Thermogravimetric curve of weight loss vs. temperature for PK-PDAPm(OH) samples immersed in a 2 M NaOH solution at 80°C for increasingly long times. (b) Variation in weight loss vs. immersion times for PK-PDAPm(OH) samples immersed in a 2 M NaOH solution.

Figure 2.19 shows the curve of σ_T vs. 1/T (overall conductivity as a function of the inverse of temperature) for the dry and wet PK-PDAPm(I) (Figure. 2.19a) and PK-PDAPm(OH) (Figure. 2.19b). This type of plot reveals four conductivity regions (I, II, III and IV) separated by the thermal transitions T_I, T_{II}, T_{III} and T_{IV}, measured by DSC (see above). The overall conductivity (σ_T) curve is simulated with the Arrhenius-like equation [164,165]:

$$\sigma_T = A_\sigma . \exp(-E_a | RT) \quad (2.3)$$

where A_σ relates to the number of charge carriers, R is the universal gas constant, and E_a is the activation energy with the Vogel-Fulcher-Tammann-like (VFT) equation [164,166-168]

$$\sigma_T = A_\sigma . exp \frac{-E_{a,VFT}}{R(T-T_o)} \quad (2.4)$$

where, $E_{a,VFT}$ is the pseudo-activation energy for conduction, and T_0 is the thermodynamic ideal glass transition temperature, with the boundary condition Tg -55 $\leq T_o \geq$ Tg -40 K [166].

The values of E_a and $E_{a,VFT}$ are given in Table 2.8. As expected, the conductivity mechanism in regions I and II in dry membranes was the result of long-range charge migration events between coordination sites in different neighboring chains (inter-chain hopping [130]) with an Arrhenius-like behavior. The σ_T shows a VFT behavior in region III, however, suggesting that charge migration was coupled with the segmental motions of the host polymer matrix. The E_a value in these regions is around 1 kJ/mol. In wet membranes, the conductivity mechanism is VFT-like, and charge migration can be expected to occur between delocalization bodies [127]. The $E_{a,VFT}$ values for PK-PDAPm(OH) in regions III and IV were of the same order of magnitude, and lower than those for PK- PDAPm(I). Figure 2.20 shows the conductivity vs. 1/T for PK-PDAPm(OH) and AMVOH [163]. The conductivity of AMVOH reveals an Arrhenius-like behavior, suggesting that the dynamics of the host polymeric matrix are not significantly involved in the long-range conduction mechanism.

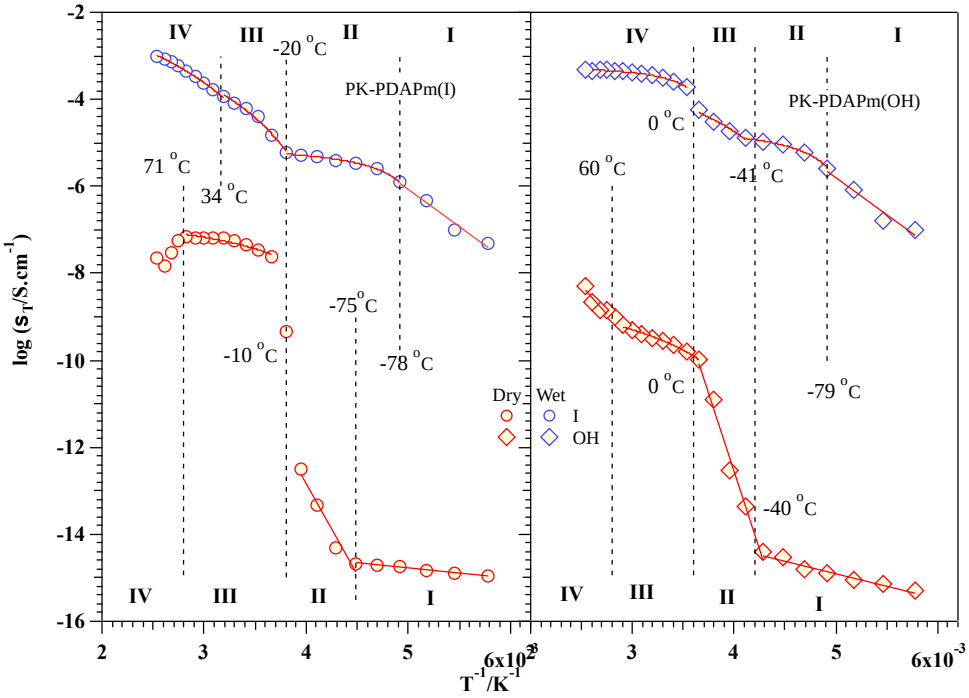

Figure 2.19: Conductivity vs 1/T for dry and wet PK-PDAPm(I) (a), and PK-PDAPm(OH) (b). Four conductivity regions are detectable (I, II, III, & IV), defined by the temperature for DSC.

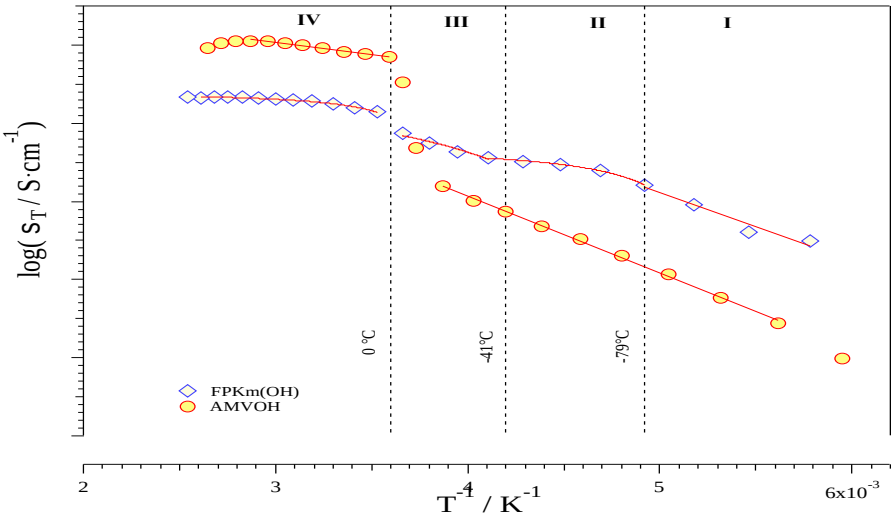

Figure 2.20: Conductivity vs 1/T for PK-PDAPm(OH) and AMVOH.

Table 2.8: Activation energy of overall conductivity (σ_T) in the four conductivity regions for dry and wet membranes (PK-PDAPm(I) and PK-PDAPm(OH)).

	Sample	**I**	**II**		**III**		**IV**	
		E_a/ kJ/mol	**E_a/** kJ/mol	**T_0 /K**	**E_a/** kJ/mol	**T_0 /K**	**E_a/** kJ/mol	**T_0 /K**
dry	I	4.44±0.38*	80.91 ±4.11*	/	1.23±0.11°	183±9	/	/
	OH	11.21±1.32*	136.7±8.31*	/	2.24±0.08°	172±9	51.02±3.06*	/
wet	I	33.03±2.09*	0.272±0.042°	197±10	3.80±0.23°	197±8	5.29±0.48°	197±6
	OH	33.08±3.01*	0.305±0.039°	187±8	1.94±0.31°	187±9	1.09±0.06°	197±5

* The value of E_a was determined by fitting the conductivity data with the Arrhenius equation.
° The value of E_a was obtained by fitting the conductivity data with the VFT equation.

2.3.8 XRD

XRD studies were conducted to gain additional information on the morphology of the polymers in terms of their crystalline and amorphous phases. The X-ray diffractograms of the PK and PK-PDAP showed the α and β crystalline phases and an amorphous part (Figure 2.21). The α phase reveals some weak reflections at 2θ =15, 24, 25, and 41°, while those in the β phase become stronger, and appear at 2θ =21 and 29° [169,170]. The crystallinity is due to the presence of polar carbonyl groups in the backbone of PK. The difference between α and β is due to chain packing. In other words, the orientation of the carbonyl group at the center of the chain differs from that at its ends [79]. The intensity of the β phase is greater than that of the α phase, and the crystals' size is larger. The β phase has practically disappeared from the PK-PDAPm, and it has become more amorphous. As discussed in the section on DSC, the thermal treatment used to prepare the membrane should have improved the order-disorder rearrangement of the materials, which was also related to a greater degree of crosslinking.

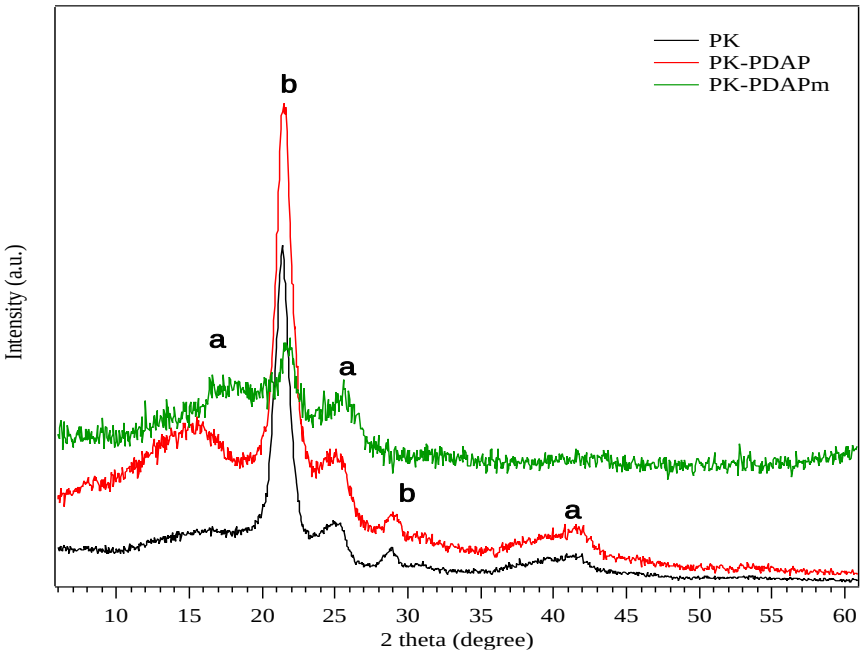

Figure 2.21: X-ray diffractograms of PK, PK-PDAP, and PK-PDAPm.

2.3.9 SEM

The SEM study on the PK and PK-PDAP (Figure 2.22[a,b]) shows that the PK and polyamine had a polymorph spherical structure with a "cauliflower-like" appearance. Figure 2.22(c,d) shows the SEM micrographs of the fractured surface of the polyamine membrane (PK-PDAPm), which has a homogeneous appearance with some spherical clusters. Micropores due to solvent evaporation become evident at higher magnifications (5000x). The SEM images of a cross-section of the membrane show a layered but homogeneous morphology throughout its thickness.

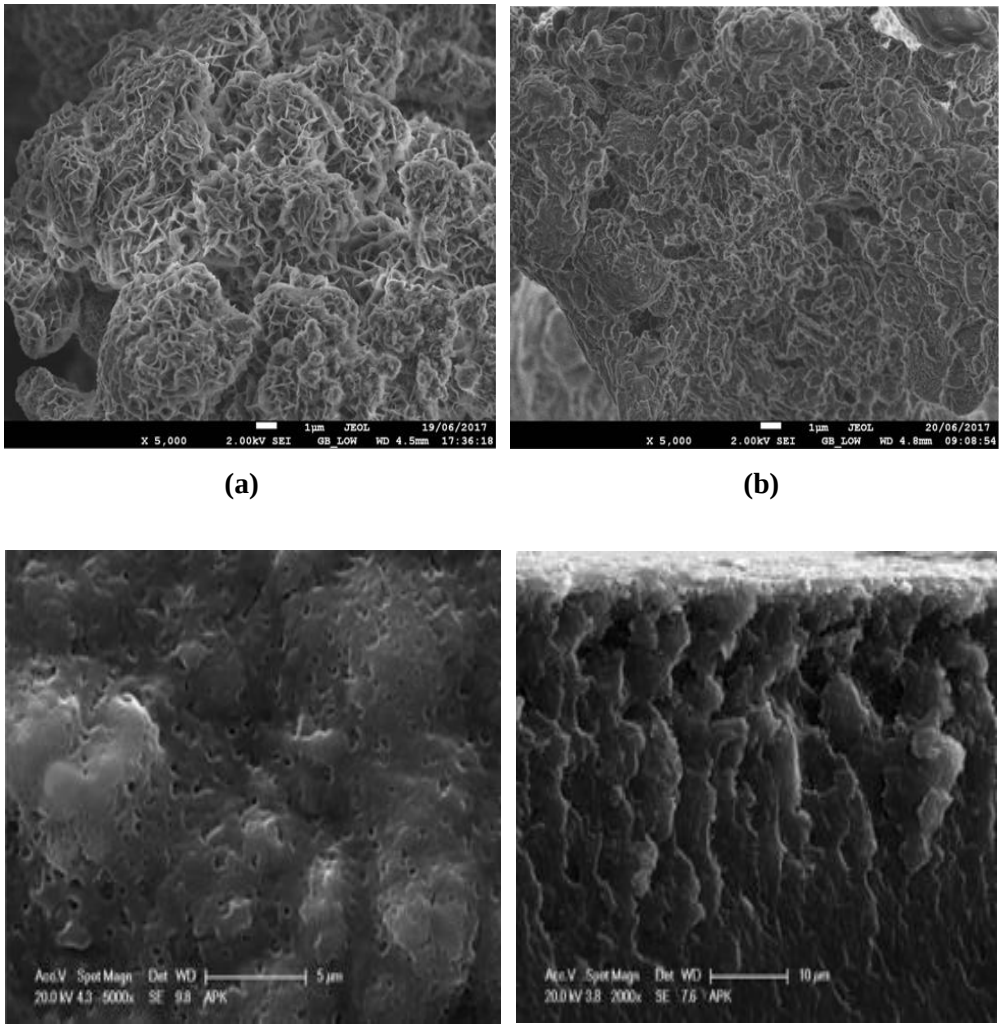

(a) **(b)**

(c) **(d)**

Figure 2.22: SEM micrographs of: (a) PK (5000x); (b) PK-PDAP (5000x); (c) PK-PDAPm (5000x); and (d) cross-section of PK-PDAPm (2000x).

2.4 Conclusions

Anion exchange membranes were successfully prepared by chemically modifying PK with primary amine, followed by solution casting, methylation and ion exchange processes. Given the low nitrogen content, polyamine has a backbone mainly consisting of PK, with some pyrrole or pyridine units inserted in it. The structure of these units, and the mechanism behind their formation can be deduced from the elemental analysis, FTIR, NMR and UV-Vis findings. The structure of the N-containing units is the result of Paal-Knorr reactions, as well as crosslinking phenomena, as observed on DSC. These structural changes can strongly affect the final properties of the modified PK. XRD analysis revealed the semicrystalline nature of the synthesized polymer and the membrane obtained. On TGA, the thermograms of all the compounds demonstrated a good thermal stability up to 200^{o}C. The ionic conductivity of the hydrated iodide and hydroxyl membranes could reach values as high as 9 x10^{-4} S cm^{-1} at 120^{o}C in the former, and 5 x10^{-4} S cm^{-1} at 90^{o}C in the latter. Our results indicate that dielectric relaxations shift to higher frequencies as the temperature rises. The electrode polarization appeared to be due to the charge accumulating between the sample and the electrode. Inter-domain polarizations can also be seen at higher temperatures because of the charge accumulating at the interfaces between domains with a different permittivity in the bulk membranes. The dielectric relaxation at low temperatures (T < 0^{o}C) and electrode polarization at higher temperatures (T > 0^{o}C) were responsible for the ionic conductivity of dry PK-PDAPm(I), whereas in dry PK-PDAPm(OH) it was due to dielectric relaxation alone. Measurements of the temperature dependence of PK-PDAPm(I) and PK-PDAPm (OH) conductivity, in both wet and dry conditions, revealed four conductivity regions (I, II, III and IV), relating to the thermal transitions measured by DSC. In dry membranes, the conductivity mechanism of regions I and II has an Arrhenius-like behavior. Our results indicate that the relationship is non-linear for all regions because the conductivity in region III followed a VFT behavior. The conductivity of the wet membranes did not obey the Arrhenius rule, however. The obtained results indicated that the modified polyketone AEM is a potential candidate for the electrochemical applications.

Chapter 3

Properties of the Polyamine-Based Anion Exchange Membrane: Effect of Functionalized Silica Particles Prepared using a Sol-Gel Method

3.1 Introduction

The main goal of this study was to obtain a new polymer material in which amino-functionalized silica (Si-NH_2) contributes synergically to the final composite's performance, improving its anion exchange properties and thermal stability. This could be achieved by means of the surface modification of inorganic nanoparticles, a topic attracting great interest because of the broad array of its potential applications in the fields of chemistry, biology and physics, in composite materials [171] or drug delivery [172], for coupling and immobilizing functional molecules and biomolecules [173], and in base catalysis [174]. The surface modification of inorganic nanoparticles can also enhance the compatibility between organic and inorganic phases [175]. Metal oxides like SiO_2 have been widely used as inorganic fillers in polymer composites [176-178]. This is thanks to: the commercial availability of SiO_2 in various particle sizes and with different morphological features; the large number of surface hydroxyl groups suitable for further modification; and the ease with which *in situ* silica can be formed using the sol-gel process on silicon alkoxides under mild reaction conditions [179,180]. Adding silica also strengthens the interface between the nanoparticles and the polymer matrices [181,182]. Basically, the functionalization of silica particles is a method for tailoring the surface properties of particles to suit target applications [183,184], and 3-amino-propyltriethoxysilane (APTES) is often used if the aim is to insert anionic groups [185-188]. The method used to prepare a polyamine-based AEM (PK-PDAPm) from a modified PK skeleton is described in detail in chapter 1. The resulting polyamine consists of a stable pyrrole ring along the backbone, and a reactive pendant amino functional group

[8]. In the present work, the hydroxyl groups of silica powder were exploited for their condensation reaction with 3-APTES under hydrolytic conditions [189-191], and the modified silica (Si-NH_2) was added to polyamine. The incorporation of the amino functional groups (Si-NH_2) in the polyamine membrane was expected to have a stable and homogeneous reinforcing effect by improving the filler-polymer interface, and thereby help to improve the membrane's IEC. As a consequence, the incorporation of Si-NH_2 within polyamine membranes to form (PA-SiNH_2)m should contribute to increasing their conductivity, retaining their water content at high temperatures and low relative humidity, improving their thermomechanical properties, and containing their thermal degradation at high temperatures. The structural and thermal properties of the end products were assessed using FTIR, NMR, XRD, TGA and DSC, and the membranes' ion exchange ability and ionic conductivity were determined.

3.2 Experimental

3.2.1 Reagents

3-aminopropyltriethoxysilane (Aldrich, 99%), ammonium hydroxide (Carlo Erba, 30%), hydrochloric acid (Baker, 36-38%), iodomethane (ABCR GmbH, 99%), polyethylene glycol 200 (Sigma Aldrich, MW 190 - 210 g/mol), potassium hydroxide (VWR), absolute ethanol (VWR), and 1,1,1,3,3,3-hexafluoroisopropanol (Sigma-Aldrich, 99%), were commercially available and used as received. The silica powder had an average diameter (agglomerated particles) of 6.20 μm. Bi-distilled water was used in all procedures.

3.2.2 Methods

PK synthesis and amination to obtain PK-PDAP were done as explained in chapter 2, pages 19 and 20 [8].

3.2.2.1 Modified silica (Si-NH_2)

After suspending 100 mg of silica in 1.5 mL of APTES and 1.5 mL of ethanol in the ultrasonic bath for 10 min, 0.1 mL of distilled water was dropped into the reaction medium to facilitate APTES hydrolysis. After 1.5 hour, 60 µL of NH_4OH catalyst was fed into the reaction mixture. Sonication was continued for 3 hours. Gelling was allowed for 1 hour. The gel was then centrifuged and washed with ethanol and distilled water (3x for 5 min at 4,000 rpm). The final material (Si-NH_2) was dried at 70°C for 24 hours [192].

3.2.2.2. Membrane preparation

Polyamine (PK-PDAP) synthesis followed the Paal-Knorr reaction. After weighing and grinding 30 mg of polyamine powder, and adding 15 mg of previously-ground modified silica (Si-NH_2), the powder was mixed with 7 mL of HFIP solvent and stirred for 1 hour at 40°C. Then 50 w% of PEG200 (0.26 mL) was added to the solution, before 60 mL of NH_4OH was added by means of a syringe. The solution was homogenized by placing it in an ultrasonic bath at 40°C for about 30 min, then leaving it stirring overnight at 40°C. The solution was then cast into a Petri dish to obtain a homogeneous, free-standing membrane. This modified membrane was named (PA-$SiNH_2$)m. To run the methylation reaction, (PA-$SiNH_2$)m was immersed in iodomethane for 24 hours, then washed thoroughly with deionized water and dried at 40°C in a vacuum for 24 hours. The methylated membrane (PA-$SiNH_2$)mI exchanged to the hydroxide ion form (PA-$SiNH_2$)mOH in a 1M KOH solution for 1 hour. This step was repeated three times. Then the (PA-$SiNH_2$)mOH was washed with distilled water and stored under a nitrogen atmosphere to prevent hydroxide anions from changing into carbonate and bicarbonate species on contact with carbon dioxide in the atmosphere.

3.2.3 Instrumental methods

FTIR spectroscopy was done with a Nicolet FT-IR Nexus spectrometer, averaging 16

scans with a resolution of 4 cm^{-1} in the range of wavenumbers between 650 and 4000 cm^{-1}. Solid-state NMR analyses were run with a Bruker 300WB spectrometer operating at a proton frequency of 300.13 MHz. Magic Angle Spinning (MAS) ^{29}Si and ^{13}C NMR spectra were acquired with single pulse experiments (SP) and cross-polarization pulse sequences (CP) under the following conditions:

- ^{29}Si frequency: 59.62 MHz, SP: $\pi/4$ pulse 2.25 μs, recycle delay 150s, 3k scans; CP: contact time 5ms, ^{1}H $\pi/2$ 3.2 μs, decoupling length 5.9 μs, recycle delay: 10 s, 5k scans;
- ^{13}C frequency: 75.48 MHz, CP: contact time 2ms, decoupling length 5.9 μs, ^{1}H $\pi/2$ 3.2 μs, recycle delay 5 s, 20k scans.

Samples were packed in 4 mm zirconia rotors, which were spun at 7 kHz under an air flow. Adamantane (Q_8M_8) was used as an external secondary reference. Si units were labelled according to the usual NMR notation, T^n and Q^n representing trifunctional ($SiCO_3$), and tetrafunctional (SiO_4) Si units, respectively, and *n* the number of bridging O atoms. The lineshape analysis was run with the Bruker Topspin 3.2 software. Using a Labsys SETARAM thermobalance, TGA was performed from 25°C to 700°C, in N_2 and in air, with a heating rate of 10°C min^{-1}. DSC analyses were conducted with a DSC92 SETARAM equipped with a liquid N_2 cooling system. Data were collected at temperatures in the range between -100°C and 400°C, with a heating rate of 10 °C min^{-1}. XRD measurements were obtained on an X'TRA diffractometer (Thermo ARL, Switzerland), based on conventional powder geometry, using a solid-state Si-Li detector, and Cu Kα radiation. The data were recorded at diffraction angles 2θ from 1° to 60° at a scanning rate of 0.025 $^{\circ}s^{-1}$. The membranes' water uptake (WU) was measured from the difference in their weight before and after immersion in deionized water. In this study, the membranes (3x3 cm, 0.1 mm thick) were soaked in deionized water at room temperature for 24 hours. Then each sample was weighed immediately after removing the surface water from the membrane (W_{wet}). Membrane samples were then dried at 40°C for 6 hours and weighed again (W_{dry}). The water uptake was calculated using the following equation:

$$\text{Water uptake (\%)} = \frac{W_{wet} - W_{dry}}{W_{dry}} \times 100 \tag{3.1}$$

The IEC was ascertained with the back titration method. A dried (PA-$SiNH_2$)mOH membrane was immersed in 30 mL of 0.1 M HCl solution for 24 hours. A NaOH (0.01 M) solution was used for back titration, using phenolphthalein as an indicator. The IEC was calculated with the following equation:

$$\text{IEC (meq/g)} = \frac{[(V_{0,NaOH} - V_{NaOH})]\ C}{m_{dry}} \tag{3.2}$$

where $V_{0,NaOH}$ and V_{NaOH} are the volumes of NaOH solution consumed for back titration without and with the membrane, respectively, C is the concentration of NaOH solution, and m_{dry} is the weight of the dry membrane.

The ionic conductivity of the membranes was measured in a range of temperatures from 30 to 130°C using two-probe impedance spectroscopy and a Parstat 4000A (Princeton Applied Research, AMETEK). The impedance measurements were obtained over a frequency ranging from 1 MHz to 100 Hz at an amplitude of 10 mV. The membranes were equilibrated in deionized water for at least 24 hours at room temperature before taking the measurements. Each hydrated membrane was then sandwiched between two stainless steel electrodes. Conductivity (σ) was calculated according to the following equation:

$$\sigma = \frac{L}{(R_b \times A)} \tag{3.3}$$

where L is the membrane's thickness, R_b is the bulk resistance obtained from the intercept on the real impedance axis (Z' axis), and A is the effective area of contact between the membrane and the electrode.

3.3 Results and discussion

3.3.1 FTIR

Figure 3.1 (a, b) shows the FTIR spectra in the 4000-650 cm^{-1} range collected on pristine silica (SiO_2), APTES, modified silica (Si-NH_2), and the modified membrane (PA-SiNH_2)m. The FTIR peak assignments in Table 3.1 were drawn from the literature. Figure 3.1(a) shows the characteristic bands of silica, with the stretching vibrations of the Si-O-Si bonds at 794, 1060 and 1217 cm^{-1}, and the Si-OH vibration at 957 cm^{-1} [193-196]. The band at 1647 cm^{-1} is attributed to the bending vibration of water molecules adsorbed on the surface of the silica [193, 196].

The characteristic functional groups of APTES included the absorption peak at 765-789 cm^{-1}, attributed to Si-C stretching, and in-phase Si-O stretching vibration [197]. The peak found at 953 cm^{-1}, attributed to the silanol groups [192], shifted to 927 cm^{-1} after the reaction of silica and APTES. The intense peaks of Si-O-C stretching of APTES at 1073 and 1101 cm^{-1} [197] were replaced in the Si-NH_2 spectrum by a broad band at 1095 cm^{-1}, indicating that hydrolysis-condensation reactions had occurred. The weak shoulder at 1018 cm^{-1}, attributed to asymmetric siloxane bond (Si-O-Si) stretching, changed into a broad moderate peak at 1004 cm^{-1} after the modification [198]. The characteristic vibrations at 1296 and 1390 cm^{-1} are attributed respectively to C-N stretching, and to the Si-CH_2 bending mode of APTES [192,152,153]. The peak at 1366 cm^{-1}, corresponding to the bending mode of CH_3 in APTES [153], disappeared after the reaction with silica, confirming APTES hydrolysis. The bands identified at 1443, 1482 and 1594 cm^{-1} are attributed to the characteristic NH_2 deformation mode of primary amines [194,198,199].

Figure 3.1(b) shows the absorption bands in the region of 3000-2800 cm^{-1}. The symmetric and asymmetric CH_2 stretching vibrations of APTES [192,197,198] merged into two broad peaks after the reaction with SiO_2, as a consequence of APTES hydrolysis

and the reaction with the silica surface. Accordingly, the absorption bands at 3379 cm^{-1} assigned to the N-H stretching vibration in pristine APTES [195, 196] had shifted to 3288 and 3357 cm^{-1} in the Si-NH_2 sample.

(PA-SiNH_2)m shows a broad band in the range from 3000 to 3600 cm^{-1} that results from the adsorbed water O-H stretching modes overlapping with the N-H and SiO-H stretching vibrations, which appeared as shoulders on the broad band [192, 194].

The above results suggest that APTES reacts with the silica powder, leading to the presence of organic molecules covalently bonded to the particles' surface, as proposed in Figure 3.2. Further investigations will be needed to support this conclusion, however.

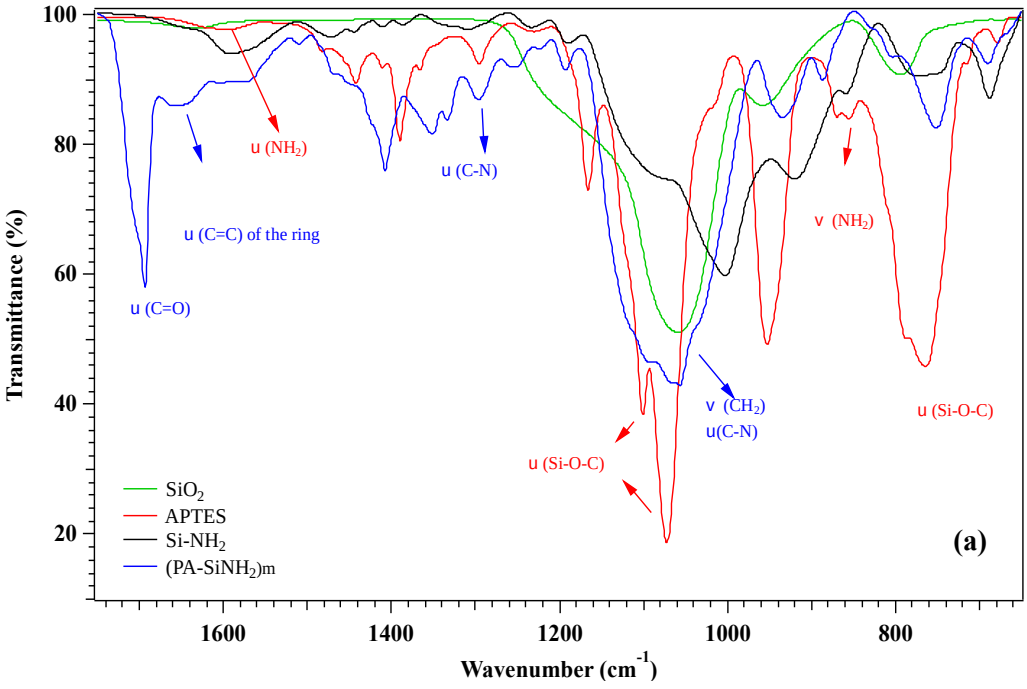

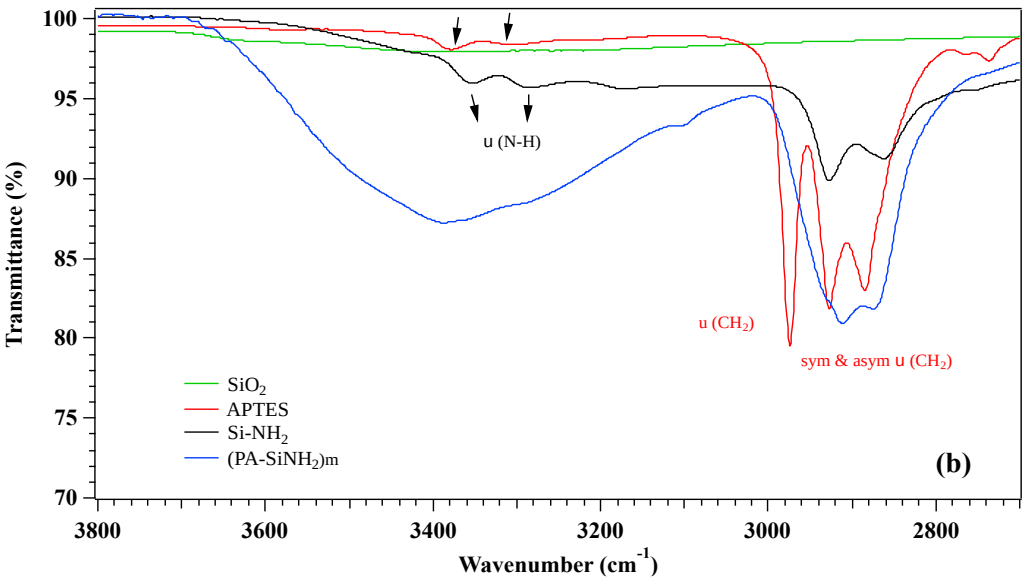

Figure 3.1: FTIR spectra of SiO_2, APTES, aminopropyl-functionalized silica ($Si\text{-}NH_2$), and the modified polyamine membrane ($PA\text{-}SiNH_2$)m: a) 1750-650 cm^{-1}; b) 3800-2700 cm^{-1}

The silica-modified polyamine matrix ($PA\text{-}SiNH_2$)m showed absorption at 1606 and 1656 cm^{-1}, proving the presence of a C-C aromatic ring [8,152,153] (Figure 3.1a). The stretching vibration of the carbonyl group belonging to PK was also seen at 1693 cm^{-1} [8,199]. The appearance of a shoulder (1704 cm^{-1}) in the C=O peak probably stems from the presence of two different PK phases, namely alpha and beta [8,9]. The peaks at 805 and 1333 cm^{-1} are assigned to polyamine CH_2 wagging and CH_3 rocking [8,144,149,150]. Compared with pure polyamine (data not shown) [8], the new absorption peak observed at 1509 cm^{-1} in ($PA\text{-}SiNH_2$)m reveals the presence of the modified silica groups in the membrane. The presence of PEG in the modified membrane was also confirmed by the appearance of a new peak at 1252 cm^{-1} assigned to the C-O-C vibration of PEG [152].

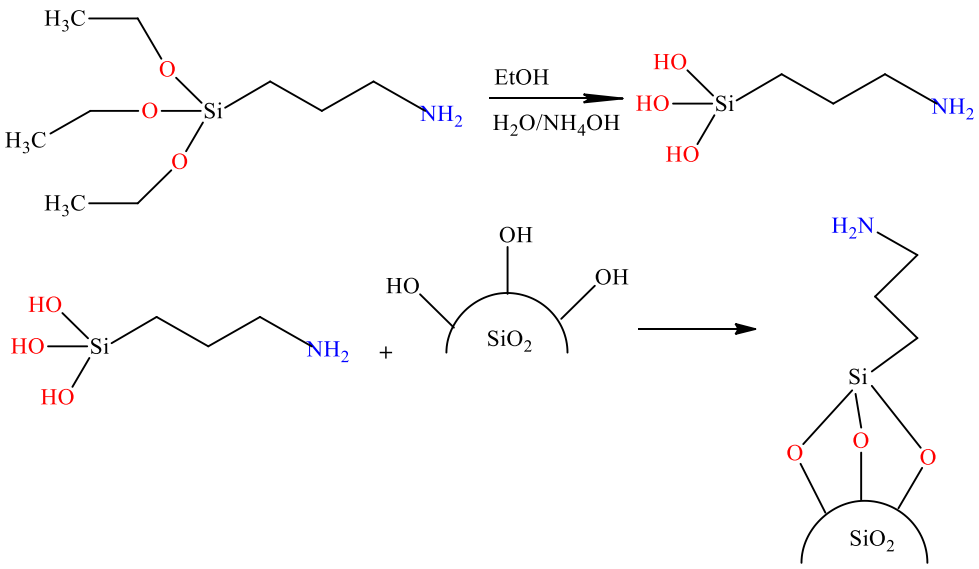

Figure 3.2: Schematic route for the modification of silica particles (Si-NH_2).

Table 3.1: FTIR peaks for SiO_2, APTES, Si-NH_2 and (PA-SiNH_2)m. Assignments were made accordingly.

Wavenumber (cm^{-1}) & intensity				Assignments	References
SiO_2	**APTES**	**Si-NH_2**	**(PA-SiNH_2)m**		
	765(s) 789(sh,m)	746 (vw) 784(vw)	751(w)	} υ(Si-C), (Si-O)	197
794(w)				υ (Si-O-Si)	193-195
			805(vw)	*p* (CH_2)	8,9,144,150
	870(w)		886(w)	ϖ (NH_2)	152,153
957(w)	953(m)	927(w)	934(w)	δ (Si-O-C), υ (Si-OH)	192,194,196
	1018(sh,vw)	1004(b,m)	1037(sh,m)	} υ (Si-O-Si)	198
			1057,1068(m)	ϖ (CH_2) υ (C-N)	8,9,152,153
1060 (m)	1073(vs) 1101(s)	1095(b,w)	1097(s)	} υ (Si-O-C)	193-197
	1167(m)	1191(vw)	1192(w)	} *asym* υ (Si-O-Si)	192
1217 (sh,vw)	1234(vw)	1233(vw)	1224(vw)		
			1252(w)	C-O-C	152
	1296(w)	1305(vw)	1296(w)	υ (C-N)	152,153
			1333(w)	ϖ (CH_2)	144,149,150
	1366(vw)		1352(w)	δ(CH_3) *sym*	153
	1390(w)	1384(vw)		δ (Si-CH_2)	192
	1412(vw)	1410(vw)	1408(w)	υ (CH_2)	149,150
	1443(w)	1444(vw)		δ (NH_2)	194,198
	1482(vw)	1472(vw)	1469(vw) 1509(vw)	} υ (NH_2)	194,198

	1594(vw)	1590w(w)	1570(w)	*sym* υ (NH_2)	198,199
1647 (vw)					193,197
			1606(w) 1656(w)	} υ (C=C) of ring	8,152,153
			1693(m) 1704 (sh,vw)	} υ (C=O)	8,9,149
	2895(m)	2861(w)	2874(m)	υ (CH_2)	194,197,198
	2927(m)	2927(w)	2913(m)	*sym* (C-H)	192,198
	2974(m)			υ (CH_2)	197
		3188	3108	*sym* υ (N-H)	196,197
		3288(vw)	3275(b,w)	*sym* υ (N-H)	195,196
	3379(vw)	3357(vw)	3365 (b,w) 3396 (b,w)	υ(Si-OH), υ(OH), υ (N–H)	192,195,196

Relative intensities are given in brackets: vs: very strong; s: strong; m: moderate; w: weak; vw: very weak; sh: shoulder. υ: stretching; δ: bending; ϖ: wagging; *p*: rocking; b: broad; asym: asymmetric; sym: symmetric

3.3.2 NMR

^{13}C NMR spectra were recorded to investigate the features of the organic counterpart in the reagents and the materials obtained. Figure 3.3 shows the CP/MAS ^{13}C NMR spectra for PK-PDAP and for the modified final membrane (PA-$SiNH_2$)m. The ^{13}C NMR spectra for the APTES, PEG200 and 1,2DAP reagents, and the MAS ^{13}C NMR spectra of the intermediate solid Si-NH_2 and PK samples, were also recorded, and are shown in Figures 3.4 and 3.5, respectively. Table 3.2 summarizes the chemical shift and peak assignments for the signals observed in the spectra for the reagents, Si-NH_2 and PK. Slight differences in the chemical shift of the same resonances in the pure reagents (Figure 3.4) and intermediate products (Figure 3.5) are to be expected because the spectra for the reagents were obtained using liquid-state NMR.

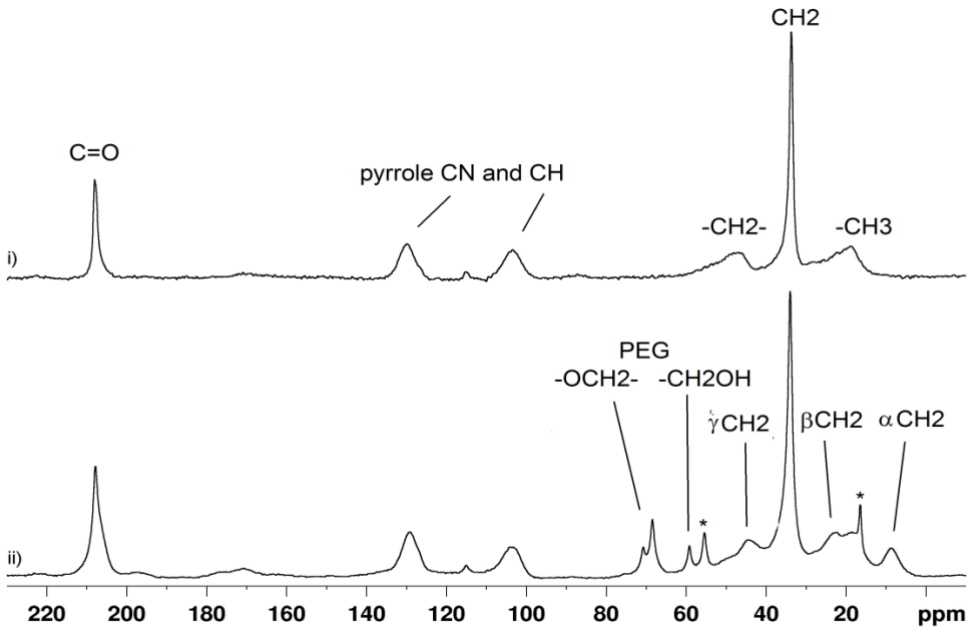

Figure 3.3: CP/MAS ^{13}C NMR spectra for: i) PK-PDAP; and ii) (PA-$SiNH_2$)m**.** Peaks marked with * are attributed to residual EtOH groups.

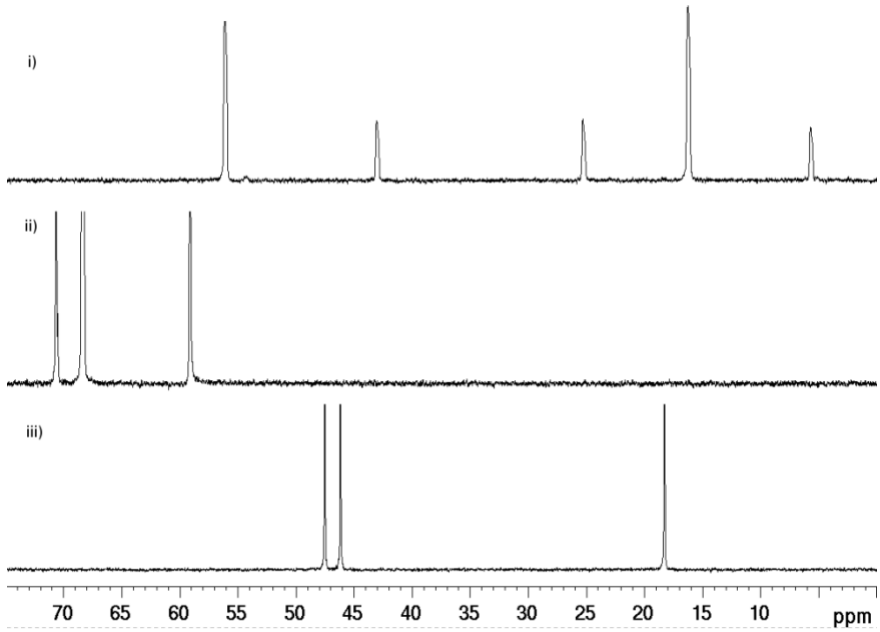

Figure 3.4: ^{13}C NMR spectra for the reagents in CDCl3: i) APTES; ii) PEG200; and iii) 1,2DAP. Spectra acquired with a Bruker 400WB spectrometer operating at a proton frequency of 400.13 MHz, and equipped with a 5 mm BBO double-channel probe**.** ^{13}C frequency: 75.48 MHz, zgig30 pulse sequence, 128 scans.

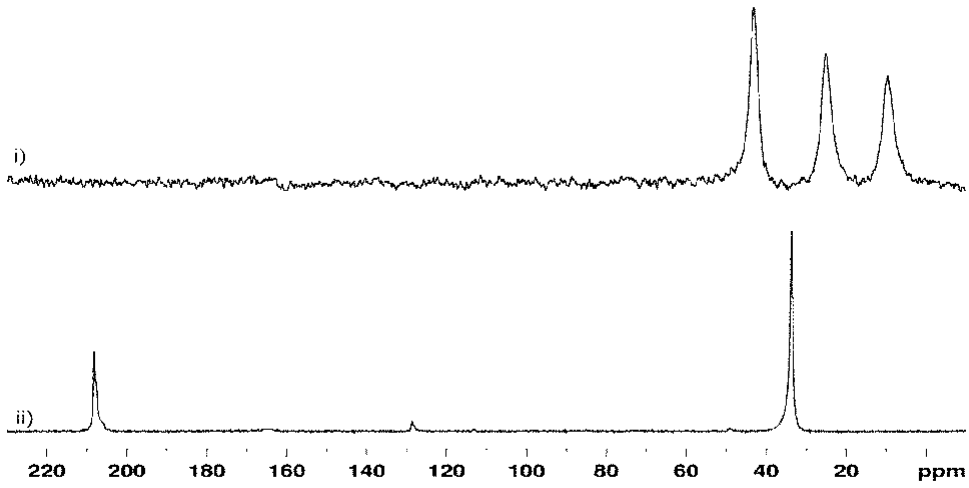

Figure 3.5: CP/MAS ^{13}C NMR spectra for: i) Si-NH_2; and ii) PK.

The Si-NH_2 spectrum (Figure 3.5) is characterized by the presence of signals due to the methylene carbon atoms in the aminopropyl chain linked to Si, while no residual ethoxide groups are detectable. Two intense, sharp peaks, due respectively to ketone and methylene groups, can be seen in the PK spectrum, and are consistent with the polymer's structure (Figure 3.5).

Figure 3.3 shows the ^{13}C NMR spectra for PK-PDAP and the (PA-SiNH_2)m membranes. According to Ataollahi et al. [8,9], Figure 3.3i shows that PK amination takes place, leading to the formation of heterocyclic units (mainly pyrrole rings), as demonstrated by the CN and CH aromatic peaks at 130 and 104 ppm, connected via methylene groups (47 ppm) to the main PK chain. The pyrrole ring keeps the residual part of 1,2DAP as a pendant group, as discernible from the signal of the methyl group (19 ppm). The different linewidths of the signals suggest that the PK chains are more mobile than the chains characterized by the polymer's pyrrole rings.

The (PA-SiNH_2)m membrane is prepared by adding PEG200 and modified silica (Si-NH_2) nanoparticles. The corresponding spectrum (Figure 3.3ii) shows the resonances due to PK-PDAP with a slight broadening, and the signals of the PEG units at 70.9 (intermediate -O$\underline{C}H_2$-), 68.6 (-O$\underline{C}$H-), and 55.5 (terminal -$\underline{C}H_2$OH) ppm, consistently with the data in Table 3.2. The PEG short chains produce sharp signals consistent with their freedom of molecular motion. The three broad signals centered at 44.3, 23.2 and 8.9 ppm, assigned to the methylene carbon atoms in the aminopropyl chain linked to Si (Table 3.2), confirm the presence of the inorganic counterpart (Si-NH_2). There are two other small, sharp peaks at 59.4 and 16.6 ppm, which are tentatively assigned to ethoxide groups linked to silicon atoms.

Table 3.2: Assignment of chemical shifts and peaks in spectra shown in Figures 3.4 and 3.5

PEG200		**1,2DAP**		**PK**		**APTES**		**Si-NH_2**	
δ (ppm)	**Assignment**	**δ (ppm)**	**Assignment**	**δ (ppm)**	**Assignment**	**δ (ppm)**	**Assignment**	**δ (ppm)**	**Assignment**
70.7	-O<u>C</u>$H_2$$CH_2$OH	47.6	H_2N<u>C</u>H<	208.2	>C=O	56.3	-O<u>C</u>$H_2$$CH_3$	-	
68.4	-O<u>C</u>H_2-	46.2	>CH<u>C</u>$H_2$$NH_2$	33.7	-CH_2-	43.2	-<u>C</u>$H_2$$NH_2$ (γ)	43.0	γ
59.2	-<u>C</u>H_2OH	18.4	-<u>C</u>H_3			25.3	-<u>C</u>H_2- (β)	25.0	β
						16.3	-OCH_2<u>C</u>H_3	-	
						5.7	Si<u>C</u>H_2- (α)	9.8	α

In Figure 3.3, the change in the shape of the C=O signal suggests the presence of different environments for the PK chains in the membranes. Figure 3.6 shows the magnification of the carbonyl region of PK, PK-PDAP and (PA-$SiNH_2$)m spectra. Pristine PK reveals two sharp components at 208.2 and 207.7 ppm, together with a broad component probably due to an amorphous phase. The same components are visible in PK-PDAP and (PA-$SiNH_2$)m, but they are much broader, especially in (PA-$SiNH_2$)m (Figure 3.6). Judging from the FTIR results, these findings are perfectly consistent with the XRD findings (chapter 2, page 57), which pointed to the presence of two PK crystalline phases (α and β), due to different chain packing, and one amorphous phase. In PK-PDAP, XRD highlighted a marked decrease in the β phase, and an increase in the amorphous nature of the sample. Accordingly, the different chain packing and the difficulty in crystallizing are clearly enhanced in the (PA-$SiNH_2$)m sample as a consequence of the reaction with modified silica.

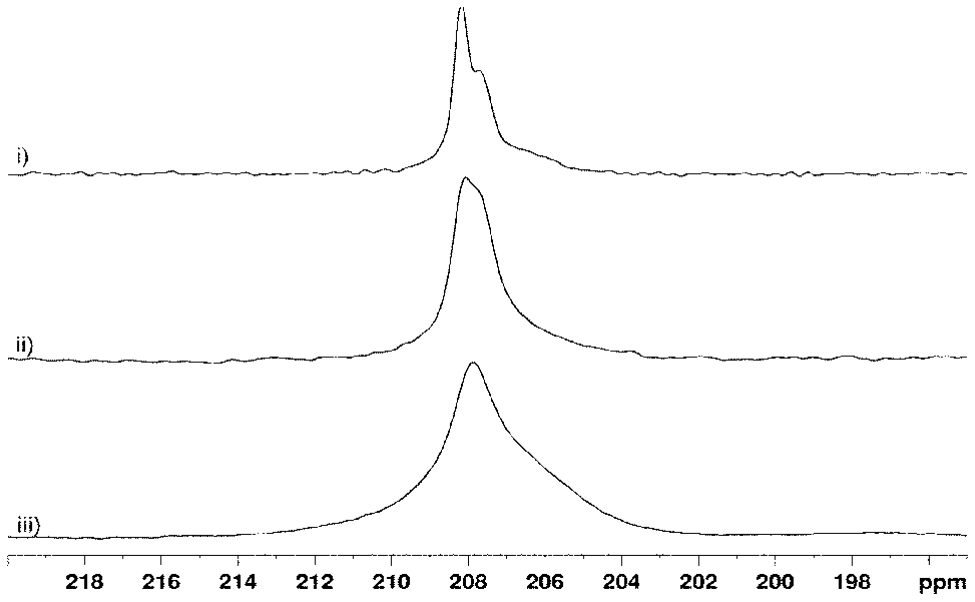

Figure 3.6: CP/MAS ^{13}C NMR magnification of the carbonyl region of the spectra for: i) PK; ii) PK-PDAP; and iii) (PA-$SiNH_2$)m.

The inorganic counterpart of the silica-polyamine composite can be analyzed using ^{29}Si NMR. Judging from the CP/MAS spectra shown in Figure 3.7, resonances due to the Q units can be seen in the spectrum of pristine silica (Figure 3.7i). Reaction with APTES leads to the appearance of signals due to the T units in the range from -50 to -70 ppm (Figure 3.7ii). T and Q resonances are both detectable in the spectrum for (PA-$SiNH_2$)m (Figure 3.7iii), with a remarkably broadening line resulting from the lesser mobility and greater local disorder of the Si units after incorporation in the polymeric network [200]. The T units, and the T^2 units in particular, are submitted in the (PA-$SiNH_2$)m sample to a 1.4 ppm downfield shift with respect to Si-NH_2. Both the broadening line and this small shift may be attributable to the interactions at the interface between the organic host polymer and the organosilica filler [200].

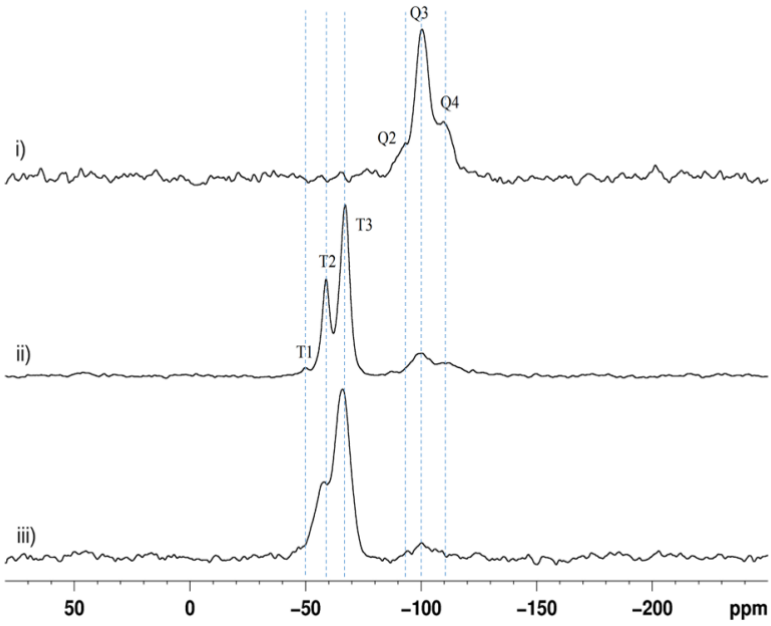

Figure 3.7: CP/MAS ^{29}Si NMR spectra of: (i) pristine SiO_2; (ii) Si-NH_2; and (iii) (PA-$SiNH_2$)m. Dotted lines make it easier to find the T and Q zones.

Table 3.3 provides a summary of the quantitative information obtained by fitting the profiles of the spectra from the MAS experiments (not shown). Comparing pristine SiO_2 with Si-NH_2 reveals the drop in Q^4 units in the modified silica. An experimental T:Q ratio of 3:1 was calculated from the area of the peaks in Si-NH_2, which differs considerably from the nominal ratio (1:1). The low amount of Q units could be due to the preferential formation of silsesquioxane domains by APTES hydrolysis-condensation, to an only partial SiO_2 surface functionalization, and to a loss of silica particles during the washing steps. These effects are probably due to siloxane bonds breaking and particles dissolving under the conditions adopted for the synthesis, i.e. in an alkaline environment and with a long sonication time. The final (PA-SiNH_2)m membrane showed a further increase in partially-condensed units (T^2 and Q^3) at the expense of fully-condensed units (T^3 and Q^4). The total amount of T units was also lower than in the Si-NH_2. These findings can again be attributed to the above-mentioned conditions experienced by the samples during the synthesizing process. As a consequence, the degree of condensation (DOC), calculated according to Figueira et al [200], decreases after the reaction of SiO_2 with APTES, and slightly further again after the incorporation of Si-NH_2 in the membrane.

Table 3.3: Quantitative analysis obtained from MAS ^{29}Si NMR data.

	T1	**T2**	**T3**	**Q3**	**Q4**	**DOC**	**T%**	**(T1+T2)/T3**	**Q3/Q4**
	-49,8	-58,0	-66,1	-99,6	-110,3				
SiO_2	-	-	-	13,5	86,5	96,6	-	-	0,2
$SiNH_2$	2,0	25,1	48,5	5,0	19,5	89,5	75,6	0,6	0,3
(PA-$SiNH_2$)m	-	20,7	21,0	25,3	33,0	87,2	41,7	1,0	0,8

3.3.3 XRD

Figure 3.8(a) shows the XRD patterns for pure the silica (SiO_2), and modified silica (Si-NH_2). Amorphous silica reveals a broad halo around 23º in the XRD pattern [201,202]. By comparison with pure silica, the XRD spectrum of Si-NH_2 shows a halo at 2θ=23º due to

Q unit domains, and a peak at 2θ=8° produced by T unit domains [203], consistently with the NMR results [203].

Figure 3.8(b) shows the XRD patterns of the PK, PK-PDAPm and (PA-$SiNH_2$)m. As reported in chapter 2 [9], both PK and the polyamine membrane revealed the crystalline phases α and β, and an amorphous region. PK-PDAPm appeared to be more amorphous than pristine PK. In particular, the intensity of the β phase in PK-PDAPm, which appeared at 2θ = 21°, was weaker. A similar pattern emerges in the spectra of (PA-$SiNH_2$)m. Due to the incorporation of modified silica in the polyamine matrix, the intensity of the diffraction peak of (PA-$SiNH_2$)m became weaker, implying that the amorphous phase of the membrane increased. These results are perfectly in line with the NMR findings.

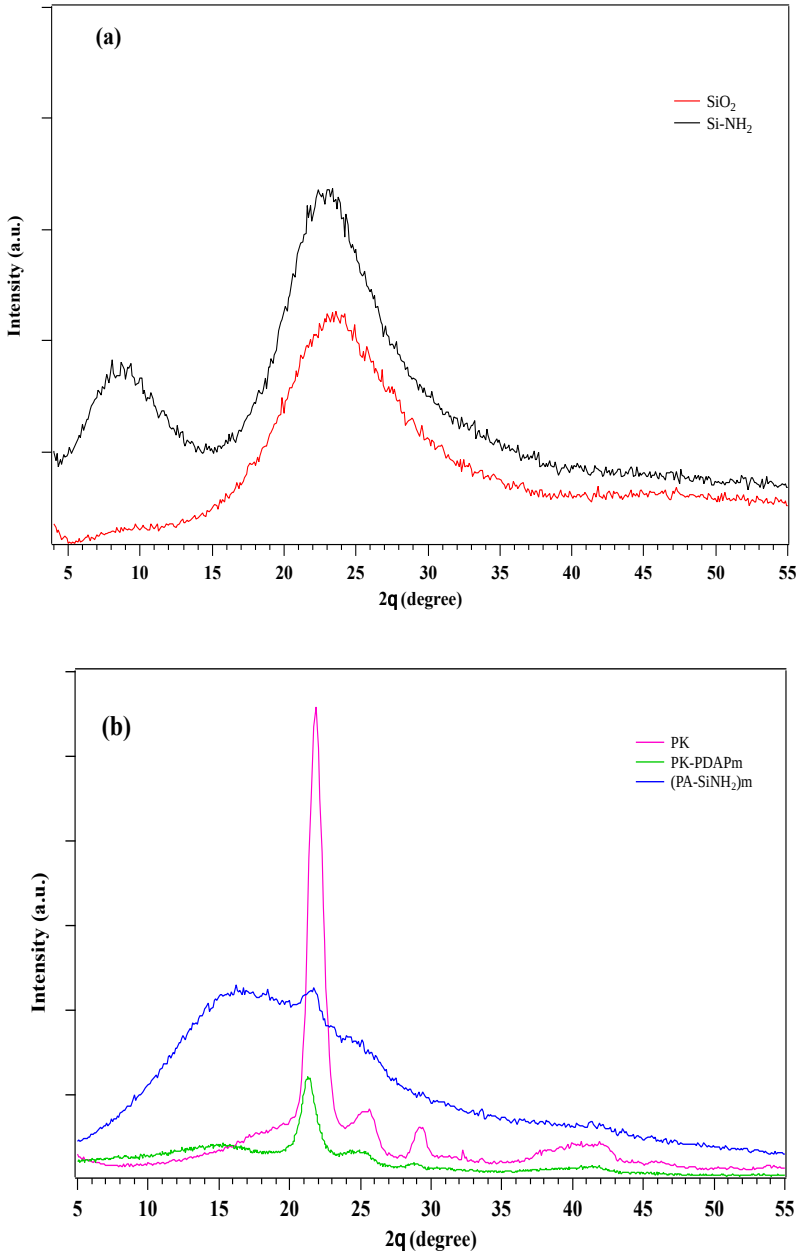

Figure 3.8: XRD spectra for: a) SiO_2 and Si-NH_2; b) PK, PK-PDAPm and (PA-$SiNH_2$)m.

3.3.4 Thermogravimetric analysis

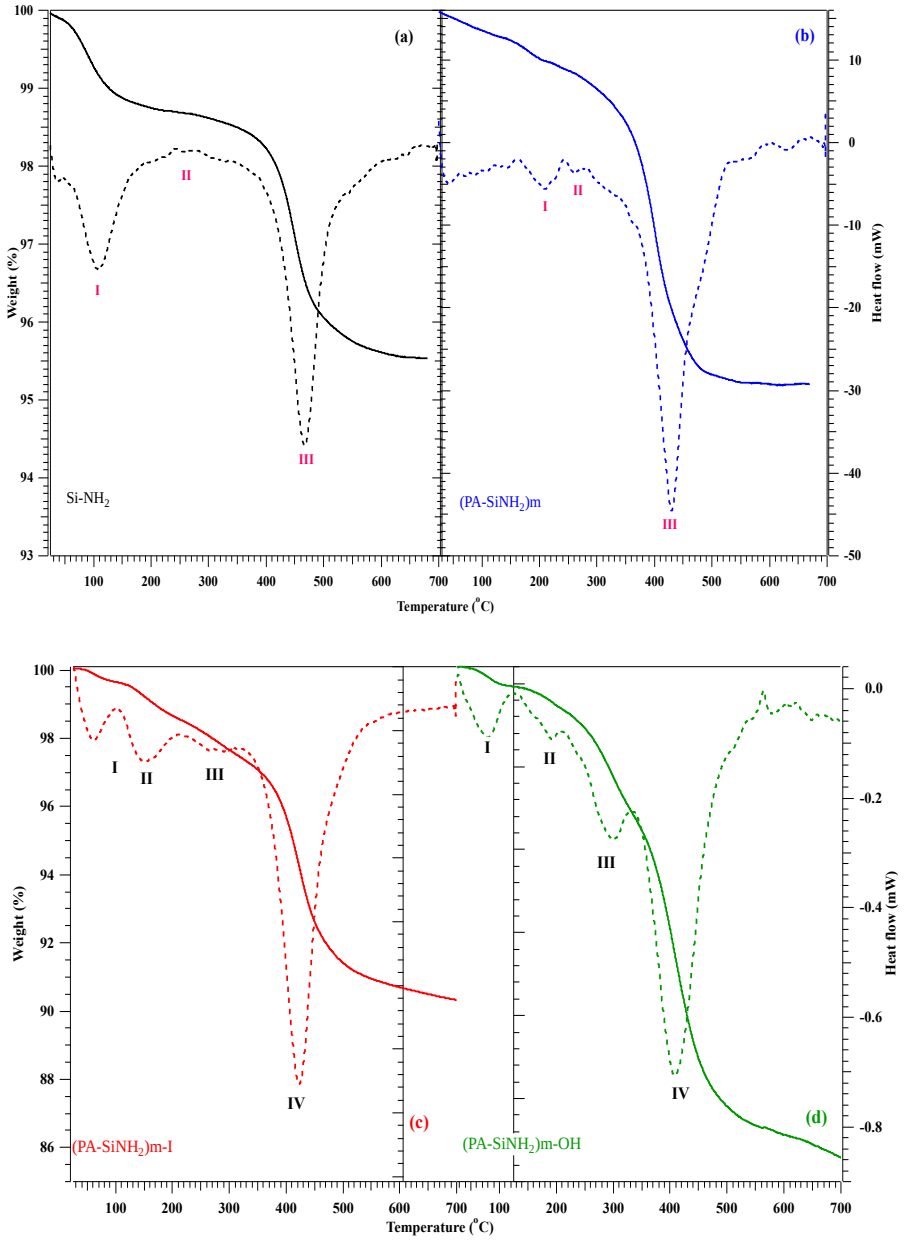

Figure 3.9: Thermogravimetric profiles for: a) Si-NH_2; b) (PA-$SiNH_2$)m; c) modified membrane in iodide form (PA-$SiNH_2$)m-I; d) modified membrane in OH form (PA-$SiNH_2$)m-OH.

Figure 3.9(a) shows the thermogravimetric curve and its derivative for aminopropyl-functionalized silica (Si-NH_2). Si-NH_2 exhibited mass loss in three stages: (I) first at temperatures in the range of 25-200^{o}C due to the elimination of adsorbed water from the silica surface and residual ethanol; (II) then gradually over the temperature range of 200-380^{o}C, with a weight loss of less than 1%, which represents the decomposition of aminopropyl groups; and finally (III) a rapid degradation above 400^{o}C with a 3% weight loss, possibly due to dehydroxylation of Si-OH residual functions leading to the formation of Si-O-Si groups [194].

Figure 3.9(b) shows the effect of functionalized silica on the thermal stability of (PA-$SiNH_2$)m. The membrane's weight loss is distributed over three stages: (I) a first weight loss of 1% at around 25-200°C, due to the elimination of trapped residual solvent; (II) a second at temperatures in the range of 200-300°C, with a 1% weight loss similar to the one seen for Si-NH_2; and (III) a third occurring above 300°C, with a weight loss of 3%, due to decomposition of the soft segment functional groups.

Figure 3.9(c) and (d) show the thermogravimetric curves for the membranes after methylation ([PA-$SiNH_2$]m-I), and after the ion exchange process ([PA-$SiNH_2$]m-OH), respectively. Both thermogravimetric curves exhibited four stages: (I) a first weight loss (1%) at temperatures in the range of 25-100°C on both thermogravimetric plots, which corresponds to the evaporation of residual solvent; (II) a second weight loss from the (PA-$SiNH_2$)m-I at about 100-200°C, due to loss of the amine group (the thermogravimetric curve for [PA-$SiNH_2$]m-OH showed the same behavior); (III) a third weight loss due to cleavage of the methylated group at 300°C with 1% and 7 % weight losses for (PA-$SiNH_2$)m-I and (PA-$SiNH_2$)m-OH, respectively; and (IV) a fourth weight loss starting from when the temperature rose above 350°C, when the polyamine matrix began to decompose. This fourth stage coincided with a 7% weight loss for (PA-$SiNH_2$)m-I, whereas the thermogravimetric profile showed that the final decomposition of (PA-$SiNH_2$)m-OH started already at 300°C, with a greater weight loss (26%). We can conclude

that adding modified silica improves the thermal stability of the membrane (up to 200°C). The interaction between the modified silica and the polymer matrix can reduce the polymer's thermal motion, and the consequently greater energy required for the segmental movement of polymer chain results in a higher thermal stability [195].

3.3.5 Differential scanning calorimetry

In the DSC thermograms for Si-NH_2, (PA-SiNH_2)m, (PA-SiNH_2)m-I and (PA-SiNH_2)m-OH, shown in Figure 3.10, the exothermic peak in the temperature range of 5-50°C is due to order-disorder molecular rearrangements and melting of the nanometric domains. Si-NH_2 exhibited a broad endothermic peak at 160°C, indicating the release of volatile fragments from the sample due to reactions of the residual starting materials and decomposition of the organo-functional group. An additional endothermic peak is visible at temperatures beyond 300°C, corresponding to dehydroxylation and the consequent internal rearrangement of the silica backbone.

The curve for (PA-SiNH_2)m reveals no remarkable exothermic phenomena up to 300°C, probably due to chemical cross-linking and intermolecular cross-linking between Si-NH_2 and the polyamine matrix. Incorporating Si-NH_2 in the polymeric matrix seems to prevent its rearrangement.

The treated membrane (PA-SiNH_2)m-I actually behaves in much the same way as Si-NH_2, and the endothermic phenomena occurred at lower temperatures. The treatment seems to have negatively affected the interaction between the reinforcement phase and the PA. This trend is confirmed by the curve for (PA-SiNH_2)m-OH), and all these results are consistent with those of the TGA, as previously discussed.

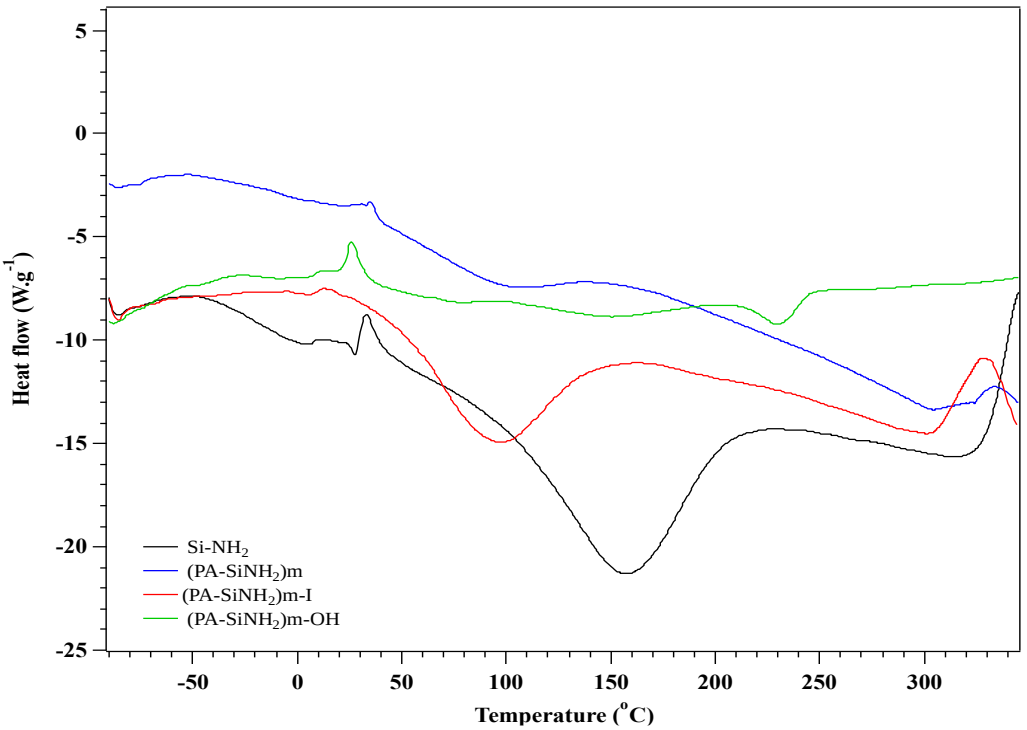

Figure 3.10: DSC thermographs for Si-NH_2, (PA-$SiNH_2$)m, the modified membrane in iodide form (PA-$SiNH_2$)m-I, and the modified membrane in OH form (PA-$SiNH_2$)m-OH.

3.3.6 Water uptake and IEC

To assess the feasibility of a conductive membrane made of these materials, the water uptake of the modified membranes was measured, and the results are shown in Table 3.4. The IEC of the membrane in OH form ([PA-Si-NH_2]mOH) was examined. Alongside the FTIR and NMR results, the IEC values seemed quite high - even compared with the results for the membrane discussed in chapter 2 (page 23) – thus confirming the presence and activity of amine groups.

Table 3.4: Water uptake of different membranes

Membrane	**WU (%)**
(PA-Si-NH_2)m	34±0.31
(PA-Si-NH_2)mI	39±0.36
(PA-Si-NH_2)mOH	43±0.25

The properties of the membranes revealed a structural dependence on the hydrophilicity of the functional group. The (PA-Si-NH_2)mOH had a higher IEC (1.25 ±0.01mmol/g), than the poly(dodoxymethylene norbornene-co-norbornene-3-(trimethylpropyl ammonium)-functionalized silica (1.19 mmol/g) described by He et al [204], implying that tails of modified silica (-NH_2) act as functional groups, improving the general properties of the membrane. The modified membrane also exhibited a relatively higher water uptake compared with the polyamine membrane [8].

3.3.7. Conductivity measurements

Figure 3.11 shows the ionic conductivity of the membranes as a function of temperature. It is clear that raising the temperature increases the ionic conductivity, which reaches a maximum value of 2.4 $\times 10^{-4}$ S cm^{-1} at 130°C for (PA-SiNH_2)m-I, and 4.8 $\times 10^{-4}$ S cm^{-1} at 120°C for (PA-SiNH_2)m-OH. The slight difference in the conductivity of the membrane in OH form may be due to the membranes in hydroxide form absorbing more water than those in the iodide form due to the thermodynamic driving forces involved in hydration [205]. The conductivity of both membranes did not differ significantly from that of the membranes synthesized without adding modified silica (PK-PDAPm[I] & PK-PDAPm[OH]) [8].

Caution is needed in comparing the conductivity values of membranes with and without modified silica for several reasons. First of all, our main aim was to improve thermal stability, and the structure was profoundly modified by adding silica which is an

insulating material. The most significant improvement was obtained in terms of thermal stability, particularly for the (PA-SiNH$_2$)m-OH membrane. This is consistent with the results of TGA (2% mass loss at temperatures in the range of 100-200^{o}C).

Second, there are the different methods used to measure conductivity, which provided different results. The conductivity of PK-PDAPm(I) and PK-PDAPm(OH) was measured using broadband electrical spectroscopy (BES) with a Novocontrol Alpha-A analyzer. The temperature can be controlled with a home-made cryostat operating with a N_2 gas jet heating and cooling system. This instrument can provide detailed information about conductivity measurements, but it is an expensive technique. We recently used Parstat 4000A equipment to perform impedance spectroscopy, which is considered a simple technique, and similar techniques have often been used for conductivity measurements described in the literature.

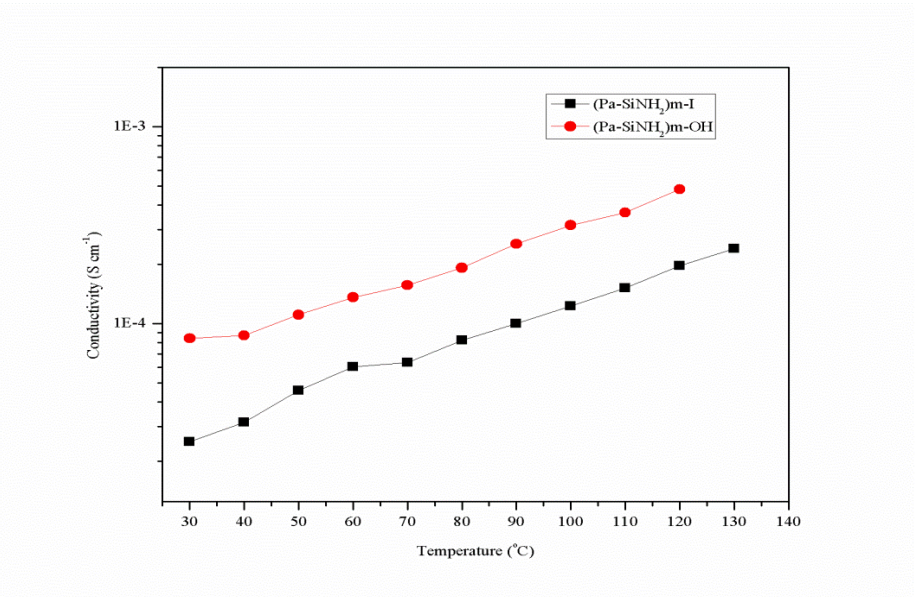

Figure 3.11: Ionic conductivity of (Pa-SiNH$_2$)m-I and (Pa-SiNH$_2$)m-OH membranes vs. temperature.

Figure 3.12 shows the dependence of conductivity on the temperature for (PA-SiNH$_2$)m-I and (PA-SiNH$_2$)m-OH, and Table 3.3 gives the activation energy E_a (kJ mol^{-1}) of the

membranes. As the temperature increases, so does the mobility of both the ions and the polymer chains, and this contributes to enhancing conductivity.

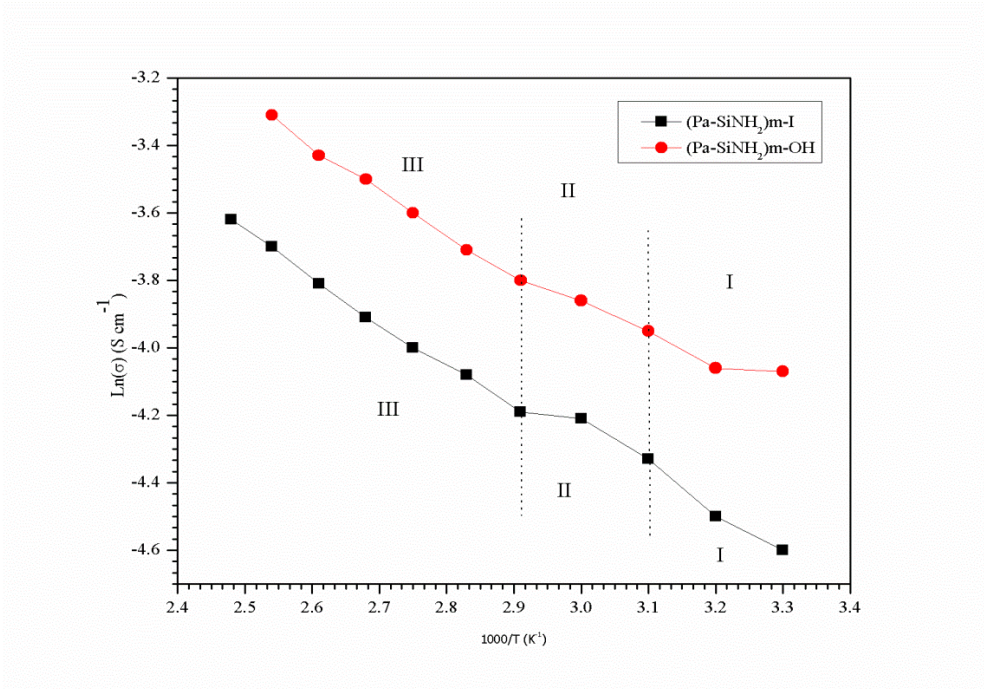

Figure 3.12: Conductivity vs 1/T for (Pa-$SiNH_2$)m-I and (Pa-$SiNH_2$)m-OH membranes. Three conductivity regions are detectable (I, II, & III).

Three conductivity regions (I, II and III) were identified (Figure 3.12). The overall conductivity (σ_T) curve was simulated with the Arrhenius-like equation [164,165]:

$$\sigma_T = A_\sigma . \exp(-E_a|RT) \quad (3.4)$$

where A_σ is the number of charge carriers, R is the universal gas constant, and E_a is the activation energy, expressed with the Vogel-Fulcher-Tammann-like (VFT) equation [164,165-168]

$$\sigma_T = A_\sigma . exp \frac{-E_{a,VFT}}{R(T-T_o)} \quad (3.5)$$

where $E_{a,VFT}$ is the pseudo-activation energy for conduction, and T_0 is the thermodynamic ideal glass transition temperature, with the boundary condition Tg -55 $\leq T_o \geq$ Tg -40 K [166].

In regions I and II, the relationship between conductivity and temperature is non-linear, indicating a VFT behavior. This means that the ionic conductivity of the polymer electrolyte relies mainly on the polymer chain's segmental motion. Region III shows a linear relationship, indicating an Arrhenius behavior. This suggests that the anion transport property is due to an ionic hopping mechanism [8, 167,168, 206]. With rising temperatures, the polymer's segmental movement promotes ionic motion by allowing the ions to transfer from one site to another in the same polymer chain, or to the neighboring polymer chain, resulting in an increased ionic conductivity [206].

Table 3.5: Activation energy of overall conductivity (σ_T) in the three conductivity regions for (Pa-$SiNH_2$)m-I and (Pa-$SiNH_2$)m-OH

Sample	**I**	**II**	**III**
	E_a (KJ/mol)	**E_a (KJ/mol)**	**E_a (KJ/mol)**
(Pa-$SiNH_2$)m-I	^{o}6.20±2.34	^{o}11.22±1.68	*10.98±0.29
(Pa-$SiNH_2$)m-OH	^{o}6.58±0.55	^{o}5.08±2.45	*10.92±0.32

*The value of Ea is determined by fitting the conductivity data with the Arrhenius equation. ^{o}The value of E_a is obtained by fitting the conductivity data with the VFT equation.

3.4 Conclusions

Amine-functionalized silica (Si-NH_2) was synthesized by co-condensation of APTES using the sol-gel method. Si-NH_2 was added to the polyamine polymer to combine the polymer matrix functionalities with the unique properties of the inorganic nanoparticles. In this work, we investigated the effect of Si-NH_2 on the polyamine membrane's thermal properties and structural changes. Combined FTIR, NMR and XRD analyses led to the complete structural characterization of the modified silica active filler, and revealed both a

reinforcement effect and structural changes resulting from its addition to the polyamine membrane. Our results show that the thermal stability of (PA-$SiNH_2$)m was better than that of the corresponding membrane without silica, even after treatments with iodomethane and KOH. (PA-Si-NH_2)mOH proved capable of a higher water uptake (WU=43 %) with an IEC of 1.25 mmol/g. The results showed that ionic conductivity increased with rising temperatures: the highest ionic conductivity being 2.4×10^{-4} S cm^{-1} at 130°C for (PA-$SiNH_2$)m-I, and 4.8×10^{-4} S cm^{-1} at 120°C for (PA-$SiNH_2$)m-OH. Further studies revealed three conductivity regions (I, II and III), indicating that ion transport in both (PA-$SiNH_2$)m-I and (PA-$SiNH_2$)m-OH in regions I and II followed a VFT-like behavior, suggesting that polymer chain segmental motion plays an important part in these regions. Region III followed an Arrhenius behavior, which involved an ion hopping mechanism.

Conclusions and Future work

Conclusions

This work describes the synthesis and characterization of AEMs derived from an alternating aliphatic PK precursor. A summary of the results obtained in the two parts of the study is presented below.

Alternating aliphatic PK, synthesized by copolymerizing carbon monoxide and ethylene using a homogeneous palladium catalyst, proved an excellent polymer building block for the synthesis of functional polymer. AEMs were successfully prepared by chemically modifying PK with primary amine, followed by solution casting, methylation and hydroxide ion exchange processes.

FTIR spectroscopy confirmed the successful synthesis of all systems. In particular, two adjacent carbonyl groups of the polymeric chain reacted with amine to form a pyrrole ring. These changes are revealed by: a lower intensity of the carbonyl group (C=O) at 1689 cm^{-1}; the presence of new peaks (around 754 cm^{-1} and at 919 cm^{-1}) due to out-of-plane vibration of (C-C) in the pyrrole ring, and to out-of-plane bending vibration of (=C-H) in the carbon-carbon double bond; a broad peak at 1567 cm^{-1} corresponding to (C=C) stretching. UV-Vis spectra and NMR spectroscopy also provided evidence of the presence of pyridine units due to molecular rearrangement and crosslinking. This was further supported by DSC, where an endothermic peak observed at T= 98°C related to crosslinking and condensation phenomena. The XRD analysis indicated that the synthesized polymers and derived membranes had a semicrystalline nature. The use of a PK precursor to form AEMs is promising because TGA of all the compounds demonstrated a good thermal stability up to 200°C. The ionic conductivity increases at higher temperatures, up to 120°C. The ionic conductivity of the iodide and

hydroxyl membranes in hydrated form can reach values as high as 9 $x10^{-4}$ $S.cm^{-1}$ at 120°C in the former, and 5 $x10^{-4}$ $S.cm^{-1}$ at 90°C in the latter, with an IEC of 1.11 mmol/g. The temperature dependence of the iodide and hydroxyl membranes' ionic conductivity was studied in both wet and dry conditions. Four conductivity regions (I, II, III and IV) were detected, which corresponded to the thermal transitions measured by DSC. In dry membranes, the conductivity mechanism of regions I and II has an Arrhenius-like behavior as a result of inter-chain ion hopping. The conductivity in region III follows a VFT behavior, indicating that the ionic conductivity depends largely on the polymer chain's segmental motions coupled with charge migration. In wet membranes, conductivity had a VFT-like behavior, suggesting that it relied mainly on the segmental motion of the polymer host.

The second part of the research focused on synthesizing amine-functionalized silica (Si-NH_2) by co-condensation of APTES using the sol-gel method. Si-NH_2 was incorporated in the polyamine polymer with the aim of combining the polymer matrix functionalities with the unique properties of the inorganic nanoparticles. The modified silica and corresponding membranes were structurally characterized with FTIR, NMR and XRD analyses, which showed a reinforcement effect and structural changes. The incorporation of Si-NH_2 clearly improved the membrane's properties, and especially its thermal stability, compared with the pristine polyamine membrane. Water uptake and IEC also improved. The maximum conductivity was obtained at 2.4 $\times10^{-4}$ S cm^{-1} at 130°C for (PA-$SiNH_2$)m-I, and at 4.8 $\times10^{-4}$ S cm^{-1} at 120°C for (PA-$SiNH_2$)m-OH. Further studies indicated that ion transport in the (PA-$SiNH_2$)m-I and (PA-$SiNH_2$)m-OH samples had both a VFT-like and an Arrhenius-like behavior. Their conductivity depended on the number of NH_2 groups. It could be improved by increasing the amine content of the modified polymer. These results demonstrate that such a membrane might have very good prospects for electrochemical applications.

Future work

Having demonstrated the feasibility of AEMs based on modified PK, it would be worth going on to increase the amine content of the modified polymer, to obtain a further improvement in its conductivity. The mechanical properties and chemical stability of the AEMs would also be well worth investigating. Further studies are also needed to better clarify the electrochemical performance of AEMs by means of impedance spectroscopy with a view to applications in vanadium redox flow batteries or alkaline fuel cells, for instance.

References

[1] M. Seno, M. Takagi, K. Takeda, Handbook of Separation Science. Kyoritsu Shuppan Co, Tokyo. (1993).

[2] H. Strathmann, Ion-Exchange Membrane Separation Processes. Elsevier, Amsterdam. (2004).

[3] I. M. Luqman, Ion Exchange Technology I - Theory and Materials. Springer Dordrecht Heidelberg New York London, (2012).

[4] R. K. Nagarale, G. S. Gohil, V. K. Shahi, Recent developments on ion-exchange membranes and electro-membrane processes. Adv Colloid Interface Sci. 119 (2006) 97-130.

[5] X. Tongwen, Ion exchange membranes: state of their development and perspective (Review). Journal of Membrane Science. 263 (2005) 1-29.

[6] M. Y. Kariduraganavar, R. K. Nagarale, A. A. Kittur, S. S. Kulkarni, Ion-exchange membranes preparative methods for electrodialysis and fuel cell applications. Desalination. 197 (2006) 225-246.

[7] Y. Tanaka, Ion exchange membranes: fundamentals and applications. Elsevier, Amsterdam, Netherlands (2007).

[8] N. Ataollahi, K. Vezzù, G. Nawn, G. Pace, G. Cavinato, F. Girardi, P. Scardi, V. Di Noto, R. Di Maggio, A polyketone-based anion exchange membrane for electrochemical applications: synthesis and characterization. Electrochimica Acta. 226 (2017) 148-157.

[9] N. Ataollahi, F. Girardi, E. Cappelletto, K. Vezzù, V. Di Noto, P. Scardi, E. Callone, R. Di Maggio, Chemical modification and structural rearrangements of polyketone-based polymer membrane. J. Appl. Polym. Sci. (2017) DOI: 10.1002/APP.45485.

[10] N. Ataollahi, E. Cappelletto, K. Vezzù, V. Di Noto, G. Cavinato, E. Callone, S. Dirè, P. Scardi, R. Di Maggio, Properties of anion exchange membrane based on polyamine: effect of functionalized silica particles prepared by sol-gel method. Solid State Ionics. (2018)

[11] M. Winter, R. J. Brodd, What are batteries, fuel cells and supercapacitors? Chemical Reviews, 104 (2004) 4245-4269.

[12] Fuel Cell Handbook, (Seventh Edition) by EG&G Technical Services, Inc. Morgantown, West Virginia, (2004).

[13] L. Carrette, K. A. Friedrich, U. Stimming, Fuel cells - fundamentals and applications. Fuel Cells, 1, 5-39 (2001).

[14] H. Strathmann, L. Giorno, E. Drioli, An introduction to membrane science and technology. CNR Servizio Pubblicazioni, (2006).

[15] A. A. Zagorondni, Ion exchange materials: properties and application. Elsevier, Amsterdam, (2006).

[16] D. E. Fenton, J. M. Parker, P.V. Wright, Complexes of alkali metal ions with poly(ethylene oxide). Polymer 14 (1973) 589-1589.

[17] M. Armand, J. Chabagno, M. Duclot, Polyethers as solid electrolytes, in: Fast ion transp. solids: electrodes electrolytes. Proc. Int. Conf., (1979) 131-136.

[18] G. B. Appetecchi, Y. Aihara, B. Scrosati, Investigation of swelling phenomena in PEO-based polymer electrolytes. II. Chemical and electrochemical characterization. Solid State Ionics 170 (2004) 63-72.

[19] H. Hou, G. Sun, R. He, B. Sun, W. Jin, H. Liu, Q. Xin, Alkali-doped polybenzimidazole membrane for alkaline direct methanol fuel cell. Int J Hydrogen Energy 33 (2008) 7172-7176.

[20] A. D. Modestov, M. R. Tarasevich, A. Y. Leykin, V.Y. Filiminov, MEA for alkaline direct ethanol fuel cell with alkali doped PBI membrane and non-platinum electrodes. J Power Sources. 188 (2009) 502-506.

[21] B. Xing, O. Savadogo, Hydrogen/oxygen polymer electrolyte membrane fuel cells (PEMFCs) based on alkaline-doped polybenzimidazole (PBI). Electrochemistry Communications 2 (2000) 697-702.

[22] M. M. Nasef, E. A. Hegazy, Ion exchange membranes by radiation-induced graft copolymerization of polar monomers onto non-polar films: preparations and applications. Prog Polym Sci. 29 (2004) 499-561.

[23] B. R. Einsla, S. Chempath, L. R. Pratt, J. M. Boncella, J. Rau, C. Macomber, B. S. Pivovar, Stability of cations for anion exchange membrane fuel cells. ECS Transactions (2007) 1173-1180.

[24] T. Sata, Studies on ion exchange membranes with permselectivity for specific ions in electrodialysis. Journal of Membrane Science 93 (1994) 117-135.

[25] A. C. Cope, E. R. Trumbull, Olefins from Amines: The Hofmann elimination reaction and amine oxide pyrolysis in organic reactions, R.E. Krieger Publ. Co., Huntington, New York, 1975.

[26] J. R. Varcoe, R. C. T. Slade, E. Lam How Yee, An alkaline polymer electrochemical interface: a breakthrough in application of alkaline anion-exchange membranes in fuel cells. Chemical Communications. (2006) 1428-1429.

[27] H. Herman, R. C. T. Slade, J. R. Varcoe, The radiation-grafting of vinylbenzyl chloride onto poly(hexafluoropropylene-co-tetrafluoroethylene) films with subsequent conversion to alkaline anion-exchange membranes: optimization of the experimental conditions and characterization. Journal of Membrane Science. 218 (2003) 147-163.

[28] T. Cohen, P. Dagard, J. Molenat, B. Brun, C. Gavach, Proton leakage through perfluorinated anion exchange membranes. Journal of Electroanalytical Chemistry. 210 (1986) 329-336.

[29] A. Elmidaoui, A. T. Cherif, J. Brunea, F. Duclert, T. Cohen, C. Gavach, Preparation of perfluorinated ion exchange membranes and their application in acid recovery. Journal of Membrane Science. 67 (1992) 263-271.

[30] K. Haagen, F. Helfferich, Ion-exchange membrane. Ger Patent 971 (1961)729.

[31] T. M. Aminabhavi, P. V. Kulkarni, M. Y. Kariduraganavar, Ion exchange membranes, methods and processes for production thereof and uses in specific applications. US Patent 6 (2004) 814-865.

[32] Y. Wan, B. Peppley, K. A. M. Creber, V. T. Bui, E. Halliop, Quaternized-chitosan membranes for possible applications in alkaline fuel cells. Journal of Power Sources. 185 (2008) 183-187.

[33] G. W. Bodamer, (Rohm and Hass) (1954) US Patents 2,681,319 (1954), 2,681,320 2,737,486 (1956).

[34] A. B. Yaroslavtsev, V. V. Nikonenko, Ion-exchange membrane materials: properties, modification, and practical application. Nanotechnol in Russia. 4 (2009)137-159.

[35] E. B. Trostyanskaya , S. B. Makarova, Anion-exchange resins in the class of onium compounds. Zh Prikl Khim. 39 (1966)1754-1760.

[36] G. Couture, A. Alaaeddine, F. Boschet, B. Ameduri, Polymeric materials as anion-exchange membranes for alkaline fuel cells. Progress in Polymer Science. 36 (2011) 1521-1557.

[37] T. Sata, M. Tsujimoto, T. Yamaguchi, K. Matsusaki, Change of anion exchange membranes in an aqueous sodium hydroxide solution at high temperature. J Membr Sci. 112 (1996) 161-170.

[38] M. L. Perry, T. F. Fuller, A historical perspective of fuel cell technology in the 20th century. Journal of the Electrochemical Society. 149 (2002) 59-67.

[39] L. Xianguo, Principles of Fuel Cells. New York: Taylor & Francis Group, (2006).

[40] S. J. Peighambardoust, S. Rowshanzamir, M. Amjadi, Review of the proton exchange membranes for fuel cell applications. International Journal of Hydrogen Eenergy. 35 (2010) 9349-9384.

[41] J. H. Reid, Process of Generating Electricity. US Patent 736,016, (1903).

[42] G. Erich, Alkaline fuel cell: a critical view. J. Power Sources, 61 (1996) 99-104.

[43] M. A. Abdel Rahim, R. M. Abdel Hameed, M. W. Khalil, Nickel as a catalyst for the electro-oxidation of methanol in alkaline medium. J. Power Sources, 134 (2004) 160-169.

[44] A. L. Dicks, Hydrogen generation from natural gas for the fuel cell systems of tomorrow. Journal of Power Sources. 61 (1996) 113-124.

[45] A. G. Stern, Design of an efficient, high-purity hydrogen generation apparatus and method for a sustainable, closed clean energy cycle. International Journal of Hydrogen Energy. 40 (2015) 9885-9906.

[46] R. D. Noble, A. S. Stern, Membrane Separations Technology: Principles and Applications, Elsevier, Amsterdam (1995).

[47] H. Zhang, H. Zhang, X. Li, Z. Mai, W. Wei, Silica modified nanofiltration membranes with improved selectivity for redox flow battery application. Energy & Environmental Science. 5 (2012) 6299-6303.

[48] B. M. Carter, B. R. Wiesenauer, R. D. Noble, D. L. Gin, Thin-film composite bicontinuous cubic lyotropic liquid crystal polymer membranes: effects of anion-exchange on water filtration performance. Journal of Membrane Science. 455 (2014) 143-151.

[49] R. J. Petersen, Composite reverse osmosis and nanofiltration membranes. J. Membr. Sci. 83 (1993) 81-150.

[50] R.W. Baker, Membrane technology and applications, McGraw-Hill, New York, (2000).

[51] H. Strathmann, Electrodialysis, a mature technology with a multitude of new applications. Desalination. 264 (2010) 268-288.

[52] N. U. Afsar, B. Erigene, M. Irfan, B. Wu, T. Xu, W. Ji, K. Emmanuel, L. Gea, T. Xu, High-performance anion exchange membrane with proton transport pathways for diffusion dialysis. Separation and Purification Technology. 193 (2018) 11-20.

[53] J. Luo, C. Wu, T. Xu, Y. Wu, Diffusion dialysis-concept, principle and applications. J. Membr. Sci. 366 (2011)1-16.

[54] D. H. Kim, A review of desalting process techniques and economic analysis of the recovery of salts from retentates. Desalination. 270 (2011)1-8.

[55] M. I. Khan, S. Akhtar, S. Zafar, A. Shaheen, M. A. Khan, R. Luque, Removal of Congo red from aqueous solution by anion exchange membrane (EBTAC): adsorption kinetics and themodynamics. Materials. 8 (2015) 4147-4161.

[56] D. Langevin, M. Pinoche, E. Se, M. Me, R. Roux, CO_2 facilitated transport through functionalized cation-exchange membranes. J. Membr. Sci. 82 (1993) 51-63.

[57] M. I. Khan, R. Luque, Sh. Akhtar, A. Shaheen, A. Mehmood, S. Idress, S. A. Buzdar, A. Rehman, Design of anion exchange membranes and electrodialysis studies for water desalination. Materials. 9 (2016) 365; doi:10.3390/ma9050365.

[58] Ch. Choia, S. Kima, R. Kima, Y. Choia, S. Kimb, H. Jungc, J. H. Yangd, H. T. Kima, A review of vanadium electrolytes for vanadium redox flow batteries. Renewable and Sustainable Energy Reviews 69 (2017) 263-274.

[59] D. Chen, M. A. Hickner, E. Agar, E. C. Kumbur, Selective anion exchange membranes for high coulombic efficiency vanadium redox flow batteries. Electrochemistry Communications. 26 (2013) 37-40.

[60] C. Berthier, W. Gorecki, M. Minier, M. B. Armand, J. M. Chabagno, P. Rigaud, Microscopic investigation of ionic conductivity in alkali metal salts-poly (ethylene oxide) adducts. Solid State Ionics 11(1) (1983) 91-95.

[61] De Grotthuss CJT. Ann Chim (Paris) 1806; 58:54.

[62] K. D. Kreuer, S. J. Paddison, E. Spohr, M. Schuster, Transport in proton conductors for fuel-cell applications: simulations, elementary reactions, and phenomenology. Chem Rev. 104 (2004) 4637-4678.

[63] A. Z. Weber, J. Newman, Transport in polymer-electrolyte membranes. II. Mathematical model. Journal of the Electrochemical Society. 151 (2004) 311-325.

[64] J. F. Nagle, H. J. Morowitz, Molecular mechanisms for proton transport in membranes, P Natl Acad Sci USA, 75 (1978) 298-302.

[65] S. J. Peighambardoust, S. Rowshanzamir, M. Amjadi, Review of the proton exchange membranes for fuel cell applications. International Journal of Hydrogen Energy. 35 (2010) 9349-9384.

[66] G. Merle, M. Wessling, K. Nijmeijer, Anion exchange membranes for alkaline fuel cells: a review. Journal of Membrane Science. 377 (2011) 1-35.

[67] M. E. Tuckerman, D. Marx, M. Parrinello, The nature and transport mechanism of hydrated hydroxide ions in aqueous solution. Nature. 417 (2002) 925-929.

[68] N. Agmon, Mechanism of hydroxide mobility. Chemical Physics Letters. 319 (2000) 247-252.

[69] C. Chen,Y. L. Steve Tse, G. E. Lindberg, C. Knight, G. A. Voth, Hydroxide solvation and transport in anion exchange membranes. Journal of the American Chemical Society. 138 (2016) 991-1000.

[70] H. Takaba, T. Hisabe, T. Shimizu, M. K. Alam, Molecular modelling of OH transport in poly(aryleneethersulfone ketone)s containing quaternized ammonio-substituted fluorenyl groups as anion exchange membranes. Journal of Membrane Science. 522 (2017) 237-244.

[71] K. N. Grew, W. K. S. Chiu, A dusty fluid model for predicting hydroxyl anion conductivity in alkaline anion exchange membranes. Journal of the Electrochemical Society. 157 (2010) 327-337.

[72] T. Luo, S. Abdu, M. Wessling, Selectivity of ion exchange membranes: a review. Journal of Membrane Science https://doi.org/10.1016/j.memsci.2018.03.051

[73] A. Amel, N. Gavish, L. Zhu, D. R. Dekel, M. A. Hickner, Y. E. Eli, Bicarbonate and chloride anion transport in anion exchange membranes. Journal of Membrane Science. 514 (2016) 125–134.

[74] D. I. Dintses, Byull. Vses. Khim. O-va im. D.I. Mendeleeva , 10 (1939) 31.

[75] DE 863711 (1941), Farbenfabriken Bayer, invs.: F. Ballauf, O. Bayer, and L. Leichmann.

[76] W. Reppe, A. Mangini, US Patent No. 2, 577, 208, (1951).

[77] W. Reppe, A. Mangini, G. Patent No. 880, 297, (1948).

[78] M. M. Brubaker, US Patent No. 2,495,286, (1950).

[79] A. Sommazzi, F. Garbassi, Olefin-carbon monoxide copolymers, Prog. Polym. Sci. 22 (1997) 1547-1605.

[80] W. C. J. Zuiderduin1, J. Hue´tink, R. J. Gaymans, Rigid particle toughening of aliphatic polyketone. Polymer. 47 (2006) 5880-5887.

[81] E. Drent, P. H. M. Budzelaar, Palladium-catalyzed alternating copolymerization of alkenes and carbon-monoxide. Chem. Rev 96 (2) (1996) 663-681.

[82] J. M. Lagarona, M. E. Vickersb, A. K. Powella, N. S. Davidson, Crystalline structure in aliphatic polyketones, Polymer .41 (2000) 3011-3017.

[83] C. Bianchini, A. Meli, Alternating copolymerization of carbon monoxide and olefins by single-site metal catalysis. Coordination Chemistry Reviews. 225 (2002) 35-66.

[84] G. A. Holt, JR., J. E. Spruiell. Melting and crystallization behavior of aliphatic polyketones. Journal of Applied Polymer Science .83 (2002) 2124-2142.

[85] W. C. J. Zuiderduin, D. S. Homminga, H. J. Hue´tink, R. J. Gaymans, Influence of molecular weight on the fracture properties of aliphatic polyketone terpolymers. Polymer .44 (2003) 6361-6370.

[86] J. T. Guo, Y. Q. Ye, Sh. Gao, Y. K. Feng, Synthesis of polyketone catalyzed by Pd/C catalyst. Journal of Molecular Catalysis A: Chemical. 307 (2009) 121-127.

[87] W. P. Mul, H. Dirkzwager, A. A. Broekhuis, H. J. Heeres, A. J. van der Linden, A. G. Orpen, Highly active, recyclable catalyst for the manufacture of viscous, low molecular weight, CO-ethene-propene-based polyketone, base component for a new class of resins. Inorg. Chim. Acta. 327 (1) (2002) 147-159.

[88] C. Bianchini, A. Meli, Alternating copolymerization of carbon monoxide and olefins by single-site metal catalysis. Coord. Chem. Rev. 225 (2002) 35-66.

[89] J. G. Bonner, A. K. Powell, In Proceedings of 213 National ACS Meeting, Chemistry Publications, San Francisco, (1997).

[90] J. G. Bonner , A. K. Powell, New Plastics'98, London, (1998).

[91] A. Akelah, A. Moet, Functionalized polymers and their applications. 1st Edition, Chapman and Hall, London, (1990).

[92] L. D. Loan, F. H. Winslow, Reactions of macromolecules. in Macromolecules: An Introduction to Polymer Science. Academic Press, New York, (1979).

[93] J. A. Moore, Reactions of polymers, Proceedings of the NATO Advanced Study Institute held at Rensselaer Polytechnic Institute, Trony, USA, (1973).

[94] E. Charles, J. R. Carraher, M. Tsuda, Introduction: Polymer modification - some problems and possibilities - areas in need of research. ACS Symposium Series; American Chemical Society: Washington, DC, (1980).

[95] M. M. Brubaker, D. D. Coffman, H. H. Hoehn, Synthesis and characterization of ethylene/carbon monoxide copolymers, a new class of polyketones. J. Am. Chem. Soc. 74 (1952) 1509-1515.

[96] J-T. Chen, Y-S. Yeh, A. Sen, Synthesis and characterization of N-substituted poly(ethylenepyrrole): functionalization of ethylene-carbone monoxide alternating copolymers. J. Chem. Soc., Chem. Commun. 14 (1989) 965-967.

[97] S-Y. Lu, R. M. Paton, M. J. Green, A. R. Lucy, Synthesis and characterization of polyketoximes derived from alkene-carbon monoxide copolymers. Eur. Polym. J. 32 (1996) 1285-1288.

[98] Z. Jiang, S. Sanganeria, A. Sen, Polymer incorporating backbone thiophene, furan, and alcohol functionalities formed through chemical modifications of alternating olefin-carbon monoxide copolymers. J. Polym. Sci., Part A: Polym. Chem. 32 (1994) 841-847.

[99] M. J. Green, A. R. Lucy, S-Y. Lu, R. M. Paton, Functionalisation of alkene-carbon monoxide alternating copolymers via tranketalisation reactions. J. Chem. Soc., Chem. Commun. 18 (1994) 2063-2064.

[100] EP 0412671A1, The British Petroleum Company p.I.c., inv.: A. R. Lucy. (1991).

[101] D. D. Coffman, H. H. Hoehn, J. T. Maynard, Reductive amination of ethylene/carbone monoxide polyketones. A new class of polyamines. J. Am. Chem. Soc. 76 (1954) 6394-6399.

[102] US 2599501, E. I. du Pont de Nemours & Company, inv.: R. W. Upson. (1952).

[103] N. Nozaki, N. Kosaka, V. M. Grabner, T. Hiyama, Macromolecules. 34 (2001) 6167.

[104] US 2495293 (1950), E. I. du Pont de Nemours & Company, inv.: S. L. Scott.

[105] R. H. Michel, W. A. Murphey, Intramolecular rearrangements of polyketones. J. Polym. Sci. 55 (1961) 741-751.

[106] B. K. Banik, I. Banik, M. Renteria, S. K. Dasgupta, A straightforward highly efficient Paal-Knorr synthesis of pyrroles. Tetrahedron Letters 46 (2005) 2643-2645.

[107] J. Chen, Y. Yeh, A. Sen, Chem Commun 1989, 965.

[108] A. Sen, Z. Jiang, J. Chen, Macromolecules 1989, 22, 2012.

[109] B. Wang, Y. Gu, Ch. Luo, T. Yang, L.Yang, J. Suo, Pyrrole synthesis in ionic liquids by Paal-Knorr condensation under mild conditions. Tetrahedron Letters. 45 (2004) 3417-3419.

[110] J. Chen, H. Wu, Z. Zheng, C. Jin, X. Zhang, W. Sua, An approach to the Paal-Knorr pyrroles synthesis catalysed by $Sc(OTf)_3$ under solvent-free conditions. Tetrahedron Letters 47 (2006) 5383-5387.

[111] Y. Zhang, A. A. Broekhuis, M. C. A. Stuart, F. Picchioni, Polymeric amines by chemical modifications of alternating aliphatic polyketones. Journal of Applied Polymer Science 107 (2008) 262-271.

[112] Y. Zhang, A. A. Broekhuis, F. Picchioni, Aqueous polymer emulsions by chemical modifications of thermosetting alternating polyketones. Journal of Applied Polymer Science. 106 (2007) 3237-3247.

[113] C. Toncelli, D. C. De Reus, F. Picchioni, A. A. Broekhuis, Properties of reversible diels-alder furan/ maleimide polymer networks as function of crosslink density macromol. Chem. Phys. 213 (2012) 157-165.

[114] A. I. Hamarneh, H. J. Heeres, A. A. Broekhuis, K. A. Sjollema, Y. Zhang, F. Picchioni, Use of soy proteins in polyketone-based wood adhesives. International Journal of Adhesion & Adhesives. 30 (2010) 626-635.

[115] A. I. Hamarneh, H. J. Heeres, A. A. Broekhuis, F. Picchioni, Extraction of Jatropha curcas proteins and application in polyketone-based wood adhesives. International Journal of Adhesion & Adhesives. 30 (2010) 615-625.

[116] C. Toncelli, S. Bouwhuis, A. A. Broekhuis, F. Picchioni, Cyclopentadiene-functionalized polyketone as self-cross-linking thermo-reversible thermoset with increased softening temperature. J. APPL. POLYM. SCI. (2016) DOI: 10.1002/APP.42924.

[117] V. Di Noto, T. A. Zawodzinski, A. M. Herring, G. A. Giffin, E. Negro, S. Lavina, Polymer electrolytes for a hydrogen economy. Int. J. Hydrogen Energy. 37 (2012) 6120-6131.

[118] J. Kim, T. Momma, T. Osaka, Cell performance of Pd-Sn catalyst in passive direct methanol alkaline fuel cell using anion exchange membrane. J. Power Sources 189 (2009) 999-1002.

[119] N. Wagner, M. Schulze, E. Gülzow, Long-term investigations of silver cathodes for alkaline fuel cells. J. Power Sources 127 (2004) 264-272.

[120] J. R. Varcoe, R. C. T. Slade, Prospects for alkaline anion-exchange membranes in low temperature fuel cells. Fuel Cells 5 (2005) 187-200.

[121] J. Wind, R. Späh, W. Kaiser, G. Böhm, Metallic bipolar plates for PEM fuel cells. J. Power Sources 105 (2002) 256-260.

[122] Y. J. Wang, J. Qiao, R. Baker, J. Zhang, Alkaline polymer electrolyte membranes for fuel cell applications. Chem. Soc. Rev 42 (2013) 5768-5787.

[123] D. Chen, M. A. Hickner, E. Agar, E. C. Kumbur, Optimized anion exchange membranes for vanadium redox flow batteries. ACS Appl. Mater. Interfaces 5 (2013) 7559–7566.

[124] Y. Leng, G. Chen, A.J. Mendoza, T.B. Tighe, M.A. Hickner, C.Y. Wang, Solid-state water electrolysis with an alkaline membrane. J. Am. Chem. Soc. 134 (2012) 9054-9057.

[125] W. Garcia-Vasquez, L. Dammaka, C. Larchet, V. Nikonenko, N. Pismenskaya, D. Grande, Evolution of anion-exchange membrane properties in a full-scale electrodialysis stack. J. Membr. Sci. 446 (2013) 255-265.

[126] T. P. Pandey, H. N. Sarode, Y. Yang, Y. Yang, K. Vezzù, V. Di Noto, S. Seifert, D. M. Knauss, M. W. Liberatore, A. M. Herring, A highly hydroxide conductive, chemically stable anion exchange membrane poly(2,6 dimethyl 1,4 phenylene oxide)-b-poly(vinyl benzyl trimethyl ammonium), for electrochemical applications. J. Electrochem. Soc. 163 (2016) 513-520.

[127] V. Di Noto, G. A. Guinevere, K. Vezzù, G. Nawn, F. Bertasi, T.-H. Tsai, A. Maes, S. Seifert, B. Coughlin, A. Herring, Interplay between solid state transitions, conductivity mechanism, and electrical relaxations in a [PVBTMA][Br]-b-PMB diblock copolymer membrane for electrochemical applications. Phys. Chem. Chem. Phys. 17 (2015) 31125-311139.

[128] T. P. Pandey, A. M. Maes, H. N. Sarode, B. D. Peters, S. Lavina, K. Vezzu, Y. Yang, S. D. Poynton, J. R. Varcoe, S. Seifert, M. W. Liberatore, V. Di Noto, A. M. Herring, Interplay between water uptake, ion interactions, and conductivity in an e-beam grafted poly(ethylene-co-tetrafluoroethylene) anion exchange membrane. Phys. Chem. Chem. Phys. 17 (2015) 4367-4378.

[129] H. Sarode, M. A. Vandiver, Y. Liu, A. M. Maes, T.P. Pandey, S. Piril Ertem, T. Tsai, B. Zhang, D. C. Herbst, G. E. Lindberg, Y.-L.S. Tse, S. Seifert, V. Di Noto, E. B. Coughlin, Y. Yan, G. A. Voth, T. A. Witten, D. Knauss, M.W. Liberatore, A. M. Herring, Thin robust anion exchange membranes for fuel cell applications. ECS Trans. 64 (2014) 1185-1194.

[130] G. A. Giffin, S. Lavina, G. Pace, V. Di Noto, Interplay between the structure and relaxations in selemion AMV hydroxide conducting membranes for AEMFC applications. J. Phys. Chem. C 116 (2012) 23965-23973.

[131] D. Valade, F. D. R. Boschet, B. Améduri, Synthesis and modification of alternating copolymers based on vinyl ethers, chlorotrifluoroethylene, and hexafluoropropylene. Macromolecules 42 (2009) 7689-7700.

[132] J. R. Varcoe, R. C. T. Slade, E. Lam How Yee, S. D. Poynton, D. J. Driscoll, D. C. Apperley, Poly (ethylene-co-tetrafluoroethylene)-derived radiation-grafted anion-exchange membrane with properties specifically tailored for application in metal-cation-free alkaline polymer electrolyte fuel cells. Chem. Mater. 19 (2007) 2686-2693.

[133] M. S. Huda, R. Kiyono, M. Tasaka, T. Yamaguchi, T. Sata, Thermal membrane potential across anion-exchange membranes with different benzyltrialkylammonium groups. Sep. Purif. Technol. 14 (1998) 10-95.

[134] E. S. Dragan, E. Avram, D. Axente, C. Marcu, Ion-exchange resins. III. Functionalization-morphology correlations in the synthesis of some macroporous, strong basic anion exchangers and uranium-sorption properties evaluation. J. Polym. Sci. A: Polym. Chem. 42 (2004) 2451-2461.

[135] V. Di Noto, E. Negro, S. Polizzi, K. Vezzù, L. Toniolo, G. Cavinato, Synthesis studies and fuel cell performance of core-shell electrocatalysts for oxygen reduction reaction based on a PtNix carbon nitride shell and pyrolyzed polyketone nanoball core. Int. J. Hydrogen Energy 39 (2014) 2812-2827.

[136] B. L. Rivas, E. D. Pereira, I. Moreno-Villoslada, Water-soluble polymer–metal ion interactions. Prog. Polym. Sci. 28 (2003) 173-208.

[137] S. Liu, S. P. Armes, Recent advances in the synthesis of polymeric surfactant. Curr. Opin. Colloid Interface Sci. 6 (2001) 249-256.

[138] T. Radeva, Physical Chemistry of Polyelectrolytes. CRC Press, 2001.

[139] A. A. Zagorodni, Ion Exchange Materials: Properties and Applications, 1st ed., Elsevier Science, 2006.

[140] C. Toncelli, A. Haijer, F. Alberts, A. A. Broekhuis, F. Picchioni, The green route from carbon monoxide fixation to functional polyamines: a class of high-performing metal ion scavengers. Ind. Eng. Chem. Res. 54 (2015) 9450-9457.

[141] G. J. Hwang, S. G. Lim, S.Y. Bong, Ch. H. Ryu, H. S. Choi, Preparation of anion exchange membrane using polyvinyl chloride (PVC) for alkaline water electrolysis. Korean J. Chem. Eng. 32 (9) (2015) 1896-1901.

[142] S. Yun, J. Parrondo, V. Ramani, Derivatized cardo-polyetherketone anion exchange membranes for all-vanadium redox flow batteries. J. Mater. Chem. A 2 (2014) 6605-6615.

[143] G. Cavinato, L. Toniolo, Carbonylation of ethene catalysed by Pd(II)-phosphine complexes. Molecules 19 (2014) 15116-15161.

[144] V. Di Noto, E. Negro, S. Polizzi, K. Vezzu, L. Toniolo, G. Cavinato, Synthesis, studies and fuel cell performance of core-shell electrocatalysts for oxygen reduction reaction based on a PtNix carbon nitride shell and a pyrolyzed polyketone nanoball core. Int. J. Hydrogen Energy 39 (2014) 2812-2827.

[145] B. Delley, From molecules to solids with the DMo1^3 approach. J. Chem. Phys. 2000, 113, 7756.

[146] http://www.astom-corp.jp/en/index.html.

[147] A. Jikihara, R. Ohashi, Y. Kakihana, M. Higa, K. Kobayashi, Electrodialytic transport properties of anion-exchange membranes prepared from poly(vinyl alcohol) and poly(vinyl alcohol-co-methacryloyl aminopropyl trimethyl ammonium chloride). Membranes 3 (2013) 1-15, doi:http://dx.doi.org/ 10.3390/membranes3010001.

[148] R. Sulcis, F. Vizza, W. Oberhauser, F. Ciardelli, R. Spiniello, N.T. Dintcheva, Recycling ground tire rubber (GTR) scraps as high-impact filler of in situ produced polyketone matrix. Polym. Adv. Technol. (2014) 1060-1068.

[149] O. Ohsawa, K.H. Lee, B.S. Kim, S. Lee, I.S. Kim, Preparation and characterization of polyketone (PK) fibrous membrane via electrospinning. Polymer 51 (2010) 2007-2012.

[150] S. De Vito, F. Ciardelli, E. Benedetti, E. Bramanti, Thermal phase-transitions of carbon monoxide-ethylene alternating copolymer- a FTIR study. Polym. Adv. Technol. 8 (1997) 53-62.

[151] H. Xia, Y. Hashimoto, T. Morita, T. Hirai, Formation of polyketone particle structure by hexafluoroisopropanol solvent evaporation and effects of plasticizer addition. J. Polym. Sci. B: Polym. Phys. 52 (2014) 887-892.

[152] The Handbook of Infrared and Raman Characteristic Frequencies of Organic Molecules, 1st ed., Lin-Vien & Colthup & Fateley & Grasselli, 1991.

[153] Introduction to Spectroscopy. Donald L. Pavia, Gary M. Lampman, George S. Kriz, 4th ed., (2009).

[154] E. B. Fox, T. Smith, T. K. Williamson, S. E. Kendrick, Aging effects on the properties of imidazolium, quaternary ammonium, pyridinium, and pyrrolidinium-based ionic liquids used in fuel and energy production. Energy Fuels 27 (2013) 6355-6636.

[155] M. Suarez, D. Molero, E. Salfran, H. Rodriguez, J. Caro, E. Saez, R. Martinez-Alvarez, N. Martin, NMR study of 1,4-dihydropyridine derivatives endowed with long alkyl and functionalized chains. J. Braz. Chem. Soc, 22 (1) (2011) 166-171.

[156] J. A. Dasilva, C. S. Barria, C. Jullian, P. Navarrete, L. N. Vergara, J. A. Squella. Unexpected diastereotopic behavior in the 1H NMR spectrum of 1,4-dihydropyridine derivatives triggered by chiral and prochiral centres. J. Braz. Chem. Soc, 16 (1) (2005)112-115.

[157] D. N. Huyen, N. T. Tung, T. D. Vinh, N. D. Thien, Synergistic effects in the gas sensitivity of polypyrrole/single wall carbon nanotube composites. Sensors 12 (2012) 7965-7974.

[158] M .A. Chougule, S.G. Pawar, P. R. Godse, R. N. Mulik, S. Sen, V.B. Patil, Synthesis and characterization of polypyrrole (PPy) thin films. Soft Nanosci. Lett.1 (2011) 6-10

[159] T. A. Sherazi, J. Y. Sohn, Y. M. Lee, M. D. Guiver, Polyethylene-based radiation grafted anion-exchange membranes for alkaline fuel cells. Journal of Membrane Science, 441 (2013) 148-157.

[160] O. Brylev, F. Alloin, M. Duclot, J.L. Souquet, J. Y. Sanchez, New family of anion conducting polymers. Synthesis and characterization. Electrochim. Acta 48 (2003) 1953-1959.

[161] N. J. Robertson, I. V. H. A. Kostalik, T. J. Clark, P. F. Mutolo, H. D. Abrun, G. W. Coates, Tunable high performance cross-linked alkaline anion exchange membranes for fuel cell applications. J. Am. Chem. Soc. 132 (2010) 3400-3404.

[162] T. J. Clark, N. J. Robertson, I. V. H. A. Kostalik, E. B. Lobkovsky, P. F. Mutolo, H. D. Abrun, G. W. Coates, A ring-opening metathesis polymerization route to alkaline anion exchange membranes: development of hydroxide-conducting thin films from an ammonium-functionalized monomer. J. Am. Chem. Soc. 131 (2009) 12888-12889.

[163] G. A. Giffin, S. Lavina, G. Pace, V. Di Noto, Interplay between the structure and relaxations in selemion AMV hydroxide conducting membranes for AEMFC applications. J. Phys. Chem. C 116 (2012) 23965-23973.

[164] V. Di Noto, G. A. Giffin, K. Vezzù, M. Piga, S. Lavina, Solid state proton conductors: properties and applications in fuel cells, in: P. Knauth, M.L. Di Vona (Eds.), Solid State Proton Conductors: Properties and Applications in Fuel Cells. John Wiley & Sons, Chichester. (2012) 109-183.

[165] V. Di Noto, Zeolitic inorganic-organic polymer electrolyte based on oligo (ethylene glycol) 600 K2PdCl4 and K3Co(CN)6. J. Phys. Chem. B 104 (2000) 10116-10125.

[166] V. Di Noto, A novel polymer electrolyte based on oligo (ethylen glycol) 600, K_2PdC_{l4}, and $K_3Fe(CN)_6$. J. Mater. Res. 12 (1997) 3393-3403.

[167] V. Di Noto, M. Vittadello, Mechanism of ionic conductivity in poly (ethylen glycol 400)/$(MgCl_2)$x polymer electrolytes: studies based on electrical spectroscopy. Solid State Ionics 147 (2002) 309-316.

[168] V. Di Noto, K. Vezzù, G. Pace, M. Vittadello, A. Bertucco, Effect of subcritical CO_2 on the structural and electrical properties of ORMOCERS-APE systems based on Zr and Al. Electrochim. Acta 50 (2005) 3904-3916.

[169] R. Sulcis, F. Vizza, W. Oberhauser, F. Ciardelli, R. Spiniello, N. Dintcheva, E. Tz.; Passaglia. Polym. Adv. Technol. 25 (2014)1060.

[170] K. I. Aly, M. I. J. Abdel Monem, Appl. Polym. Sci.98 (2005) 2394.

[171] K. C. Chang, C. Y. Lin, H. F. Lin, Sh. Ch. Chiou, W. Ch. Huang, J. M. Yeh, J. Ch. Yang, Thermally and mechanically enhanced epoxy resin-silica hybrid materials containing primary amine-modified silica nanoparticles. J. Appl. Polym. Sci., 108 (2008) 1629-1635.

[172] B. Munoz, A. Ramila, J. Perez-Pariente, I. Diaz, M. Vallet-Regi, MCM-41 organic modificationas drug delivery rate regulator. Chem. Mater., 15 (2003) 500-503.

[173] C. Lei, Y. Shin, J. Liu, E. J. Ackerman, Entrapping enzyme in a functionalized nanoporous support. J. Am. Chem. Soc., 124 (2002)11242-11243.

[174] X. Wang, Y. H. Tseng, J. C. C. Chan, S. Cheng, Catalytic applications of aminopropylated mesoporous silica prepared Catalytic by a template-free route in flavanones synthesis. J. Catal., 233 (2005) 266-275.

[175] Hsu Tung Lu, Synthesis and characterization of amino functionalized silica

nanoparticles. Colloid Journal, 75(3) (2013) 311–318.

[176] A. K. Sahu, G. Selvarani, S. Pitchumani, P. Sridhar, A. K. A. Shukla, Sol-gel modified alternative Nafion-silica composite membrane for polymer electrolyte fuel cells. J Electrochem Soc, 154 (2007) 123–132.

[177] Ch. Lee, S. M. Jo, J. Choi, K-Y. Baek, Y.B. Truong, I.L. Kyratzis, Y.G. Shul, SiO_2/sulfonated poly ether ether ketone (SPEEK) composite nanofiber mat supported proton exchange membranes for fuel cells. J Mater Sci, 48 (2013) 3665–3671.

[178] N. H. Jalani, K. Dunn, R. Datta, Synthesis and characterization of Nafion-MO_2 (M = Zr, Si, Ti) nanocomposite membranes for high temperature PEM fuel cells. Electrochimica Acta, 51 (2005) 553-560.

[179] H.W. Rhee, L.J. Ghil, Polymer Nanocomposites in Fuel Cells. Woodhead Publishing Limited (2012) 433-471.

[180] L. Wahba, M. D'Arienzo, S. Dirè, R. Donetti, T. Hanel, F. Morazzoni, M. Niederberger, N. Santo, L. Tadiello, R. Scotti, Novel non-aqueous sol-gel route for the in-situ synthesis of high loaded silica-rubber nanocomposites. Soft Matter, 10 (2014) 2234-2244.

[181] Y. Taniguchi, M. Ogawa, W. Gang, H. Saitoh, K. Fujiki, T. Yamauchi, et al., Preparation of hyperfunctional carbon black by grafting of hyperbranched polyester onto the surface. Materials Chemistry and Physics, 108 (2008) 397–402.

[182] R. Walter, K. Friedrich, V. Privalko, A.J. Savadori, On modulus and fracture toughness of rigid particulate filled high density polyethylene. Journal of Adhesion, 64 (1997) 87–109.

[183] H. J. Han, S. M. Koo, Surface modification of PTMS particles with organosilanes: TEOS-, VTMS and MTMS-modified particles. Journal of Sol-Gel Science and Technology. 31 (2004) 117-121.

[184] Sh. Nakagaki, G. K. B. Ferreira, A. L. Marçal, K. Ciuffi, Metalloporphyrins immobilized on silica and modified silica as catalysts in heterogeneous processes. Current Organic Synthesis, 11 (2014) 67-88.

[185] C. B. Hansen, G. J. Hoogers, W. Drenth, Anchored manganese and ruthenium porphyrins as catalysts in the decomposition of cyclohexyl hydroperoxide. J. Mol. Catal. 79(1-3) (1993) 153-163.

[186] A. Gomathi, S. J. Hoseini, C. N. R. Rao. Functionalization and solubilization of inorganic nanostructures and carbon nanotubes by employing organosilicon and organotin

reagents. J. Mater Chem. 19 (2009) 988–995.

[187] Z. Hamzah, N. Narawi, H. Md Rasid, A. N. Md Yusoff, Synthesis and characterization of mesoporous material functionalized with different silylating agent and their capability to remove cu^{2+}. The Malaysian Journal of Analytical Sciences. 16(3) (2012) 290-296.

[188] B. Qiao, T. J. Wang, H. Gao, Y. Jin, High density silanization of nano-silica particles using -aminopropyltriethoxysilane (APTES). Applied Surface Science. 351 (2015) 646-654.

[189] C. J. Brinker, G. W. Scherer, Sol-Gel Science. The Physics and Chemistry of Sol-Gel Processing. Academic Press: San Diego, 1990.

[190] Z. H. Huang, K. Y. Qiu, Preparation and thermal property of poly(methyl methacrylate) silicate hybrid materials by the in-situ sol-gel process. Polymer Bulletin, 35(1995) 607-613.

[191] S. Sakka, Handbook of Sol-Gel Science and Technology, Processing, Characterization and Applications, Chapter 11. Kluwer Academic Publishers (2005).

[192] I. A. Rahman, M. Jafarzadeh, C. S. Sipaut, Synthesis of organo-functionalized nanosilica via a co-condensation modification using g-aminopropyltriethoxysilane (APTES). Ceramics International 35 (2009) 1883-1888.

[193] R. V. Ghorpade, C. R. Rajan, N. N. Chavan, S. Ponrathnam, Synthesis of novel silica-polyimide nanocomposite films using aromatic-amino modified silica nanoparticles: mechanical, thermal and morphological investigations. eXPRESS Polymer Letters. 9 (5) (2015) 469-479.

[194] M. Sándor, C. L. Nistor, G. Szalontai, R. Stoica, C. A. Nicolae, E. Alexandrescu, J. Fazakas, F. Oancea, D. Donescu, Aminopropyl-silica hybrid particles as supports for humic acids immobilization. Materials. 9(34) (2016) doi:10.3390/ma9010034.

[195] M. Namvar-Mahboub, M. Pakizeh, Development of a novel thin film composite membrane by interfacial polymerization on polyetherimide/modified SiO_2 support for organic solvent nanofiltration. Separation and Purification Technology. 119 (2013) 35–45.

[196] P. Vejayakumaran, I. A. Rahmana, C. S. Sipaut, J. Ismail, C. K. Chee, Structural and thermal characterizations of silica nanoparticles grafted with pendant maleimide and epoxide groups. Journal of Colloid and Interface Science. 328 (2008) 81-91.

[197] Z. Hou, W. Qu, Ch. Kan, Synthesis and properties of triethoxysilane-terminated anionic polyurethane and its waterborne dispersions. J Polym Res 22 (2015) 111-119.

[198] N. S. K. Gunda , M. Singh, L. Norman, K. Kaur, S. K. Mitra, Optimization and characterization of biomolecule immobilization on silicon substrates using (3-aminopropyl)triethoxysilane (APTES) and glutaraldehyde linker. Applied Surface Science. 305 (2014) 522–530.

[199] J. Kim, J. Cho, P. M. Seidler, N. E. Kurland,V. K. Yadavalli, Investigations of chemical modifications of amino-terminated organic films on silicon substrates and controlled protein immobilization. Langmuir. 26(4) (2010) 2599–2608.

[200] R. Figueira , E. Callone, C. Silva, E. Pereira, S. Dirè, Hybrid coatings enriched with tetraethoxysilane for corrosion mitigation of hot-dip galvanized steel in chloride contaminated simulated concrete pore solutions. Materials, 10 (2017), 306.

[201] S. N. Abdollahi, M. Naderi, G. Amoabediny, Synthesis and physicochemical characterization of tunable silica-gold nanoshells via seed growth method. Colloids and Surfaces A: Physicochem. Eng. Aspects, 414 (2012) 345–351.

[202] M. Jafarzadeh, I. A. Rahman, C. S. Sipaut, Optical properties of amorphous organo-modified silica nanoparticles produced via co-condensation method. Ceramics International, 36 (2010) 333–338.

[203] E. Borovin, E. Callone, R. Ceccato, A. Quaranta, S. Dirè, Adsorptive properties of sol gel derived hybrid organic/inorganic coatings. Materials Chemistry and Physics, 147 (2014) 954-962.

[204] X. He, X. Jiang, Z. Wang, Y. Deng, Z. Han, Y. Yang, D. Chen, Crosslinked hydroxyl-conductive copolymer/silica composite membranes based on addition-type polynorbornene for alkaline anion exchange membrane fuel cell applications. Polymer Engineering and Science, DOI 10.1002/pen.24524 (2018).

[205] W. Wang, S. Wang, X. Xie, Y. Iv, V. K. Ramani, Hydroxide-ion induced degradation pathway for dimethylimidazolium groups in anion exchange membranes. Journal of Membrane Science 462 (2014) 112-118.

[206] N. Ataollahi, A. Ahmad, H. Hamzah, M. Y. A. Rahman, N. S. Mohamed, Preparation and characterization of PVDF-HFP/MG49 based polymer blend electrolyte. Int. J. Electrochem. Sci., 7 (2012) 6693 - 6703.